

# On the application of “ $Z^0 + jet$ ” events for setting the absolute jet energy scale and determining the gluon distribution in a proton at the LHC.

D.V. Bandurin, N.B. Skachkov

*Joint Institute for Nuclear Research, Dubna, Russia*

## Abstract

A possibility of jet energy scale setting by help of “ $pp \rightarrow Z^0 + jet + X$ ” process at LHC is studied. The effect of new set of cuts, proposed in our previous works, on the improvement of  $P_t^Z - P_t^{jet}$  balance is demonstrated. The distributions of the selected events over  $P_t^Z$  and  $\eta^{jet}$  are presented. A possibility of background events suppression by use of the “ $Z^0 + jet$ ” events selection criteria is shown.

It is also found that the samples of “ $Z^0 + jet$ ” events, gained with the cuts for the jet energy calibration, may have enough statistics for determining the gluon distribution inside a proton in the region of  $2 \cdot 10^{-4} \leq x \leq 1.0$  with  $0.9 \cdot 10^3 \leq Q^2 \leq 4 \cdot 10^4$  ( $GeV/c$ )<sup>2</sup>.

Monte Carlo events produced by the PYTHIA 5.7 generator are used here.

# 1 Introduction.

A precise reconstruction of the jet energy is the extremely important task in many high energy physics experiments. The previous studies of possibilities to apply for this aim different physical processes (like " $Z^0/\gamma + jet$ " and others), done in D0, CDF, CMS and ATLAS collaborations may be found in [1]–[16].

“ $Z^0 + jet$ ” events with one high- $P_t$  jet can provide a useful sample to perform *in situ* determination of a jet transverse momentum via a transverse momentum of  $Z^0$  boson reconstructed from the precisely measured leptonic  $Z^0$  decay ( $Z^0 \rightarrow \mu^+\mu^-, e^+e^-$ ).

In this paper we limit our consideration to  $Z^0 \rightarrow \mu^+\mu^-$  decay only. The amount of material in front and inside the muon detector system guarantees absorbing most hadronic background. Besides, by using the track segments matching between the muon system and the tracker one can reach a high enough reconstruction efficiency of a muon track with a good momentum resolution (of order of  $0.5 - 1\%$ )<sup>1)</sup>. A selection of “ $Z^0 + jet$ ” events with the consequent decay  $Z^0 \rightarrow e^+e^-$  would require a supplementary introduction of isolation criteria for  $e^\pm$  tracks to perform a confident reconstruction of  $e^\pm$  signal in the cells of electromagnetic calorimeter (ECAL)<sup>2)</sup>. Our study has shown that a background to the “ $Z^0 + jet$ ” events with  $e^+e^-$  decay channel of  $Z^0$  boson is about the same as one to the “ $Z^0 + jet$ ” events with  $\mu^+\mu^-$  decay channel.

“ $Z^0 + jet$ ” events is a useful tool to cross-check a setting an absolute jet energy scale with help of other processes like “ $\gamma + jet$ ” [12]–[16] and “ $W \rightarrow 2 \text{ jets}$ ” events [8], for example.

Here we present results of the analysis of “ $Z^0 + jet$ ” events generated by using PYTHIA 5.7 Monte-Carlo event simulation package [19].

Section 2 is an introduction into the problem. General features of “ $Z^0 + jet$ ” processes at LHC energies as well as the sources of the disbalance between transverse momenta of  $Z^0$  and jet are presented here. We list here a set of the selection cuts used to identify signal “ $Z^0 + jet$ ” events (implying subsequent  $Z^0$  decay to the muon pair). New criteria (introduced for the first time in [12]) of  $P_t$  activity suppression beyond the “ $Z^0 + jet$ ” system are also described there. Vector and scalar forms of the balance equation of the event as a whole are given in this section.

In Section 3 we briefly describe an estimation of non-detectable part of jet  $P_t$  without taking into account of the detector effects.

Section 4 is devoted to the study of the influence of  $P_{tCUT}^{clust}$  and  $P_{tCUT}^{out}$  as well as the angle between  $\vec{P}_t^Z$  and  $\vec{P}_t^{jet}$  on the initial state radiation (ISR) suppression. The rates of “ $Z^0 + jet$ ” events with jet covering Barrel, Endcap and Forward parts of the calorimeter are also given in this section.

In Sections 5 and 6 we confine ourselves by consideration of “ $Z^0 + jet$ ” events with the jet entirely contained in the Barrel region. The dependences of various physical variables on  $P_{tCUT}^{clust}$  and  $P_{tCUT}^{out}$  are analyzed there and shown in the tables of Appendices 2–5. The values of the disbalance between  $P_t^Z$  and  $P_t^{jet}$  with for three  $P_t^Z$  intervals and various  $P_{tCUT}^{clust}$  and  $P_{tCUT}^{out}$  values are presented in Appendix 6.

In Section 7 we study a possibility of background events suppression for different  $P_t^Z$  intervals.

The number of events for determination of the gluon density in a proton by using “ $Z^0 + jet$ ” events is estimated in Section 8. The event rates and contributions of various processes are calculated there for different  $x$  and  $Q^2$  intervals. It is shown that the kinematic region for the gluon density determination in the intervals:  $2 \cdot 10^{-4} \leq x \leq 1.0$  with  $0.9 \cdot 10^3 \leq Q^2 \leq 4 \cdot 10^4 \text{ (GeV}/c)^2$  can be covered by studying the “ $Z^0 + jet$ ” events.

---

<sup>1)</sup> see [17]

<sup>2)</sup> For instance, by requiring (1) a total transverse momentum  $E_t^{tot}$  around an electron with  $E_t^e$  in the cone with  $R = 0.3$  to be  $E_t^{tot} < 5 \text{ GeV}$  and (2)  $E_t^{tot}/E_t^e < 0.1$  (e.g. see [18]) we additionally reduce a number of signal events by 2 – 4%.

## 2 Generalities of the “ $Z^0 + jet$ ” process.

### 2.1 Leading order picture and sources of $P_t^Z$ and $P_t^{jet}$ disbalance.

In this section we observe briefly the main effects that lead to the disbalance between  $P_t^Z$  and  $P_t^{jet}$ <sup>3)</sup>.

The process of  $Z^0 + jet$  production

$$pp \rightarrow Z^0 + 1\text{ jet} + X \quad (1)$$

is caused at the parton level by two subprocesses: Compton-like scattering

$$gg \rightarrow q + Z^0 \quad (2a)$$

and the annihilation process

$$q\bar{q} \rightarrow g + Z^0. \quad (2b)$$

Some leading order Feynman diagrams of these processes are shown in Fig. 1.

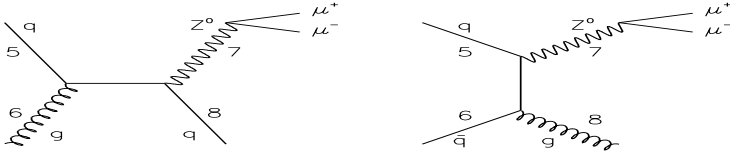


Figure 1: Some leading order Feynman diagrams for  $Z^0$  production.

If the initial state radiation (ISR) is absent, the total transverse momentum of the final state in the subprocesses (2a) or (2b) is equal to zero, i.e. the  $P_t$  balance equation for  $Z^0$  and final parton would look as

$$\vec{P}_t^{Z+part} = \vec{P}_t^Z + \vec{P}_t^{part} = 0. \quad (2)$$

Thus, having neglected hadronization effect we could expect that a jet transverse momentum  $P_t^{jet}$  is close enough to  $Z^0$  boson transverse momentum, i.e.  $\vec{P}_t^{jet} \approx -\vec{P}_t^Z$ .

A radiation of a gluon in the initial state with a non-zero transverse momentum  $P_t^{gluon} \equiv P_t^{ISR} \neq 0$  can produce a disbalance between  $P_t^Z$  and  $P_t^{part}$  and, thus, between transverse momenta of  $Z^0$  boson and the jet originated from this proton. The corresponding next-to-leading order diagrams are shown in Fig. 2.

Following [12], we choose the sum of the modulus of the transverse momentum vectors  $\vec{P}_t^5$  and  $\vec{P}_t^6$  of the incoming (into  $2 \rightarrow 2$  fundamental QCD subprocesses  $5 + 6 \rightarrow 7 + 8$ ) partons (lines 5 and 6 in Fig. 2):

$$P_{t56} = |P_t^5| + |P_t^6| \quad (3)$$

as a quantitative measure to estimate the  $P_t$  disbalance caused by ISR.

The numerical notations in the Feynman diagrams shown in Figs. 1 and 2 and in formula (2) are chosen to be in correspondence with those used in the PYTHIA event listing for description of the parton–parton subprocess displayed schematically in Fig. 3. The “ISR” block describes the initial state radiation process that can take place before the fundamental hard  $2 \rightarrow 2$  process.

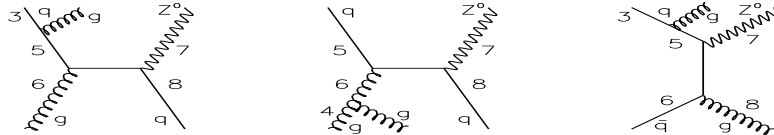


Figure 2: Some Feynman diagrams of  $Z^0$  production including gluon radiation in the initial state.

<sup>3)</sup> The more detailed consideration is given in our papers [12, 22] devoted to the jet energy calibration by using “ $\gamma + jet$ ” events.

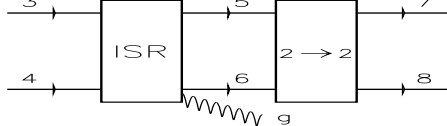


Figure 3: PYTHIA “diagram” of a fundamental  $2 \rightarrow 2$  process ( $5+6 \rightarrow 7+8$ ) following the block ( $3+4 \rightarrow 5+6$ ) of initial state radiation (ISR).

Let us consider fundamental subprocesses in which there is no initial state radiation but instead final state radiation (FSR) takes place. Some Feynman diagrams of the signal subprocesses with the FSR are shown in Fig. 4. An appearance of a gluon in the final state may also cause a disbalance between transverse momenta of  $Z^0$  and jet. But because it manifests itself as some extra jets or clusters, like in the case of ISR, the same selection criteria (see below) as for suppression of ISR can be used.

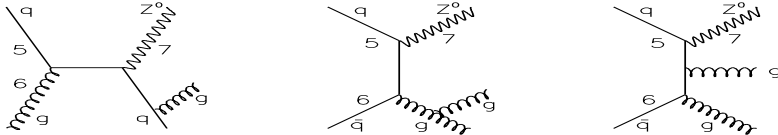


Figure 4: Some of Feynman diagrams of  $Z^0$  production including gluon radiation in the final state.

A possible non-zero value of the intrinsic transverse momentum of a parton inside a colliding proton ( $k_T$ ) may be another source of the  $P_t^Z$  and  $P_t^{part}$  disbalance in the final state. Its reasonable value is supposed to lead to the value of  $k_T \leq 1.0 \text{ GeV}/c$ . In what follows we shall keep the value of  $k_T$  to be fixed by the PYTHIA default value  $\langle k_T \rangle = 0.44 \text{ GeV}/c$ . The dependence of the disbalance between  $P_t^Z$  and  $P_t^{Jet}$  on a possible variation of  $k_T$  is discussed in detail in [16, 22]. The general conclusion is that the variation of  $k_T$  within reasonable boundaries does not produce a large effect when the initial state radiation is taken into account. The latter makes a dominant contribution.

Another non-perturbative effect that results in the  $P_t^Z$  and  $P_t^{Jet}$  disbalance is an hadronization of the parton, produced in the fundamental  $2 \rightarrow 2$  subprocess, into a jet. The contribution of the hadronization to this disbalance is calculated within the Lund string fragmentation scheme used by default in PYTHIA. The mean values of the relative  $P_t^{Jet} - P_t^{part}$  disbalance are presented in the tables of Appendices 2 – 5 for three different jetfinders (UA1, UA2 and LUCELL<sup>4)</sup>) as a function of the variable which limit a cluster activity beyond the “ $Z^0 + jet$ ” system (see Section 2.2 and [14]).

## 2.2 Definition of selection cuts.

1. We shall select the events with  $Z^0$  boson<sup>5)</sup> and one jet with

$$P_t^Z \geq 40 \text{ GeV}/c \quad \text{and} \quad P_t^{Jet} \geq 30 \text{ GeV}/c. \quad (4)$$

For most of our applications the jet is defined according to the PYTHIA jetfinding algorithm LUCELL. The jet cone radius  $R$  in the  $\eta - \phi$  space counted from the jet initiator cell (ic) is taken to be  $R_{ic} = ((\Delta\eta)^2 + (\Delta\phi)^2)^{1/2} = 0.7$ . Comparison with the UA1 and UA2 jetfinding algorithms is presented in Sections 5 and 6.

2. To guarantee a clear identification of a muon track from  $Z^0$  decay in the muon and tracker systems and determination of its parameters we put the following restrictions on muons<sup>6)</sup>:

(a) on the  $P_t$  value of any considered muon:

$$P_t^\mu \geq 10 \text{ GeV}/c; \quad (5)$$

(b) on the  $P_t$  value of the most energetic muon in a pair:

$$P_{tmax}^\mu \geq P_{tCUT}^\mu \quad (6)$$

$(P_{tCUT}^\mu \geq 20 \text{ GeV}/c \text{ and depends on the energy scale; see Fig. 6 of Section 4.3);}$

<sup>4)</sup> UA1 and UA2 algorithms are taken from the CMSJET program of fast simulation [18], while LUCELL is the PYTHIA’s default jetfinding algorithm [19].

<sup>5)</sup> Here and below in the paper speaking about  $Z^0$  boson we imply a signal reconstructed from the muon pair with muons selected by the criteria 2 – 4 of this section.

<sup>6)</sup> Most of the muon selection cuts are taken from [17, 18].

(c) on the value of the ratio of  $P_t^{isol}$ , i.e. the scalar sum of  $P_t$  of all particles surrounding a muon, to  $P_t^\mu$  ( $P_t^{isol}/P_t^\mu$ ) in the cone of radius  $R = 0.3$  and on the value of maximal  $P_t$  of a charged particle surrounding a muon in this cone:

$$P_t^{isol}/P_t^\mu \leq 0.10, \quad P_t^{ch} \leq 2 \text{ GeV}/c. \quad (7)$$

The isolated high- $P_t$  tracks can be reconstructed with a good efficiency (at least 98% over all pseudorapidity region  $|\eta| < 2.4$ ; see [17]) and with generation of a low number of fake and ghost tracks.

3. A muon is selected in the region of the muon system acceptance:

$$|\eta^\mu| < 2.4. \quad (8)$$

4. To select muon pairs only from the  $Z^0$  decay we limit the value of invariant mass of a muon pair  $M_{inv}^{ll}$  by:

$$|M^Z - M_{inv}^{ll}| \leq 5 \text{ GeV}/c^2. \quad (9)$$

5. We select the events with the vector  $\vec{P}_t^{jet}$  being “back-to-back” to the vector  $\vec{P}_t^Z$  (in the plane transverse to the beam line) within  $\Delta\phi$  defined by the equation:

$$\phi_{(Z,jet)} = 180^\circ \pm \Delta\phi \quad (10)$$

where  $\phi_{(Z,jet)}$  is the angle between the  $\vec{P}_t^Z$  and  $\vec{P}_t^{jet}$  vectors:  $\vec{P}_t^Z \cdot \vec{P}_t^{jet} = P_t^Z P_t^{jet} \cos(\phi_{(Z,jet)})$ , where  $P_t^Z = |\vec{P}_t^Z|$ ,  $P_t^{jet} = |\vec{P}_t^{jet}|$ .  $\Delta\phi$  defined in the interval  $5 - 15^\circ$  is the most effective choice.

6. The initial and final state radiations (ISR and FSR) manifest themselves most clearly as some final state mini-jets or clusters activity (see the previous section and [12]–[16]). To suppress it, we impose a new cut condition that was not formulated in an evident form in previous experiments: we choose the “ $Z^0 + jet$ ” events that do not have any other jet-like or cluster high  $P_t$  activity by taking values of  $P_t^{clust}$  (the cluster cone  $R_{clust}(\eta, \phi) = 0.7$ ), being smaller than some threshold  $P_{tCUT}^{clust}$  value, i.e. we select the events with

$$P_t^{clust} \leq P_{tCUT}^{clust}. \quad (11)$$

7. We limit the value of the modulus of the vector sum of  $\vec{P}_t$  of all particles that do not belong to the “ $Z^0 + jet$ ” system but fit into the region  $|\eta| < 5$  covered by the calorimeter system, i.e., we limit the signal in the cells “beyond the jet and  $Z^0$ ” regions by the following cut:

$$\left| \sum_{i \notin Jet, Z^0} \vec{P}_t^i \right| \equiv P_t^{out} \leq P_{tCUT}^{out}, \quad |\eta| < 5. \quad (12)$$

The importance of  $P_{tCUT}^{out}$  and  $P_{tCUT}^{clust}$  for selection of events with a good balance of  $P_t^Z$  and  $P_t^{jet}$  was already shown in [12] – [16] and in [22]. In Sections 5 and 6 it will be demonstrated once again for the case of “ $Z^0 + jet$ ” events. The set of selection cuts 1 – 7 we call as “Selection 1”.

8. By analogy with [12] – [16] and [22] we use a “jet isolation” requirement (introduced for the first time in [12]), i.e. the presence of a “clean enough” (in the sense of limited  $P_t$  activity) region inside the ring of  $\Delta R = 0.3$  around the jet. Following this picture, we restrict the ratio of the scalar sum of transverse momenta of particles belonging to this ring, i.e.

$$P_t^{ring}/P_t^{jet} \equiv \epsilon^{jet}, \quad \text{where} \quad P_t^{ring} = \sum_{i \in 0.7 < R < 1} |\vec{P}_t^i| \quad (13)$$

with  $\epsilon^{jet} \leq 3 - 8\%$  (see Sections 6 and 7). The set of events that pass cuts 1 – 7 will be called “Selection 2”.

9. As in [12, 22] in the following “Selection 3” we shall keep only those events in which one and the same jet (i.e. up to good accuracy having the same values of  $P_t^{jet}$ ,  $R^{jet}$  and  $\Delta\phi$ ) is found simultaneously by every of three jetfinders used here: UA1, UA2 and LUCELL. For these jets (and also clusters) we require the following conditions:

$$P_t^{jet} > 30 \text{ GeV}/c, \quad P_t^{clust} < P_{tCUT}^{clust}, \quad \Delta\phi < 15^\circ, \quad \epsilon^{jet} \leq 5\%. \quad (14)$$

10. As we shown in [12, 22] One can expect reasonable results of modeling the jet energy calibration procedure and subsequent practical realization only if one uses a set of selected events with small missing transverse momentum  $P_t^{miss}$ . We define it here as a  $P_t$  vector sum of all the particles flying mostly in the direction of the non-instrumented region  $|\eta| > 5.0$  and neutrinos with  $|\eta| < 5.0$ :

$$\vec{P}_t^{miss} = \vec{P}_t^{|\eta|>5.0} + \sum_{i \in |\eta|<5.0} \vec{P}_{t(\nu)}^i. \quad (15)$$

Here  $\vec{P}_t^{|\eta|>5}$  is the total transverse momentum of non-observable particles  $i$  flying in the direction of the non-instrumented forward part of the CMS detector ( $|\eta| > 5$ ):

$$\sum_{i \in |\eta|>5} \vec{P}_t^i \equiv \vec{P}_t^{|\eta|>5}. \quad (16)$$

We shall use the following cut on  $P_t^{miss}$ :

$$P_t^{miss} \leq P_{tCUT}^{miss}. \quad (17)$$

The aim of the event selection with small  $P_t^{miss}$  is quite obvious: we need a set of events with a reduced  $P_t^{jet}$  uncertainty due to a possible presence of a non-detectable neutrino contribution to a jet, for example.

The exact values of the cut parameters  $P_{tCUT}^\mu$ ,  $\epsilon^{jet}$ ,  $P_{tCUT}^{clust}$ ,  $P_{tCUT}^{out}$  will be specified below, since they may be different, for instance, for various  $P_t^Z$  intervals.

### 2.3 The $P_t$ -balance equation of “ $Z^0 + jet$ ” event.

The conservation law for “ $Z^0 + jet$ ” events as a whole can be written in the following vector form [12, 22]:

$$\vec{P}_t^Z + \vec{P}_t^{jet} + \vec{P}_t^O + \vec{P}_t^{|\eta|>5} = 0. \quad (18)$$

$\vec{P}_t^{|\eta|>5}$  is defined in (16) and  $\vec{P}_t^O$  is a total transverse momentum of all other ( $O$ ) particles besides “jet particles and muons from  $Z^0$  decay” (“ $Z^0 + jet$ ” system) in the  $|\eta| < 5$  region and defined as:

$$\vec{P}_t^O = \vec{P}_t^{out} + \vec{P}_{t(\nu)}^O + \vec{P}_{t(\mu, |\eta^\mu|>2.4)}^O. \quad (19)$$

In its turn,  $\vec{P}_t^{out}$  is a sum of clusters  $P_t$  (with  $P_t^{clust}$  smaller than  $P_t^{jet}$ ) and  $P_t$  of single hadrons ( $h$ ), photons ( $\gamma$ ) and electrons ( $e$ ) with  $|\eta| < 5$  and muons ( $\mu$ ) with  $|\eta^\mu| < 2.4$  that are out of the “ $Z^0 + jet$ ” system:

$$\vec{P}_t^{out} = \vec{P}_t^{clust} + \vec{P}_{t(h)}^{sing} + \vec{P}_{t(\gamma)}^{nondir} + \vec{P}_{t(e)}^O + \vec{P}_{t(\mu, |\eta^\mu|<2.4)}^O, \quad |\eta| < 5. \quad (20)$$

The last two terms in equation (19) are the transverse momentum carried out by the neutrinos that do not belong to the jet but that are contained in the  $|\eta| < 5$  region ( $\vec{P}_{t(\nu)}^O$ ) and non-detectable muons flying with  $|\eta^\mu| > 2.4$  ( $\vec{P}_{t(\mu, |\eta^\mu|>2.4)}^O$ ).

To conclude this section, let us rewrite the basic vector  $P_t$ -balance equation in the following scalar form, more suitable to present the final results:

$$\frac{P_t^Z - P_t^{jet}}{P_t^Z} = (1 - \cos\Delta\phi) + P_t(O + \eta > 5)/P_t^Z, \quad (21)$$

where  $P_t(O + \eta > 5) \equiv (\vec{P}_t^O + \vec{P}_t^{|\eta|>5}) \cdot \vec{n}^{jet}$  with  $\vec{n}^{jet} = \vec{P}_t^{jet}/P_t^{jet}$  and  $\Delta\phi$  is the angle that enters equation (10).

As will be shown in Section 6, the first term on the right-hand side of equation (21) is negligibly small and tends to decrease fast with growing  $P_t^{jet}$ . So, the main contribution to the  $P_t$  disbalance in the “ $Z^0 + jet$ ” system is caused by the term  $P_t(O + \eta > 5)/P_t^Z$  [12]–[16], [22].

### 3 Estimation of a non-detectable part of $P_t^{jet}$ .

This subject is considered in detail in [12]. Here we outline the main results for the case of “ $Z^0 + jet$ ” events. One of the main sources of this part, that can be estimated on the particle level, is non-detectable particles (like neutrinos and muons with  $|\eta| > 2.4$ )<sup>7)</sup>

The missing transverse momentum  $P_t^{miss}$  (see (15)) and a  $P_t$  contribution to a jet from non-detectable particles are estimated here in the framework of simulation with PYTHIA<sup>8)</sup>. The detailed information about the transverse momenta of non-detectable neutrinos  $P_{t(\nu)}^{Jet}$  averaged over all events (no cut on  $P_t^{miss}$  was used) as well as about mean  $P_t$  values of muons belonging to jets  $\langle P_{t(\mu)}^{Jet} \rangle$  is presented in Tables 1–12 of Appendix 1 for the sample of events with jets which are entirely contained in the barrel region of the calorimeter ( $|\eta^{jet}| < 1.4$ , “HB-events”, see Section 4 and 5). In these tables the ratio of number of the events with non-zero  $P_{t(\nu)}^{Jet}$  to the total number of events is denoted by  $R_{event}^{\nu \in Jet}$  and the ratio of the number of events with non-zero  $P_{t(\mu)}^{Jet}$  to the total number of events is denoted by  $R_{event}^{\mu \in Jet}$ .

A wide variation of  $P_{tCUT}^{miss}$  as well as the case of allowed  $K^\pm$  decays in the calorimeter volume were presented in detail in [12]. We choose here for the following analysis  $P_{tCUT}^{miss} = 10 \text{ GeV}/c$  found to be optimal in [12].

### 4 Event rates for different $P_t^Z$ and $\eta^Z$ intervals.

#### 4.1 Dependence of the distribution of the number of events on the “back-to-back” angle $\phi_{(Z,jet)}$ and on $P_t^{ISR}$ .

Here we study the spectrum of the variable  $P_t56$  for the sample of signal events<sup>9)</sup>. For this aim four samples of “ $Z^0 + jet$ ” events (each by  $5 \cdot 10^6$ ) were generated by using PYTHIA with 2 subprocesses (2a) and (2b) and with minimal  $P_t$  of hard  $2 \rightarrow 2$  scattering<sup>10)</sup>  $\hat{p}_\perp^{min} = 20, 35, 50, 75 \text{ GeV}/c$  to cover four  $P_t^Z$  intervals: 40–50, 70–85, 100–120, 150–200  $\text{GeV}/c$ , respectively. The obtained cross sections for these subprocesses are given in Table 1.

Table 1: The cross sections (in *microbarns*) of the  $qg \rightarrow q + Z^0$  and  $q\bar{q} \rightarrow g + Z^0$  subprocesses for four  $\hat{p}_\perp^{min}$  values.

Subprocess type	$\hat{p}_\perp^{min}$ values ( $\text{GeV}/c$ )			
	20	35	50	75
$qg \rightarrow q + Z^0$	$3.83 \cdot 10^{-4}$	$1.71 \cdot 10^{-4}$	$9.14 \cdot 10^{-5}$	$3.80 \cdot 10^{-5}$
$q\bar{q} \rightarrow g + Z^0$	$1.20 \cdot 10^{-4}$	$0.42 \cdot 10^{-4}$	$1.93 \cdot 10^{-5}$	$0.69 \cdot 10^{-5}$
Total	$5.03 \cdot 10^{-4}$	$2.13 \cdot 10^{-4}$	$1.11 \cdot 10^{-4}$	$4.59 \cdot 10^{-5}$

For our analysis we used cuts (4) – (12) and the following cut parameters:

$$P_{tmax}^\mu > 20 \text{ GeV}/c, \quad \Delta\phi < 15^\circ, \quad P_{tCUT}^{clust} = 30 \text{ GeV}/c. \quad (22)$$

In Tables 2, 3 and 5, 6 we study (as in [12])  $P_t56$  spectra for two most illustrative cases of  $P_t^Z$  intervals  $40 < P_t^Z < 50 \text{ GeV}/c$  (Tables 2 and 5) and  $100 < P_t^Z < 120 \text{ GeV}/c$  (Tables 3 and 6). The distributions of the number of events for the integrated luminosity  $L_{int} = 10 \text{ fb}^{-1}$  in different  $P_t56$  intervals and for different “back-to-back” angle intervals  $\phi_{(Z,jet)} = 180^\circ \pm \Delta\phi$  (with  $\Delta\phi = 15^\circ, 10^\circ$  and  $5^\circ$  as well as without any restriction on  $\Delta\phi$ , i.e. for the whole  $\phi$  interval  $\Delta\phi = 180^\circ$ ) are given there. The LUCELL jetfinder was used to find jets and clusters. Tables 2 and 3 correspond to the events selected with cuts  $P_t^{clust} < 30 \text{ GeV}/c$  and without any limit on  $P_t^{out}$  value, while Tables 5 and 6 correspond to more restrictive selection cuts  $P_t^{clust} < 10 \text{ GeV}/c$  and  $P_t^{out} < 10 \text{ GeV}/c$ .

First, from the last summary lines of Tables 2, 3 and 5, 6 we can make a general conclusion about the  $\Delta\phi$  dependence of the event spectrum. In the case when no restriction is used we can see that for the  $40 \leq P_t^Z \leq 50 \text{ GeV}/c$

<sup>7)</sup> In a real experiment, of course, it can be also conditioned by many other reasons as, for instance, the energy leakage due to constructive features of the detector, magnetic field effects and so on.

<sup>8)</sup> We have considered the case of switched-off decays of  $\pi^\pm$  and  $K^\pm$  mesons (according to the PYTHIA default agreement,  $\pi^\pm$  and  $K^\pm$  mesons are stable).

<sup>9)</sup>  $P_t56$  is approximately proportional to  $P_t^{ISR}$  up to the value of intrinsic parton transverse momentum  $k_T$  inside a proton ( $\langle k_T \rangle$  was taken to be fixed at the PYTHIA default value, i.e.  $\langle k_T \rangle = 0.44 \text{ GeV}/c$ ).

<sup>10)</sup> CKIN(3) parameter in PYTHIA

Table 2: Number of events dependence on  $P_t 56$  and  $\Delta\phi$  for  $40 \leq P_t^Z \leq 50 \text{ GeV}/c$  and  $P_{t,CUT}^{clust} = 30 \text{ GeV}/c$  for  $L_{int}=10 \text{ fb}^{-1}$ .

$P_t 56$ (GeV/c)	$\Delta\phi_{max}$			
	180°	15°	10°	5°
0 – 5	18525	16965	15880	12708
5 – 10	29094	26671	23419	13579
10 – 15	24192	19935	14042	7033
15 – 20	18168	10910	7088	3481
20 – 25	13424	5833	3924	1968
25 – 30	10169	3604	2380	1172
30 – 40	14070	4114	2677	1311
40 – 50	7544	1833	1184	618
50 – 100	5904	1727	1097	550
100 – 300	8	3	2	0
300 – 500	0	0	0	0
30 – 500	141095	91594	71694	42423

Table 3: Number of events dependence on  $P_t 56$  and  $\Delta\phi$  for  $100 \leq P_t^Z \leq 120 \text{ GeV}/c$  and  $P_{t,CUT}^{clust} = 30 \text{ GeV}/c$  for  $L_{int}=10 \text{ fb}^{-1}$ .

$P_t 56$ (GeV/c)	$\Delta\phi_{max}$			
	180°	15°	10°	5°
0 – 5	1849	1837	1790	1616
5 – 10	3798	3770	3667	3247
10 – 15	3635	3600	3477	2542
15 – 20	3065	3025	2847	1592
20 – 25	2491	2424	1976	986
25 – 30	2115	2000	1418	709
30 – 40	2507	2039	1398	721
40 – 50	1061	744	527	289
50 – 100	1105	768	582	325
100 – 300	194	147	107	63
300 – 500	2	2	1	0
0 – 500	21826	20356	17797	12094

Table 4: Number of events dependence on  $\Delta\phi$  and on  $P_t^Z$  for  $L_{int} = 10 \text{ fb}^{-1}$ .  
 $P_{t,CUT}^{clust} = 30 \text{ GeV}/c$  (summary).

$P_t^Z$ (GeV/c)	$\Delta\phi_{max}$			
	180°	15°	10°	5°
40 – 50	141095	91591	71694	42423
70 – 80	40032	32551	26710	16794
100 – 120	2182	20356	17797	12094
150 – 200	8649	8558	8134	6182

Table 5: Number of events dependence on  $P_t 56$  and  $\Delta\phi$  for  $40 \leq P_t^Z \leq 50 \text{ GeV}/c$  and  $P_{t,CUT}^{clust} = 10 \text{ GeV}/c$  and  $P_{t,CUT}^{out} = 10 \text{ GeV}/c$  for  $L_{int}=10 \text{ fb}^{-1}$ .

$P_t 56$ (GeV/c)	$\Delta\phi_{max}$			
	$180^\circ$	$15^\circ$	$10^\circ$	$5^\circ$
0 – 5	11619	11603	11409	9603
5 – 10	15329	15258	14288	8767
10 – 15	6787	6479	5156	2768
15 – 20	1810	1533	1204	645
20 – 25	677	527	432	253
25 – 30	305	238	195	119
30 – 40	277	222	193	111
40 – 50	127	111	91	44
50 – 100	36	32	24	12
100 – 300	0	0	0	0
300 – 500	0	0	0	0
0 – 500	36967	35996	32987	22315

Table 6: Number of events dependence on  $P_t 56$  and  $\Delta\phi$  for  $100 \leq P_t^Z \leq 120 \text{ GeV}/c$  and  $P_{t,CUT}^{clust} = 10 \text{ GeV}/c$  and  $P_{t,CUT}^{out} = 10 \text{ GeV}/c$  for  $L_{int}=10 \text{ fb}^{-1}$ .

$P_t 56$ (GeV/c)	$\Delta\phi_{max}$			
	$180^\circ$	$15^\circ$	$10^\circ$	$5^\circ$
0 – 5	1133	1133	1133	1121
5 – 10	1932	1932	1932	1877
10 – 15	1002	1002	1002	867
15 – 20	309	309	309	234
20 – 25	95	95	91	63
25 – 30	49	49	45	33
30 – 40	48	44	40	32
40 – 50	27	25	25	25
50 – 100	44	44	44	40
100 – 300	5	5	5	5
300 – 500	0	0	0	0
0 – 500	4641	4637	4621	4293

Table 7: Number of events dependence on  $\Delta\phi$  and on  $P_t^Z$  for  $L_{int} = 10 \text{ fb}^{-1}$ .  
 $P_{t,CUT}^{clust} = 10 \text{ GeV}/c$  and  $P_{t,CUT}^{out} = 10 \text{ GeV}/c$  (summary).

$P_t^Z$ (GeV/c)	$\Delta\phi_{max}$			
	$180^\circ$	$15^\circ$	$10^\circ$	$5^\circ$
40 – 50	36967	35996	32987	22315
70 – 80	8688	8657	8542	7033
100 – 120	4641	4637	4621	4293
150 – 200	1746	1746	1742	1719

(Table 2) interval about 65% of events are concentrated in the  $\Delta\phi < 15^\circ$  range, while 30% of events are in the  $\Delta\phi < 5^\circ$  range. At the same time the analogous summary line of Table 3 shows us that for  $100 \leq P_t^Z \leq 120 \text{ GeV}/c$  the event spectrum moves noticeably to the small  $\Delta\phi$  region: more than 94% of events have  $\Delta\phi < 15^\circ$  and 56% of them have  $\Delta\phi < 5^\circ$ .

We observe a tendency of the distributions of the number of signal “ $Z^0 + jet$ ” events to be concentrated in a rather narrow back-to-back angle interval  $\Delta\phi < 15^\circ$  with  $P_t^Z$  growing. It becomes more distinct with a more restrictive cuts  $P_{t,CUT}^{out} = 10 \text{ GeV}/c$  and  $P_{t,CUT}^{out} = 10 \text{ GeV}/c$  (Tables 5 and 6). From the last summary line of Table 5 we see for these cuts that in the case of  $40 \leq P_t^Z \leq 50 \text{ GeV}/c$  more than 96% of the events have  $\Delta\phi < 15^\circ$ , while 60% of them are in the  $\Delta\phi < 5^\circ$  range. For  $100 \leq P_t^Z \leq 120 \text{ GeV}/c$  (see Table 6) more than 92% of the events, subject to these cuts, have  $\Delta\phi < 5^\circ$ . It means that while suppressing  $P_t$  activity beyond the “ $Z^0 + jet$ ” system by imposing  $P_{t,CUT}^{clust} = 10 \text{ GeV}/c$  and  $P_{t,CUT}^{out} = 10 \text{ GeV}/c$  we can select the sample of events with a clean back-to-back ( $\Delta\phi < 15^\circ$ ) topology of  $\vec{P}_t^Z$  and  $\vec{P}_t^{jet}$  orientation<sup>11)</sup>.

The other lines of Tables 2, 3 and 5, 6 contain the information about the  $P_t 56$  spectrum (or, up to  $k_T$  effect,  $P_t^{ISR}$  spectrum).

From the comparison of Table 2 with Table 5 (as well as from Tables 3 and 6) one can conclude that the width of the most populated part of the  $P_t 56$  (or  $P_t^{ISR}$ ) spectrum is noticeably reduced with restricting  $P_{t,CUT}^{clust}$  and  $P_{t,CUT}^{out}$ .

We supply Tables 2, 3 and 5, 6 with summarizing Tables 4 and 7 containing an illustrative information on  $\Delta\phi$  dependence of the total number of events. They include more  $P_t^Z$  intervals and contain analogous numbers of events that can be collected in different  $\Delta\phi$  intervals for  $P_{t,CUT}^{clust}$ ,  $P_{t,CUT}^{out}$  and other cuts, defined by (22), at  $L_{int} = 10 \text{ fb}^{-1}$ .

We can conclude from Tables 2–7 that restriction on the  $P_{t,CUT}^{clust}$  and  $P_{t,CUT}^{out}$  variables are good tools to reduce ISR while by limiting  $\Delta\phi$  angle the ISR remains, in fact, without a change. Meanwhile, in spite of about twofold spectra reduction of the ISR (or  $P_t 56$ ), see Tables 4 and 7, it continues to be noticeable at the LHC energies<sup>12)</sup>.

## 4.2 $P_t^Z$ , $\eta^Z$ and $P_t^\mu$ dependence of rates.

In Table 8 we present the number of events calculated after passing selection cuts (4)–(12) for different  $P_t^Z$  and  $\eta^Z$  intervals (lines and columns of the table, respectively). The last column of this table contains the total number of events (at  $L_{int} = 10 \text{ fb}^{-1}$ ) at  $|\eta^Z| < 5.0$  for a given  $P_t^Z$  interval. We see that the number of events decreases fast with growing  $P_t^Z$  (but it decreases much slower as compared with decrease in  $P_t^\gamma$  spectrum in the case of “ $\gamma + jet$ ” events, see [12]). It also drops with growing  $|\eta^Z|$  starting from  $|\eta^Z| \approx 2.0$  and has weak dependence on  $\eta^Z$  in the interval  $|\eta^Z| < 2.0$ . The analogous information is illustrated by Fig. 5 for three  $P_t^Z$  intervals<sup>13)</sup>.

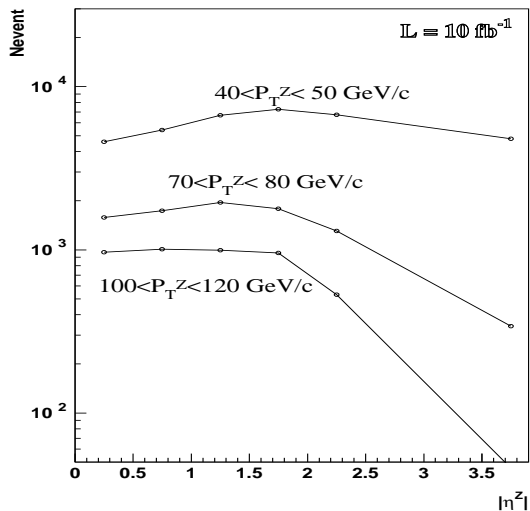


Fig. 5:  $\eta$ -dependence of rates for different  $P_t^Z$  intervals.

In Fig. 6 we have plotted a normalized distributions of the number of events over  $P_t$  of muons from  $Z^0$  decay for two  $P_t^Z$  intervals:  $40 < P_t^Z < 50$  and  $100 < P_t^Z < 120 \text{ GeV}/c$ . The muon spectra are limited by the condition (4)  $P_t^\mu > 10 \text{ GeV}/c$ . We also see that the spectra with muons having maximal  $P_t$  in the pair starts at  $20 \text{ GeV}/c$  for  $40 < P_t^Z < 50 \text{ GeV}/c$  and at  $50 \text{ GeV}/c$  for  $100 < P_t^Z < 120 \text{ GeV}/c$ . It explains our choice in (5) for  $P_{t,max}^\mu$  restriction.

<sup>11)</sup> An increase in  $P_t^Z$  produces the same effect, as is seen from Tables 3 and 5, and will be demonstrated in more detail in Section 6 and Appendices 2–5.

<sup>12)</sup> The analogous conclusion was done by studying “ $\gamma + jet$ ” events in [12].

<sup>13)</sup> We have limited  $Z^0$  pseudorapidity spectrum from above in Fig. 5 and Table 8 only to give understanding about its behavior inside this  $\eta^Z$  interval and, certainly, have not used those limits as cuts anywhere in this paper.

Table 8: Rates for  $L_{int} = 10 \text{ fb}^{-1}$  for different intervals of  $P_t^Z$  and  $\eta^Z$  ( $P_{tCUT}^{clust} = 10 \text{ GeV}/c$ ,  $P_{tCUT}^{out} = 10 \text{ GeV}/c$  and  $\Delta\phi \leq 15^\circ$ ).

$P_t^Z$ (GeV/c)	$ \Delta\eta^Z $ intervals						all $ \eta^Z $ 0.0-5.0
	0.0-0.5	0.5-1.0	1.0-1.5	1.5-2.0	2.0-2.5	2.5-5.0	
40 – 50	4594	5425	6673	7267	6732	4796	35486
50 – 60	3128	3509	4297	4570	3976	2000	21471
60 – 70	2253	2443	2855	2934	2229	851	13567
70 – 80	1580	1734	1948	1786	1307	341	8692
80 – 90	1152	1148	1267	1236	824	170	5790
90 – 100	741	859	812	808	523	59	3802
100 – 110	582	590	594	546	305	36	2657
110 – 120	384	428	451	412	226	8	1905
120 – 140	523	582	562	531	293	12	2503
140 – 170	392	380	368	341	190	4	1675
170 – 200	170	186	162	170	63	2	756
200 – 240	111	103	99	91	40	0	444
240 – 300	71	51	44	48	20	0	238

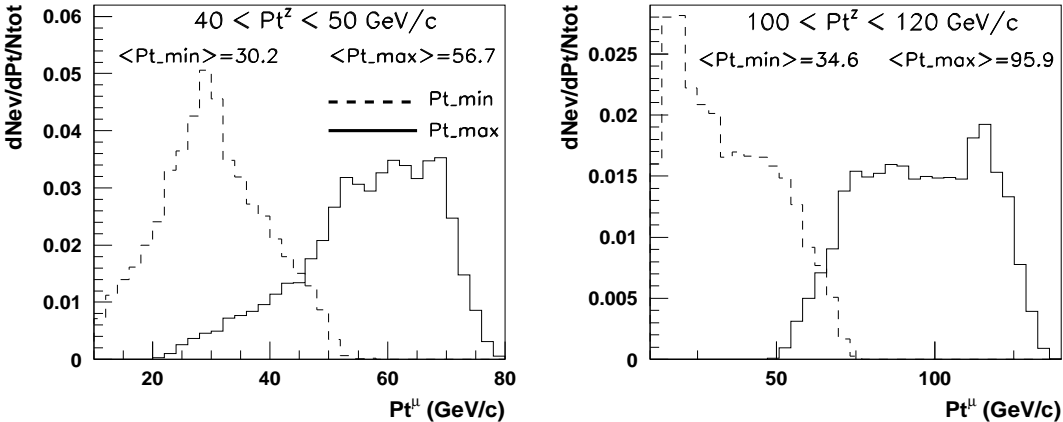


Figure 6: A normalized distributions of the number of events over  $P_t$  of muons from  $Z^0$  decay: for a muon with maximal  $P_t$  (full line) and for a muon with minimal  $P_t$  (dashed line) in the pair.

### 4.3 Estimation of “ $Z^0 + jet$ ” event rates for the HB, HE and HF regions.

Since a jet is a wide-spread object, we present the  $\eta^{jet}$  dependence of rates (for different  $P_t^Z$  intervals) in a different way. Namely, Tables 9–12 include the rates of events (at  $L_{int} = 10 \text{ fb}^{-1}$ ) for different  $\eta^{jet}$  intervals, covered by the Barrel, Endcap and Forward (HB, HE and HF) parts of the calorimeter. The events are selected after the cuts (4) – (12) (Selection 1) with the following values of the cut parameters:

$$\Delta\phi < 15^\circ, \quad P_{tCUT}^{clust} = 10 \text{ GeV}/c, \quad P_{tCUT}^{out} = 10 \text{ GeV}/c. \quad (23)$$

The first columns of these tables give the number of events with jets (found by the LUCCELL jetfinding algorithm of PYTHIA), all particles of which are comprised entirely (100%) in the Barrel part (HB) and there is a 0% sharing ( $\Delta P_t^{jet} = 0$ ) of  $P_t^{jet}$  between the HB and the neighboring HE part of the calorimeter. The second columns of the tables contain the number of events in which  $P_t$  of the jet is shared between the HB and HE regions. The same sequence of restriction conditions takes place in the next columns. Thus, the HE and HF columns include the number of events with jets entirely contained in these regions, while the HE+HF column gives the number of events where the jet covers both the HE and HF regions. From these tables we can see what number of events can, in principle, be suitable for the most precise jet energy calibration procedure, carried out separately for the HB, HE and HF parts of the calorimeter in different  $P_t^Z$  ( $\approx P_t^{jet}$ ) intervals. Less restrictive conditions, when up to 10%

of the jet  $P_t$  are allowed to be shared between the HB, HE and HF parts of the calorimeter, are given in Tables 10 and 12. Tables 9 and 10 correspond to the case of Selection 1. Tables 11 and 12 contain the number of events collected with the added Selection 2 restriction (with  $e^{jet} < 5\%$ ), i.e. they include only the events with “isolated jets” (defined in Section 2.2). The reduction factor of about 2 for the number of events can be found by comparing Tables 9 and 10 with Tables 11 and 12.

From the last summarizing line of Table 9 we see that for the whole interval  $40 < P_t^Z < 300 \text{ GeV}/c$  PYTHIA predicts about 45 000 events for HB, 16 000 events for HE and about 2 000 events for HF at  $L_{int}=10 \text{ fb}^{-1}$ .

Table 9: Selection 1.  $\Delta P_t^{jet}/P_t^{jet} = 0.00$  ( $L_{int}=10 \text{ fb}^{-1}$ ).

$P_t^Z$	HB	HB+HE	HE	HE+HF	HF
40 – 50	15072	11179	5417	3045	729
50 – 60	9076	7037	3231	1734	376
60 – 70	5813	4447	2055	1030	218
70 – 80	3726	2903	1275	669	123
80 – 90	2542	1901	847	432	67
90 – 100	1711	1243	558	246	44
100 – 110	1263	879	352	150	12
110 – 120	836	681	289	107	20
120 – 140	1085	836	400	154	8
140 – 170	752	626	218	71	8
170 – 200	348	261	103	44	0
200 – 240	206	139	75	20	0
240 – 300	111	95	28	4	0
40 – 300	44554	34076	15789	8510	2020

Table 10: Selection 1.  $\Delta P_t^{jet}/P_t^{jet} \leq 0.10$  ( $L_{int}=10 \text{ fb}^{-1}$ ).

$P_t^Z$	HB	HB+HE	HE	HE+HF	HF
40 – 50	19610	3251	10328	887	1366
50 – 60	12161	1667	6439	420	768
60 – 70	7797	950	4166	202	444
70 – 80	5077	570	2633	162	253
80 – 90	3453	372	1734	83	147
90 – 100	2261	242	1152	48	95
100 – 110	1683	170	729	32	40
110 – 120	1176	87	582	16	45
120 – 140	1465	139	816	36	43
140 – 170	1026	115	511	12	12
170 – 200	475	48	222	5	8
200 – 240	273	17	147	3	4
240 – 300	158	15	59	0	0
40 – 300	59392	8169	31395	2127	3861

An additional information on the numbers of “ $Z^0 + jet$ ” events with jets produced by  $c$  and  $b$  quarks (see also [12] and [42, 43]), given for the integrated luminosity  $L_{int} = 10 \text{ fb}^{-1}$  for different  $P_t^Z (\approx P_t^{Jet})$  intervals 45–55, 70–85, 100–120 and 150–200  $\text{GeV}/c$  is contained in Tables 1–12 of Appendix 1 (they denoted as  $N_{\text{event}}^{(c)}$  and  $N_{\text{event}}^{(b)}$  there). They also show the ratio of the number of events caused by gluonic Compton-like subprocess (2a) to the number of events due to the sum of subprocesses (2a) and (2b) ( $30\text{sub/all}$ ) and averaged jet radii  $\langle R_{gc}^{jet} \rangle$ .

Table 11: Selection 2.  $\Delta P_t^{jet} / P_t^{jet} = 0.00$  ( $L_{int}=10 \text{ fb}^{-1}$ ).

$P_t^Z$	HB	HB+HE	HE	HE+HF	HF
40 – 50	6039	4221	2364	1152	352
50 – 60	4578	3398	1810	847	182
60 – 70	3461	2637	1319	645	154
70 – 80	2542	2020	915	447	91
80 – 90	1936	1382	681	329	55
90 – 100	1390	962	475	190	36
100 – 110	1093	717	305	123	13
110 – 120	744	614	273	79	15
120 – 140	990	760	376	158	9
140 – 170	713	602	210	71	7
170 – 200	341	257	103	45	1
200 – 240	206	131	75	19	0
240 – 300	111	95	28	4	0
40 – 300	24912	18489	9393	4499	1169

Table 12: Selection 2.  $\Delta P_t^{jet} / P_t^{jet} \leq 0.10$  ( $L_{int}=10 \text{ fb}^{-1}$ ).

$P_t^Z$	HB	HB+HE	HE	HE+HF	HF
40 – 50	7770	1148	4297	309	602
50 – 60	6083	729	3425	190	384
60 – 70	4629	554	2602	119	305
70 – 80	3465	388	1885	99	178
80 – 90	2610	249	1350	59	115
90 – 100	1806	190	950	37	79
100 – 110	1434	139	610	23	36
110 – 120	1057	85	635	31	40
120 – 140	1338	117	656	21	37
140 – 170	974	111	491	12	11
170 – 200	467	48	218	4	9
200 – 240	273	18	143	4	3
240 – 300	158	14	59	0	0
40 – 300	33117	3952	18224	990	2174

## 5 Features of “ $Z^0 + jet$ ” events in the Barrel region.

### 5.1 Influence of the $P_{t\text{cut}}^{\text{clust}}$ parameter on the balance between $Z^0$ and jet transverse momenta and on the initial state radiation suppression.

Here we shall study a correlation of  $P_t^{\text{clust}}$  with  $P_t^{\text{ISR}}$ . The samples of 1-jet “ $Z^0 + jet$ ” events, gained from the PYTHIA simulation of  $5 \cdot 10^6$  signal “ $Z^0 + jet$ ” events in two  $P_t^Z$  intervals  $45 - 55$  and  $100 - 120 \text{ GeV}/c$ , will be used here. The observables defined in Section 2 will be restricted here by Selection 1 cuts (4) – (12) of Section 2.2 with  $P_{t\text{CUT}}^{\text{clust}} = 30 \text{ GeV}/c$ .  $P_{t\text{CUT}}^{\text{out}}$  is not limited here.

The influence of the  $P_{t\text{CUT}}^{\text{clust}}$  variation on the distribution of some important physical variables is shown in Fig. 7 for  $45 < P_t^Z < 55 \text{ GeV}/c$  and in Fig. 8 for  $100 < P_t^Z < 120 \text{ GeV}/c$ . Besides of distributions for three auxiliary variables  $P_t^{\text{56}}$ ,  $P_t^{\eta>5}$ ,  $P_t^{\text{out}}$  (defined by (2), (16), (18)) we present distributions for  $P_t(O+\eta > 5)$  and  $(1-\cos\Delta\phi)$  which define the right-hand side of equation (21). The distribution of the back-to-back  $\Delta\phi$  angle (10), defining the second variable  $(1-\cos\Delta\phi)$ , is also presented in Figs. 7, 8.

The  $P_t^{\text{56}}$  variable and both components defining  $P_t^Z$  and  $P_t^{\text{jet}}$  disbalance,  $(1 - \cos\Delta\phi)$  and  $P_t(O+\eta > 5)$ , as well as two others variables,  $P_t^{\text{out}}$  and  $\Delta\phi$ , show a tendency to become smaller (as the mean values as the widths of distributions) by restricting an upper limit on the  $P_t^{\text{clust}}$  value (see also tables of Appendices 2–5). It means that the precision of jet energy setting may increase with decreasing  $P_{t\text{CUT}}^{\text{clust}}$ . The origin of this improvement becomes clear from the  $P_t^{\text{56}}$  density plot which demonstrates ISR suppression (or  $P_t^{\text{ISR}}$ ) as a more restrictive cut is imposed on  $P_t^{\text{clust}}$ .

Comparison of Fig. 7 (for  $45 < P_t^Z < 55 \text{ GeV}/c$ ) and Fig. 8 (for  $100 < P_t^Z < 120 \text{ GeV}/c$ ) shows that  $\Delta\phi$  as a degree of back-to-backness of  $Z^0$  boson and jet  $P_t$  vectors in the  $\phi$ -plane decreases with increasing  $P_t^Z$ . At the same time  $P_t^{\text{ISR}}$  distribution becomes wider, while the  $P_t^{\eta>5}$  and  $P_t^{\text{out}}$  distributions practically do not depend on  $P_t^Z$  (see for details Appendices 2–5).

It should be mentioned that the results presented in Figs. 7 and 8 were obtained with the LUCELL jetfinder of PYTHIA <sup>14)</sup>.

### 5.2 $P_t$ distribution inside and outside of a jet.

Now let us see how the space outside the jet may be populated by  $P_t$  in the “ $Z^0 + jet$ ” HB events. For this purpose we calculate a vector sum  $\vec{P}_t^{\text{sum}}$  of individual transverse momenta of the calorimeter cells included by a jetfinder into a jet and of cells in a larger volume that surrounds a jet. In the latter case this procedure can be viewed as straightforward enlarging of the jet radius in the  $\eta - \phi$  space.

The plots that present the ratio  $P_t^{\text{sum}}/P_t^Z$  as a function of the distance  $R(\eta, \phi)$  counted from a jet gravity center towards its boundary and further into the space outside a jet are shown in the left-hand columns of Figs. 9 and 10 for two  $P_t^Z$  intervals ( $45 < P_t^Z < 55 \text{ GeV}/c$  and  $100 < P_t^Z < 120 \text{ GeV}/c$ ) and three jetfinding algorithms (UA1, UA2 and LUCELL).

From these figures we see that the space surrounding the jet is in general far from being empty. We also see that the average value of  $P_t^{\text{sum}}$  increases with increasing volume around a jet and it exceeds  $P_t^Z$  at  $R = 0.7 - 0.8$  (see Figs. 9 and 10).

From the right-hand columns of Figs. 11 and 12 we see that the vector disbalance measure

$$P_t^{Z+\text{sum}} = |\vec{P}_t^Z + \vec{P}_t^{\text{sum}}| \quad (24)$$

achieves its minimum again at  $R \approx 0.7 - 0.8$  for all jetfinding algorithms. (The minimum of the vector sum  $P_t^{Z+\text{sum}}$  can serve as an illustration of the  $P_t^Z - P_t^{\text{jet}}$  disbalance minimum.)

The value of  $P_t^{Z+\text{sum}}$  (as well as  $P_t^{\text{sum}}/P_t^Z$ ) continues to grow rapidly for  $40 < P_t^Z < 50 \text{ GeV}/c$  and more slowly for  $100 < P_t^Z < 120 \text{ GeV}/c$  with increasing  $R$  after the point  $R = 0.7 - 0.8$  (see Figs. 9 and 10). This means that at higher  $P_t^Z$  (or  $P_t^{\text{jet}}$ ) the topology of “ $Z^0 + jet$ ” events becomes more distinct and we get a clearer picture of an “isolated” jet. This feature clarifies the motivation of introducing the “Selection 2” criteria in Section 2.2 for selection of events with isolated jets.

---

<sup>14)</sup> The results obtained with all jetfinders and  $P_t^Z$  and  $P_t^{\text{jet}}$  balance will be discussed in Sections 7 in more detail.

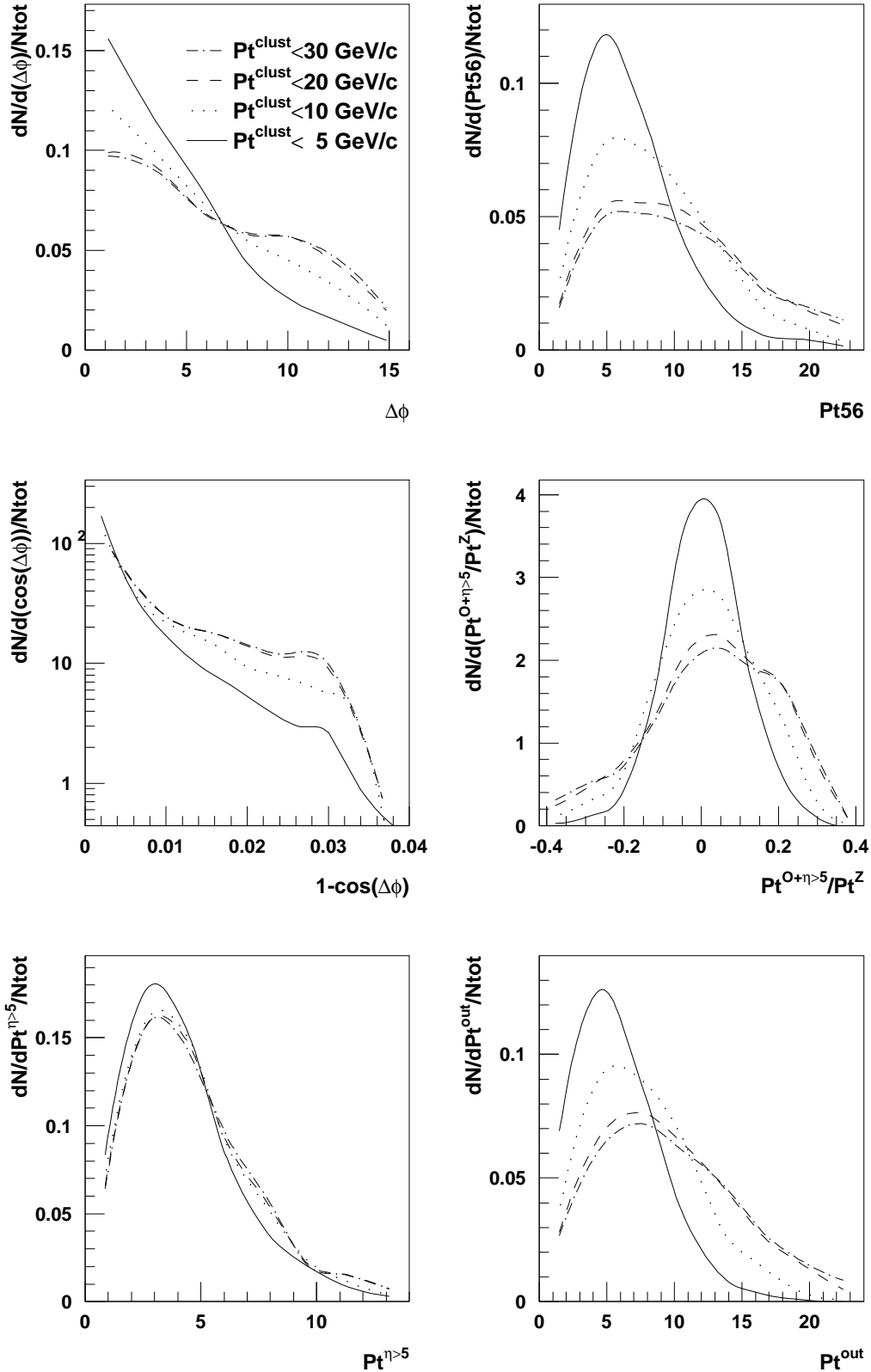


Figure 7: LUCELL algorithm,  $\Delta\phi < 15^\circ$ ,  $45 < Pt^Z < 55 \text{ GeV}/c$ . Selection 1.

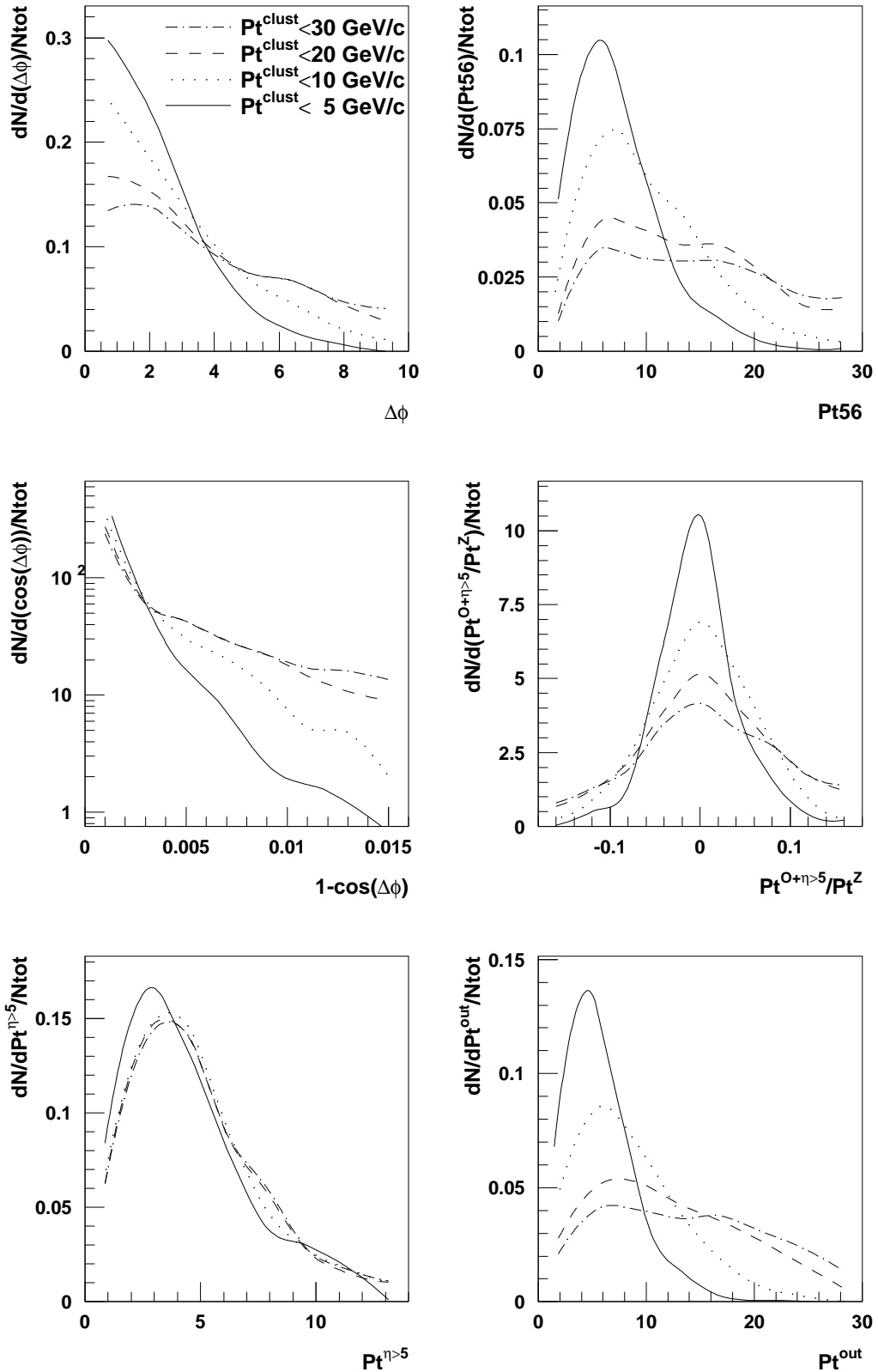


Figure 8: LUCELL algorithm,  $\Delta\phi < 15^\circ$ ,  $100 < P_t^Z < 120 \text{ GeV}/c$ . Selection 1.

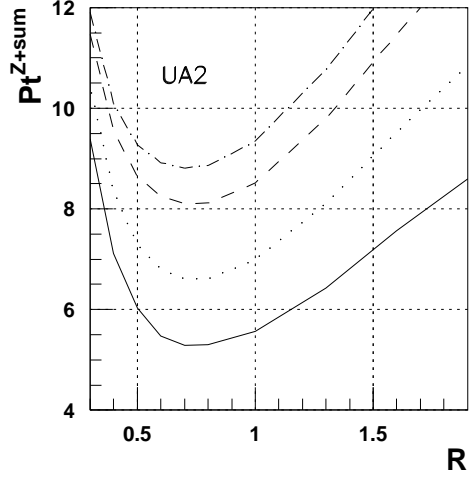
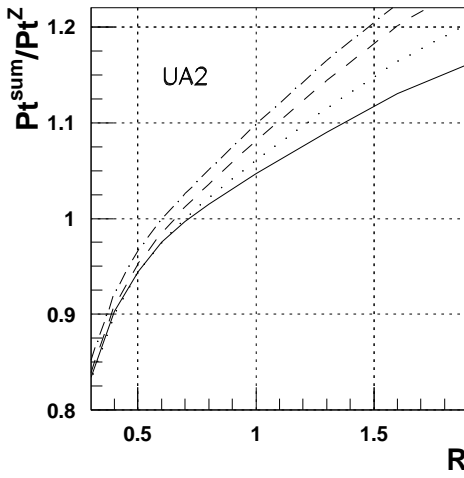
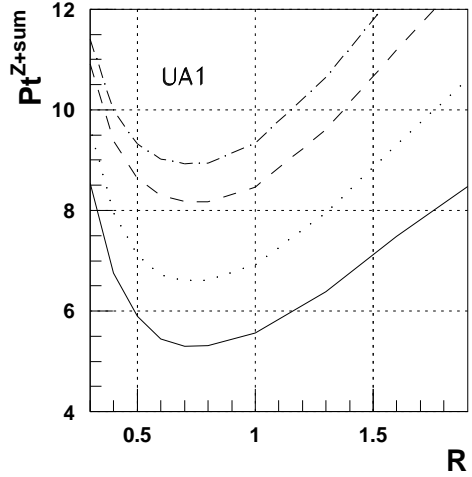
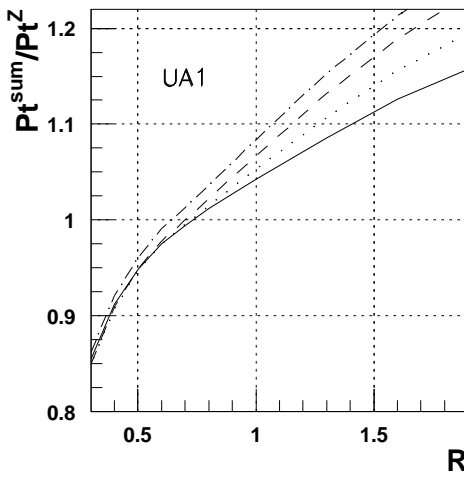
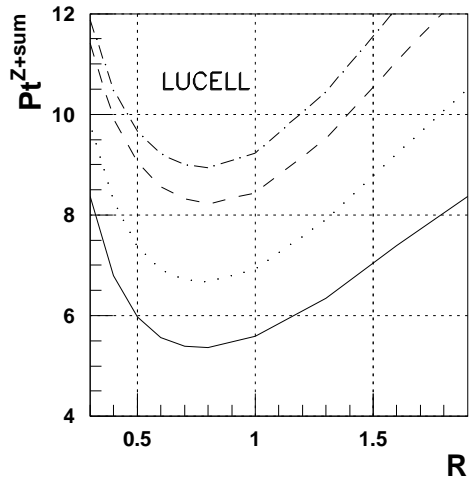
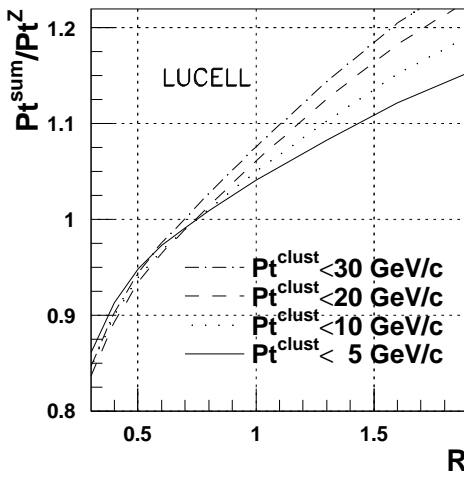


Figure 9: LUCCELL, UA1 and UA2 algorithms,  $\Delta\phi < 15^\circ$ ,  $45 < Pt^Z < 55 \text{ GeV}/c$ .

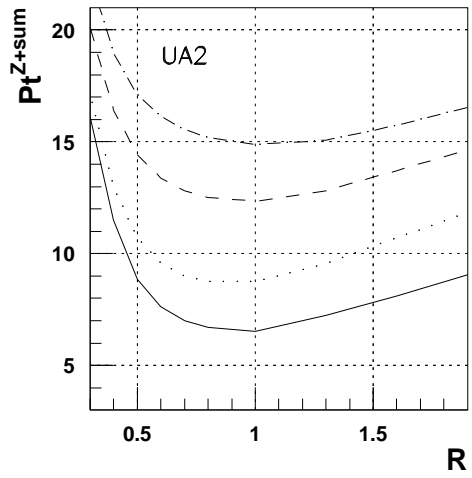
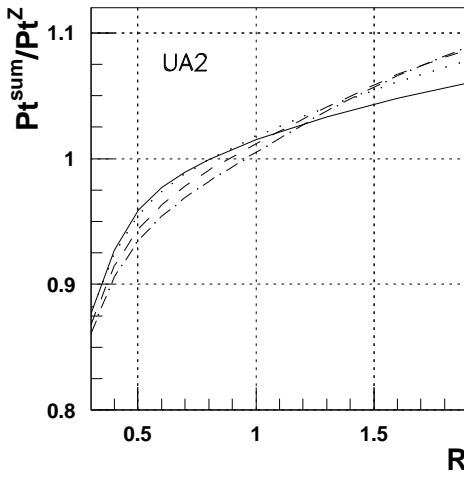
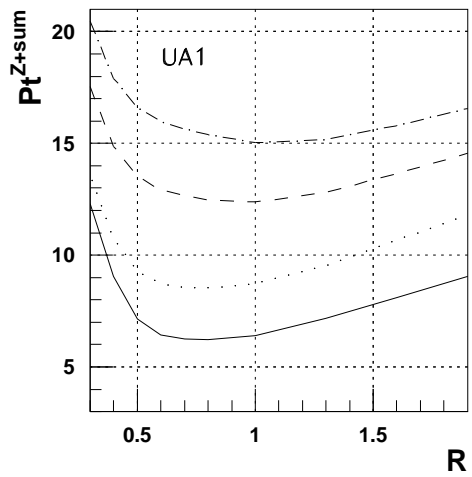
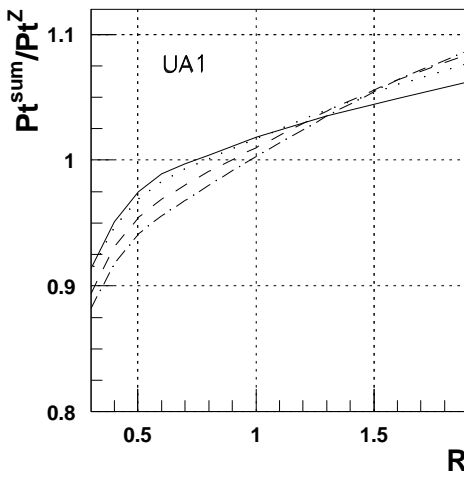
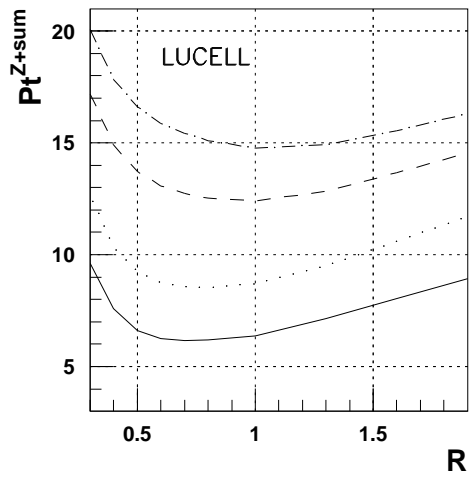
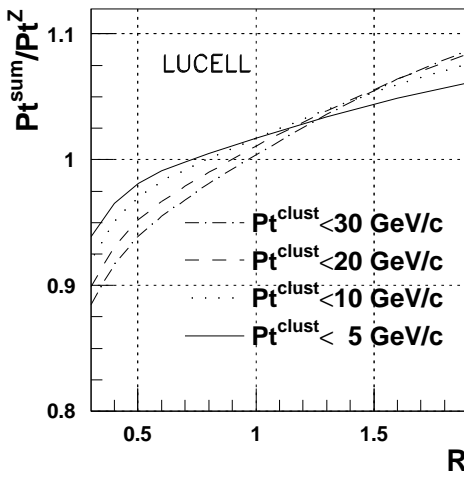


Figure 10: LUCELL, UA1 and UA2 algorithms,  $\Delta\phi < 15^\circ$ ,  $100 < Pt^Z < 120 \text{ GeV}/c$ .

## 6 Dependence of the disbalance between $P_t^Z$ and $P_t^{Jet}$ on the $P_{tCUT}^{clust}$ and $P_{tCUT}^{out}$ parameters.

Here we shall study in detail a dependence of the  $P_t^Z - P_t^{Jet}$  disbalance on the values of  $P_{tCUT}^{clust}$  and  $P_{tCUT}^{out}$ . For this aim the four samples of “ $Z^0 + jet$ ” events described in the beginning of Section 4 were used.

The mean values of the most important variables used in our analyses that reflect the main features of “ $Z^0 + jet$ ” events with the jet completely contained in the Barrel region, i.e. “HB events” (see Section 5) are given in the tables of Appendices 2–5.

Appendix 2 contains the tables for events inside  $45 < P_t^Z < 55 \text{ GeV}/c$  interval. In these tables we present the values of interest found with UA1, UA2 and LUCELL jetfinders for three different Selections mentioned in Section 2.2. Each page corresponds to a definite value of  $\Delta\phi$  as a measure of deviation from the absolute back-to-back orientation of  $\vec{P}_t^Z$  and  $\vec{P}_t^{Jet}$  vectors. The first four pages of each Appendix contain the information about variables that characterize the  $P_t^Z - P_t^{Jet}$  balance for events passed the cuts (4)–(12) (Selection 1).

On the fifth page of each of Appendices 2–5 we present Tables 13 – 15 (for the cut  $\Delta\phi < 15^\circ$ ) that correspond to Selection 2 (see Section 2.2). We have limited  $\epsilon^{jet} \leq 9\%$  for  $45 < P_t^Z < 55$  with a gradual change to  $\epsilon^{jet} \leq 3\%$  for  $P_t^Z \geq 100 \text{ GeV}/c$ . The best result for UA2 in the case of  $45 < P_t^Z < 55$  is obtained with  $\epsilon^{jet} \leq 6\%$  instead of the cut  $\epsilon^{jet} \leq 9\%$  chosen for UA1 and LUCELL algorithms <sup>15)</sup>. The results obtained with Selection 3 are given on the sixth page of Appendices 2–5 <sup>16)</sup>, while on the seventh page Selection 3 is used to find jets found simultaneously by UA1 and LUCELL jetfinders only.

The columns in tables of Appendices 2–5 correspond to five values of  $P_{tCUT}^{clust} = 30, 20, 15, 10$  and  $5 \text{ GeV}/c$ . The upper lines of these tables contain the expected numbers  $N_{event}$  of “HB events” for the integrated luminosity  $L_{int} = 10 \text{ fb}^{-1}$ .

In the next four lines of the tables we put the values of  $P_{t56}$ ,  $\Delta\phi$ ,  $P_t^{out}$ ,  $P_t^{\eta>5}$  defined by formulas (2), (9), (18) and (16), respectively, and averaged over the events selected with a chosen  $P_{tCUT}^{clust}$  value. From the tables we see, firstly, that the averaged values of  $P_t^{\eta>5}$  show very weak dependence on it (practically constant) <sup>17)</sup>, what is in complete agreement with behavior of these variables in the case of “ $\gamma + jet$ ” events [14]. At the same time, the values of  $P_{t56}$ ,  $\Delta\phi$ ,  $P_t^{out}$  decrease fast with decreasing  $P_{tCUT}^{clust}$ . The  $P_{t56}$  variable (non-observable one) that serves, according to (2), as measure of the initial state radiation transverse momentum  $P_t^{ISR}$ , i.e. one of the main source of the  $P_t$  disbalance in the subprocesses (2a) and (2b). So, variation of  $P_{tCUT}^{clust}$  from 30 to 10  $\text{GeV}/c$  for  $\Delta\phi < 15^\circ$  leads to suppression of the  $P_{t56}$  value (or  $P_t^{ISR}$ ) approximately by  $\approx 40 - 45\%$  for all  $P_t^Z$ .

The following three lines (from 6-th to 8-th) show the average values of the variables  $(P_t^Z - P_t^{part})/P_t^Z$ ,  $(P_t^J - P_t^{part})/P_t^J$ ,  $(P_t^Z - P_t^J)/P_t^Z$  (here  $J \equiv \text{Jet}$ ). These lines correspond to the relative  $P_t$  balance at the  $Z^0$ -parton level (final state of the fundamental subprocess  $2 \rightarrow 2$ ), the relative difference of the parton  $P_t$  and the jet  $P_t$  (parton hadronization effect) and the relative  $P_t$  balance of the jet and  $Z^0$  boson.

The lines 9 and 10 include the averaged values of  $P_t(O + \eta > 5)/P_t^Z$  and  $(1 - \cos(\Delta\phi))$  that appear on the right-hand side of the  $P_t$ -balance equation (21).

As a rule, the value of  $\langle 1 - \cos(\Delta\phi) \rangle$  is smaller than the value of  $\langle P_t(O + \eta > 5)/P_t^Z \rangle$  for the cut  $\Delta\phi < 15^\circ$  and tends to decrease more with growing energy. So, we can conclude that the main source of the  $P_t$  disbalance in the “ $Z^0 + jet$ ” system is defined by the term  $P_t(O + \eta > 5)/P_t^Z$ .

The following line contains the averaged values of the standard deviations of  $(P_t^Z - P_t^J)/P_t^Z (\equiv Db[Z, J])$ . The values of this variable drop approximately by a factor of two (and even more for all intervals with  $P_t^Z > 100 \text{ GeV}/c$ ) while moving from  $P_{tCUT}^{clust} = 30 \text{ GeV}/c$  to  $P_{tCUT}^{clust} = 5 \text{ GeV}/c$  for all jetfinding algorithms.

The last lines of the tables present the number of generated events, i.e. entries left after cuts.

A decrease in  $P_{tCUT}^{clust}$  leads to a decrease in the  $(P_t^Z - P_t^J)/P_t^Z$  ratio (mean values as well as standard deviations), i.e. we select the events that can be used to improve the jet energy calibration accuracy. For instance, in the case

<sup>15)</sup> In [12] – [16] the Selection 2 criterion was considered with a more severe cut  $\epsilon^{jet} \leq 2\%$ .

<sup>16)</sup> Selection 3 (see Section 2.2) leaves only those events in which jets are found simultaneously by UA1, UA2 and LUCELL jetfinders i.e. events with jets having up to a good accuracy equal coordinates of the center of gravity,  $P_t^{jet}$  and  $\phi_{(Z,jet)}$ .

<sup>17)</sup> Compare with Figs. 7 and 8.

of  $70 < P_t^Z < 85 \text{ GeV}/c$  the mean value of  $(P_t^Z - P_t^J)/P_t^Z$  drops from  $4.5 - 4.9\%$  to  $0.9 - 1.5\%$  (see Tables 4, 6 of Appendix 3) and in the case of  $100 < P_t^Z < 120 \text{ GeV}/c$  the mean value of this variable drops from  $3.4 - 3.7\%$  to less than  $0.6 - 1.0\%$  for UA1 and LUCELL jetfinders (Tables 4, 6 of Appendix 4). A worse situation is seen for the  $45 < P_t^Z < 55 \text{ GeV}/c$  interval, where the disbalance changes, e.g. for LUCELL algorithm, as  $2.1 \rightarrow 1.8\%$ . Meantime, RMS values with the same variations of  $P_{tCUT}^{clust}$  (from 30 to 10  $\text{GeV}/c$ ) decrease by  $40 - 50\%$ .

After imposing the jet isolation requirement (see Tables 13 – 15 of Appendices 2–5) we observe that for  $P_t^Z \geq 100 \text{ GeV}/c$  the mean values of  $(P_t^Z - P_t^J)/P_t^Z$  are contained inside the 1% window for any  $P_{tCUT}^{clust}$ . For  $45 < P_t^Z < 55 \text{ GeV}/c$  we see that with Selection 1  $P_{tCUT}^{clust}$  works more effectively than in the case of Selection 1. Thus,  $P_{tCUT}^{clust} = 15 \text{ GeV}/c$  allows to reduce  $(P_t^Z - P_t^J)/P_t^Z$  to less than 1% level for all algorithms. The Selection 2 criterion leaves quite a sufficient number of events with a jet contained completely in the barrel region: about 10 000 – 18 000<sup>18)</sup> for  $45 < P_t^Z < 55 \text{ GeV}/c$  with  $P_{tCUT}^{clust} = 15 \text{ GeV}/c$  and about 4 500 for  $100 < P_t^Z < 120 \text{ GeV}/c$  with  $P_{tCUT}^{clust} = 20 \text{ GeV}/c$  at  $L_{int} = 10 \text{ fb}^{-1}$  (see Tables 13 – 15 of Appendices 2, 3).

The analogous results for Selection 3 are presented in Tables 16–18 of Appendices 2–5. Let us consider first the most difficult interval  $45 < P_t^Z < 55 \text{ GeV}/c$ . From the tables of Appendix 2 one can see that this selection leads to approximately 20% reduction of the number of selected events as compared with the case of Selection 2. A combined usage of all three jetfinders (Tables 16–18) worsen the balance values. A requirement of simultaneous jet finding by only UA1 and LUCELL algorithms practically does not change values of the  $P_t^Z - P_t^{jet}$  balance and other variables, presented in Tables 19, 20, as compared with the case of Selection 2 and gives a better result (from point of view of the  $P_t^Z - P_t^{jet}$  balance values as well as from point of view of the number of selected events) as compared with the case of combined usage of all three jetfinders for this aim. This fact stresses a good compatibility of UA1 and LUCELL jetfinders. For other considered  $P_t^Z$  intervals UA1, UA2 and LUCELL algorithms give more or less close results and a passage to Selection 3 does not worsen a situation.

We also can note that Selections 2 and 3, besides improving the  $P_t^Z$  and  $P_t^{jet}$  balance value, are important for selecting events with a clean jet topology and rising the confidence level of a jet determination.

The influence of a wide variation of cuts  $P_{tCUT}^{clust}$  and  $P_{tCUT}^{out}$  on

- (a) the number of selected events (for  $L_{int} = 10 \text{ fb}^{-1}$ ),
- (b) the mean value of  $F \equiv (P_t^Z - P_t^{jet})/P_t^Z$  and
- (c) the standard deviation value  $\sigma(F)$

is presented in rows and columns of Tables 1–9 for Selection 1 of Appendix 6. The set of selection cuts (4)–(10) (Section 2.2) was applied to preselect “ $Z^0 + jet$ ” events for the tables of Appendix 6. The jets (as well as clusters) in these events, unlike the jets in the events analyzed in Appendices 2–5, were found by LUCELL jetfinder for the whole  $\eta$  region  $|\eta^{jet}| < 5.0$ .

Tables 1–3 of Appendix 6 correspond to the “ $Z^0 + jet$ ” events selection in the interval  $40 \leq P_t^Z \leq 70 \text{ GeV}/c$  Tables 4–6 to that for  $70 \leq P_t^Z \leq 100 \text{ GeV}/c$  and Tables 7–9 to that for  $100 \leq P_t^Z \leq 140 \text{ GeV}/c$ .

We see that the restriction of  $P_{tCUT}^{clust}$  and  $P_{tCUT}^{out}$  are necessary to improve the jet energy setting accuracy. So, Tables 2 (for  $40 \leq P_t^Z \leq 70 \text{ GeV}/c$ ) and 8 (for  $100 \leq P_t^Z \leq 140 \text{ GeV}/c$ ) of Appendix 6 show that the mean values of the fraction  $F \equiv (P_t^Z - P_t^{jet})/P_t^Z$  decreases with variation of the two cuts from  $P_{tCUT}^{clust} = 30 \text{ GeV}/c$  and  $P_{tCUT}^{out} = 1000 \text{ GeV}/c$  (i.e. without limits) to  $P_{tCUT}^{clust} = 10 \text{ GeV}/c$  and  $P_{tCUT}^{out} = 10 \text{ GeV}/c$  as 0.049 to 0.018 and as 0.036 to 0.012, respectively. At the same time this restriction noticeably decreases the width of the Gaussian  $\sigma(F)$  (see Tables 3, 6 and 9 of Appendix 6). So, it drops from 0.200 to 0.103 for  $40 \leq P_t^Z \leq 70 \text{ GeV}/c$  and from 0.138 to 0.066 for  $100 \leq P_t^Z \leq 140 \text{ GeV}/c$  (i.e. about in a factor of two) for the same variation of  $P_{tCUT}^{clust}$  and  $P_{tCUT}^{out}$ .

Again, the reason is caused by the term  $P_t(O + \eta > 5)/P_t^Z$  of the  $P_t$ -balance equation (19) (as we noted above, the contribution of  $(1 - \cos\Delta\phi)$  to the  $P_t^Z - P_t^{jet}$  disbalance is negligibly small). This term can be decreased by decreasing  $P_t$  activity in the space *out* of the “ $Z^0 + jet$ ” system, i.e. by limiting  $P_{tCUT}^{clust}$  and  $P_{tCUT}^{out}$ .

The numbers of events at the integrated luminosity  $L_{int} = 10 \text{ fb}^{-1}$  for different  $P_{tCUT}^{clust}$  and  $P_{tCUT}^{out}$  are given in Tables 1, 5 and 9 of Appendix 6. One can see that even with such strict  $P_{tCUT}^{clust}$  and  $P_{tCUT}^{out}$  values as 10  $\text{GeV}/c$  for both, for example, we would have 69 600, 18 100 and 6 860 for  $40 \leq P_t^Z \leq 70 \text{ GeV}/c$ ,  $70 \leq P_t^Z \leq 100 \text{ GeV}/c$  and  $100 \leq P_t^Z \leq 140 \text{ GeV}/c$  respectively.

In addition, we present in Tables 10–18 of Appendix 6 the results obtained with Selection 2. They contain the

<sup>18)</sup> the lower value corresponds to UA2 algorithm for which the stricter jet isolation cut was used

information analogous to that in Tables 1–12 but for the case of imposing jet isolation requirement:  $\epsilon^{jet} = 8\%$  at  $40 \leq P_t^Z \leq 70 \text{ GeV}/c$  and  $\epsilon^{jet} = 5\%$  at  $70 \leq P_t^Z \leq 100 \text{ GeV}/c$  and  $100 \leq P_t^Z \leq 140 \text{ GeV}/c$ . From these tables we see that with the same (and with even weaker) cuts  $P_{tCUT}^{clust} = P_{tCUT}^{out} = 10 \text{ GeV}/c$  one can obtain a much better fractional balance  $F$ , less than 1% for all  $P_t^Z$  intervals (with almost the same values of  $\sigma(F)$ ), at the statistics of about 50 800, 13 200 and 6 150 events for intervals  $40 \leq P_t^Z \leq 70 \text{ GeV}/c$ ,  $70 \leq P_t^Z \leq 100 \text{ GeV}/c$  and  $100 \leq P_t^Z \leq 140 \text{ GeV}/c$ , respectively.

The behavior of number of the selected events for  $L_{int} = 10 \text{ fb}^{-1}$ , the mean values of  $(P_t^Z - P_t^{jet})/P_t^Z$  and its standard deviation  $\sigma(F)$  as a function of  $P_{tCUT}^{out}$  for  $P_{tCUT}^{clust} = 20 \text{ GeV}/c$  is displayed in Fig. 11 for non-isolated (left-hand column) and isolated jets with  $\epsilon^{jet} = 8\%$  at  $40 \leq P_t^Z \leq 70 \text{ GeV}/c$  and  $\epsilon^{jet} = 5\%$  at  $70 \leq P_t^Z \leq 100 \text{ GeV}/c$  and  $100 \leq P_t^Z \leq 140 \text{ GeV}/c$  (right-hand column).

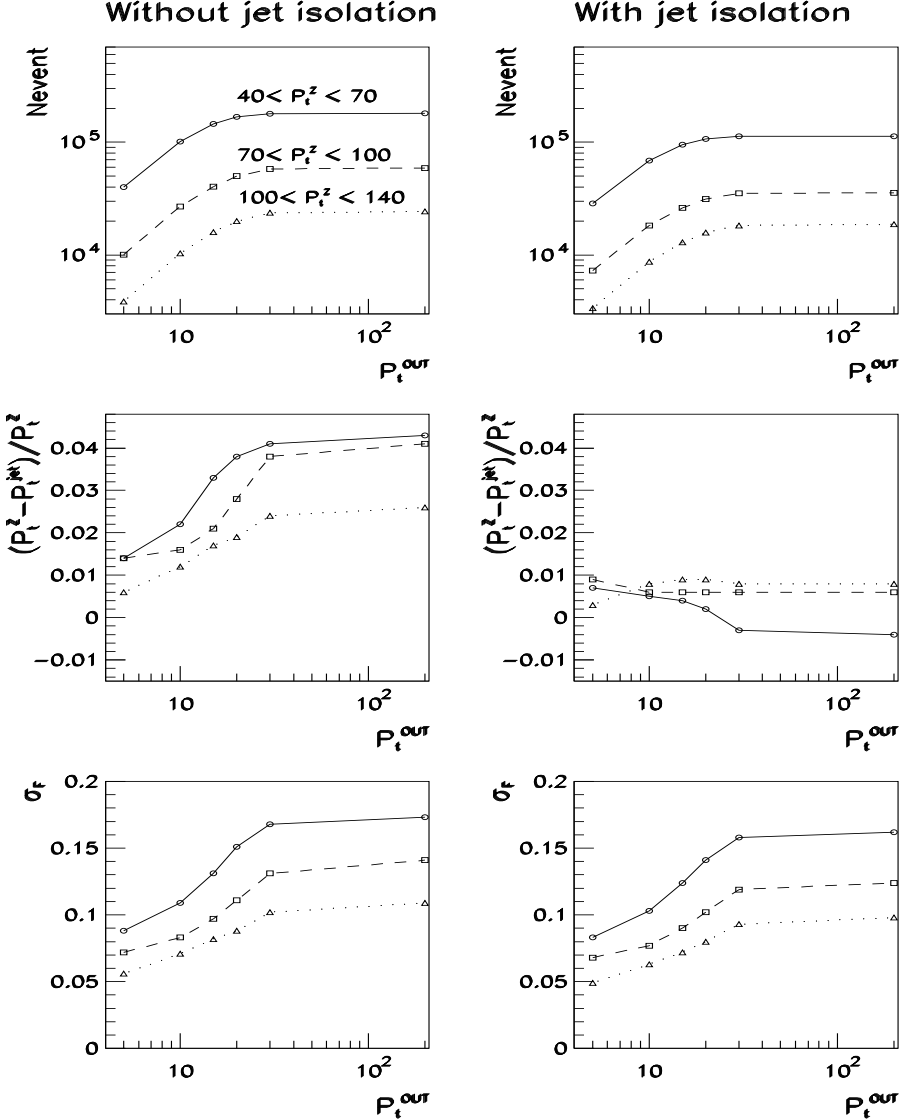


Figure 11: Number of events at  $L_{int} = 10 \text{ fb}^{-1}$ , mean value  $(P_t^Z - P_t^{jet})/P_t^Z (\equiv F)$ , its standard deviation  $\sigma_F$  as a function of  $P_{tCUT}^{out}$  value.  $P_{tCUT}^{clust}$  value is limited by  $20 \text{ GeV}/c$ . Full line corresponds to the event selection with  $40 \leq P_t^Z \leq 70 \text{ GeV}/c$ , dashed line to that with  $70 \leq P_t^Z \leq 100 \text{ GeV}/c$  and dotted line to that with  $100 \leq P_t^Z \leq 140 \text{ GeV}/c$  ( $\epsilon^{jet} = 8\%, 5\%, 5\%$  in these  $P_t^Z$  intervals, respectively).

## 7 The study of background suppression.

In principle, there is a probability, that some combination of muons in the events, based on the QCD subprocesses with much larger cross sections (by about 5 orders of magnitude) than ones of the signal subprocesses, can be registered as the  $Z^0$  signal. This type of background we call as “combinatorial background”. To study a rejection possibility of such type of events by about 40 million events with a mixture of all QCD and SM subprocesses with large cross sections existing in PYTHIA<sup>19)</sup> including also the signal subprocesses (2a) and (2b) were generated. Three generations were performed with different minimal  $P_t$  of the hard  $2 \rightarrow 2$  subprocess<sup>20)</sup>  $\hat{p}_\perp^{min}$  values:  $\hat{p}_\perp^{min}=40, 70 and }100\text{ GeV}/c$ . The cross sections of different subprocesses serve in simulation as weight factors and, thus, determine the final statistics of the corresponding physical events. The generated events were analyzed by use of the cuts given in Table 13 (see also Section 2.2).

Table 13: List of the applied cuts used in Tables 14, 15.

- 
- 0. Total number of  $\mu^+\mu^-$  pairs (No selection);
  - 1.  $P_t^\mu > 10 \text{ GeV}/c, |\eta^\mu| < 2.4$ ;
  - 2.  $|M_Z - M_{inv}^{ll}| < 20 \text{ GeV}/c^2$ ;
  - 3. 1 jet events selected;
  - 4.  $P_t^{isol}/P_t^\mu \leq 0.10, P_t^{ch} < 2 \text{ GeV}/c$ ;
  - 5.  $|M_Z - M_{inv}^{ll}| < 5 \text{ GeV}/c^2$ ;
  - 6.  $\Delta\phi < 15^\circ$ .
- 

To trace the effect of their application let us consider first the case of one (intermediate) energy, i.e. the generation with  $\hat{p}_\perp^{min}=70 \text{ GeV}/c$ . Each line of Table 14 corresponds to the respective cut of Table 13. The numbers in columns “Signal” and “Bkgd” show the number of signal and (combinatorial) background events remained after a cut. Column “ $Eff_{S(B)}$ ” demonstrates the efficiency of a cut. The efficiencies  $Eff_{S(B)}$  (with their errors) are defined as a ratio of the number of signal (background) events that passed under a cut (1–6) to the number of the preselected events after the first cut of Table 13 (The number of events after the first cuts is taken as 100%).

Table 14: A demonstration of cut-by-cut efficiencies and  $S/B$  ratios for generation with  $\hat{p}_\perp^{min}=70 \text{ GeV}/c$ .

Selection	Signal	Bkgd	$Eff_S(\%)$	$Eff_B(\%)$	$S/B$
0	401	850821			$5 \cdot 10^{-4}$
1	245	15842	$100.00 \pm 0.00$	$100.00 \pm 0.000$	0.02
2	226	467	$92.24 \pm 8.51$	$2.948 \pm 0.138$	0.5
3	99	12	$40.41 \pm 4.81$	$0.076 \pm 0.022$	8.3
4	81	10	$33.00 \pm 4.24$	$0.063 \pm 0.020$	8.1
5	72	4	$29.39 \pm 3.94$	$0.025 \pm 0.013$	18.0
6	62	0	$25.31 \pm 3.60$	$0.000 \pm 0.000$	–

Table 15: Values of efficiencies and  $S/B$  ratios for generations with  $\hat{p}_\perp^{min}=40, 70$  and  $100 \text{ GeV}/c$ .

$\hat{p}_\perp^{min}$	Cuts	Signal	Bkgd	$Eff_S(\%)$	$Eff_B(\%)$	$S/B$
$(GeV/c)$	Preselection (1)	89	1090	$100.00 \pm 0.00$	$100.00 \pm 0.00$	0.08
	Main (1 – 5)	30	0	$33.71 \pm 7.12$	$0.00 \pm 0.00$	–
$(GeV/c)$	Preselection (1)	245	15842	$100.00 \pm 0.00$	$100.00 \pm 0.00$	0.02
	Main (1 – 5)	72	4	$29.39 \pm 3.94$	$0.025 \pm 0.013$	18.0
$(GeV/c)$	Preselection (1)	497	37118	$100.00 \pm 0.00$	$100.00 \pm 0.00$	0.01
	Main (1 – 5)	127	4	$25.55 \pm 2.54$	$0.011 \pm 0.005$	31.8

We see from Table 14 that initial ratio of  $\mu^+\mu^-$  pairs in signal and background events is very small ( $5 \cdot 10^{-4}$ )<sup>21)</sup>. A weak restriction of the muon transverse momentum and pseudorapidity in the 1st selection increase  $S/B$  by

<sup>19)</sup> (namely, ISUB=11–20, 28–31, 53, 68)

<sup>20)</sup> i.e CKIN(3) parameter in PYTHIA

about 2 order (as  $5 \cdot 10^{-4} \rightarrow 2 \cdot 10^{-2}$ ). The invariant mass criterion and one-jet events selection make  $S/B = 18.0$  and the last criterion on the azimuthal angle between  $Z^0$  and jet ( $\Delta\phi < 15^\circ$ ) suppresses the background events completely.

The information on other intervals (i.e. on the event generations with  $\hat{p}_\perp^{min} = 40$  and  $\hat{p}_\perp^{min} = 100 \text{ GeV}/c$ ) is presented in Table 15. Line “Preselection (1)” corresponds to the first cuts in Table 13 ( $P_t^\mu > 10 \text{ GeV}/c$ ,  $|\eta^\mu| < 2.4$ ) while line “Main (1–5)” corresponds to the result of application of criteria from 1 to 5 of Table 13. *After application of all six criteria of Table 13 we have observed no background events in all of the  $P_t^Z$  intervals with the signal events selection efficiency of 25–33%.*

The practical absence of a background to the “ $Z^0 + \text{jet}$ ” events allow to use them for an extraction of the gluon distribution in a proton  $f_p^g(x, Q^2)$ .

## 8 Estimation of rates for gluon distribution determination at the LHC using “ $Z^0 + \text{jet}$ ” events.

Many theoretical predictions for production of new particles (Higgs, SUSY) at the LHC are based on model estimations of the gluon density behavior at low  $x$  and high  $Q^2$ . Thus, determining the proton gluon density  $f_p^g(x, Q^2)$  for this kinematic region directly in LHC experiments would be obviously very useful.

One of the channels for this determination is a high  $P_t$  direct photon production  $pp \rightarrow \gamma^{dir} + X$  (see [24]). The region of high  $P_t$ , reached by UA1 [25], UA2 [26], CDF [27] and D0 [28] extends up to  $P_t \approx 60 \text{ GeV}/c$  and recently up to  $P_t = 105 \text{ GeV}/c$  [29]. These data together with the later ones (see references in [30]–[39]) and recent E706 [40] and UA6 [41] results give an opportunity for tuning the form of gluon distribution (see [33], [36]). The rates and estimated cross sections of inclusive direct photon production at the LHC are given in [24].

A more promising process that can be used for measuring  $f_p^g(x, Q^2)$  is  $pp \rightarrow \gamma^{dir} + 1 \text{ jet} + X$  defined at the leading order by two QCD subprocesses  $qg \rightarrow q + \gamma$  and  $q\bar{q} \rightarrow g + \gamma$  was considered in [20, 21] (see also [42] and for experimental results see [44], [45]).

Here to estimate a possibility of extraction of information on the gluon density in a proton we shall consider the “ $Z^0 + \text{jet}$ ” production process (1) (analogous to the “ $\gamma + \text{jet}$ ” process above), where  $Z^0$  boson decays to the muon pair, a signal from which can be perfectly measured in the detector.

In the case of  $pp \rightarrow Z^0/\gamma^{dir} + 1 \text{ jet} + X$  for  $P_t^{jet} \geq 30 \text{ GeV}/c$  (i.e. in the region where  $k_T$  smearing effects are not important, see [37]) the cross section is expressed directly in terms of parton distribution functions  $f^a(x_a, Q^2)$  (see, for example, [34]):

$$\frac{d\sigma}{d\eta_1 d\eta_2 dP_t^2} = \sum_{a,b} x_a f^a(x_a, Q^2) x_b f^b(x_b, Q^2) \frac{d\sigma}{dt}(a b \rightarrow 1 2) \quad (25)$$

where  $x_{a,b}$  are defined by

$$x_{a,b} = P_t / \sqrt{s} \cdot (\exp(\pm\eta_1) + \exp(\pm\eta_2)). \quad (26)$$

We also used the following designations above:  $\eta_1 = \eta^Z$ ,  $\eta_2 = \eta^{jet}$ ;  $P_t = P_t^Z$ ;  $a, b = q, \bar{q}, g$ ;  $1, 2 = q, \bar{q}, g, Z^0$ . Formula (25) and the knowledge of the results of independent measurements of  $q, \bar{q}$  distributions [42] allow the gluon distribution  $f_p^g(x, Q^2)$  to be determined with an account of the selection efficiencies of “ $Z^0 + \text{jet}$ ” events.

In Table 16 we present the  $Q^2 (\equiv (P_t^Z)^2)$  and  $x$  distribution (with  $x$  defined by (26)) of the number of all events, i.e. the events, based on the subprocesses  $qg \rightarrow Z^0 + q$  and  $q\bar{q} \rightarrow g + Z^0$  (with the decay  $Z^0 \rightarrow \mu^+ \mu^-$ ) for integrated luminosity  $L_{int} = 20 \text{ fb}^{-1}$ . These events satisfy the cuts (4)–(12) of Section 2.2 with the parameter values:

$$|\eta^{jet}| < 5.0, \quad P_{tmax}^\mu \geq 20 \text{ GeV}/c, \quad \Delta\phi < 15^\circ, \quad P_{tCUT}^{clust} = 10 \text{ GeV}/c, \quad P_{tCUT}^{out} = 10 \text{ GeV}/c. \quad (27)$$

The contributions (in %) of the events originated from the subprocesses (2a) and (2b) (and passed the cuts (4)–(12) of Section 2.2) as functions of  $P_t^Z$  are presented in Fig. 12. From this figure one can see that the contribution of the events from the Compton scattering (2a) varies from 67% at  $P_t^Z \approx 40 \text{ GeV}/c$  to 85% at  $P_t^Z \approx 120 \text{ GeV}/c$ .

<sup>21)</sup> That is mainly due to the huge difference in the cross sections of “ $Z^0 + \text{jet}$ ” events (from subprocesses (2a), (2b)) and the QCD events.

The area that can be covered by studying the process (1) with the subsequent decay  $Z^0 \rightarrow \mu^+ \mu^-$  is shown in Fig. 13. The number of events in different  $x$  and  $Q^2$  intervals of this area is given in Table 16. From this figure (and Tables 16) it is seen that during first two years of LHC running at low luminosity ( $L = 10^{33} \text{ cm}^{-2} \text{s}^{-1}$ ) it would be possible to extract an information for the gluon distribution determination  $f_p^g(x, Q^2)$  in a proton in the region of  $0.9 \cdot 10^3 \leq Q^2 \leq 4 \cdot 10^4 (\text{GeV}/c)^2$  with as small  $x$  values as accessible at HERA but at higher  $Q^2$  values (by 1–2 orders of magnitude). It is also worth emphasizing that the sample of the “ $Z^0 + \text{jet}$ ” events selected for this aim can be used to perform a cross-check of  $f_p^g(x, Q^2)$  determination with help of “ $\gamma + \text{jet}$ ” events [20, 21]. The area covered with “ $\gamma + \text{jet}$ ” events is also shown in Fig. 13 by dashed lines.

Table 16: Numbers of “ $Z^0 + \text{jet}$ ” events (with  $Z^0 \rightarrow \mu^+ \mu^-$ ) in  $Q^2$  and  $x$  intervals for  $L_{\text{int}} = 20 \text{ fb}^{-1}$ .

$Q^2$ ( $\text{GeV}/c$ ) <sup>2</sup>	x values of a parton				All x	$P_t^Z$ ( $\text{GeV}/c$ )
	$10^{-4}\text{--}10^{-3}$	$10^{-3}\text{--}10^{-2}$	$10^{-2}\text{--}10^{-1}$	$10^{-1}\text{--}10^0$		
900-1600	18409	45844	47453	2479	114185	30–40
1600-2500	7417	28361	28702	1854	66333	40–50
2500-3600	2479	16574	19015	1533	39599	50–60
3600-5000	1097	10406	12941	1533	25977	60–71
5000-6400	227	5846	6944	1022	14039	71–80
6400-8100	170	4238	5430	624	10463	80–90
8100-10000	19	2989	4049	719	7776	90–100
10000-14400	19	2819	4579	908	8325	100–120
14400-20000	0	1400	2781	454	4635	120–141
20000-40000	0	908	2195	719	3822	141–200
				<b>295 144</b>		

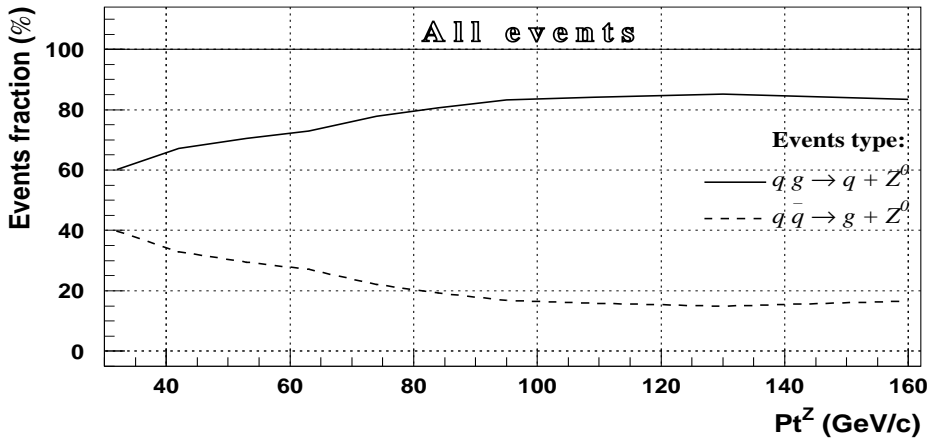


Figure 12: The contributions of the events originated from the subprocesses (2a) and (2b) as a function of  $P_t^Z$ . Full line corresponds to the “ $qg \rightarrow q + Z^0$ ” events, dashed line – to the “ $q\bar{q} \rightarrow g + Z^0$ ” events.

## 9 Summary.

A possibility of the absolute jet energy scale setting with help of “ $Z^0 + \text{jet}$ ” events based on the  $qg \rightarrow q + Z^0$  and  $q\bar{q} \rightarrow g + Z^0$  subprocesses with subsequent  $Z^0$  decay to the muon pair is studied. The PYTHIA event generator is applied here to find the selection criteria of the “ $Z^0 + \text{jet}$ ” events that would provide a good  $P_t^Z - P_t^{\text{Jet}}$  balance.

It is shown here (by analogy with [12]–[16]) that the limitation of the clusters  $P_t$  that may be found in an event in addition to the main jet as well as the limitation of  $P_t$  activity of all particles beyond the “ $Z^0 + \text{jet}$ ” system (see Section 2) leads to an improvement of the  $P_t^Z - P_t^{\text{Jet}}$  balance value. A further improvement of the  $P_t^Z - P_t^{\text{Jet}}$  balance can be reached by selection of events having the isolated jets only. Besides, this criterion (as well as the simultaneous jet finding by two or three algorithms; see Selection 3 in Section 2.2) is also important for selecting events with a clean jet topology and rising the confidence level of a jet determination. The summarizing results of our study of the jet energy scale setting are presented in Appendices 2–6 (see also Fig. 11).

It is demonstrated (Section 7) that the used selection criteria guarantee practically complete suppression of the combinatorial background from the QCD events.

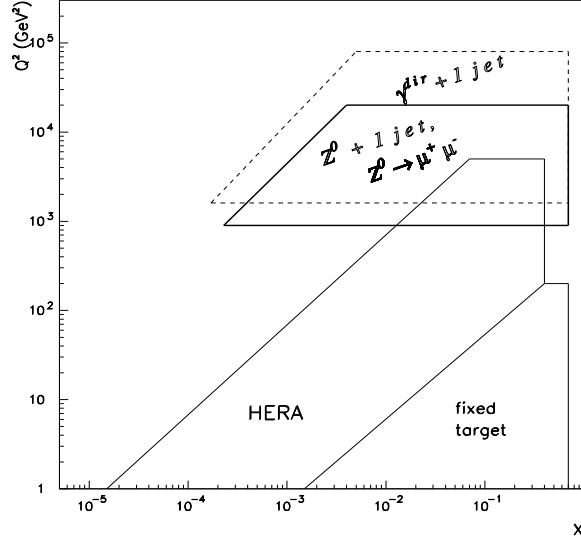


Figure 13: LHC ( $x, Q^2$ ) kinematic region for the process  $pp \rightarrow Z^0 + \text{jet} + X$  (with  $Z^0 \rightarrow \mu^+\mu^-$ ).

It is worth emphasizing that the number of events presented here were not our main goal as they may depend on the used event generator and on the particular choice of a long set of its parameters. The most important result of our work is demonstration that the set of new selection criteria (limitation of  $P_t^{clust}$ ,  $P_t^{out}$  and jet isolation found earlier in [12]–[16]) are also very useful for the jet energy scale determination by help of “ $Z^0 + \text{jet}$ ” events.

It is also shown that the selected sample of the “ $Z^0 + \text{jet}$ ” events, most suitable for the absolute jet energy scale setting at the LHC energy, can provide useful information for the gluon density determination inside a proton in the kinematic region with  $x$  values as small as accessible at HERA but at much higher  $Q^2$  values (by about 1–2 orders of magnitude):  $2 \cdot 10^{-4} \leq x \leq 1.0$  with  $0.9 \cdot 10^3 \leq Q^2 \leq 4 \cdot 10^4 (\text{GeV}/c)^2$ . This sample of “ $Z^0 + \text{jet}$ ” events can be used to perform a cross-check of the  $f_p^g(x, Q^2)$  determination by help of “ $\gamma + \text{jet}$ ” events [20, 21]. The  $x - Q^2$  kinematic area that can be covered by the “ $Z^0 + \text{jet}$ ” events (with  $Z^0 \rightarrow \mu^+\mu^-$ ) as well as by the “ $\gamma + \text{jet}$ ” events is shown in Fig. 13.

## Acknowledgments.

We are greatly thankful to D. Denegri for having offered this theme to study, fruitful discussions and permanent support and encouragement. It is a pleasure for us to express our recognition for helpful discussions to P. Aurenche, M. Dittmar, M. Fontannaz, J.Ph. Guillet, M.L. Mangano, E. Pilon, H. Rohringer, S. Tapprogge and especially to J. Womersley for supplying us with the preliminary version of paper [1].

## References

- [1] D0 Collaboration, F. Abachi *et al.*, NIM **A424** (1999)352.
- [2] CDF Collaboration. F. Abe *et al.*, Phys.Rev. **D50** (1994)2966; F. Abe *et al.*, Phys.Rev.Lett. **73** (1994)225.
- [3] D. Denegri, R. Kinnunen, A. Nikitenko, CMS Note 1997/039 “Study of calorimeter calibration with  $\tau$ ’s in CMS”.
- [4] R. Kinnunen, A. Nikitenko, CMS Note 1997/097 “Study of calorimeter calibration with pions from jets in CMS”.
- [5] J. Womersley, A talk at CMS physics group meeting at CMS Week, Aachen, 1996. See also <http://cmsdoc.cern.ch/doc/gen/agendas/960908-1>.
- [6] J. Freeman, W. Wu, **draft** “In situ calibration of CMS HCAL calorimeter”.
- [7] R. Mehdiyev, I. Vichou, ATLAS Note ATL-COM-PHYS-99-054 (1999) “Hadronic jet energy scale calibration using  $Z + \text{jet}$  events”.

- [8] P. Savard, ATLAS Note CAL-NO-092 (1997), “The  $W \rightarrow jet - jet$  and top mass reconstructions with the ATLAS detector”.
- [9] ATLAS Detector and Physics Performance, Technical Design Report, Volumes **1**, **2**, 1999. CERN/LHCC 99-14.
- [10] N.B. Skachkov, V.F. Konoplyanikov, D.V. Bandourin, “Photon – jet events for calibration of HCAL”. Second Annual RDMS CMS Collaboration Meeting. CMS-Document, 1996–213. CERN, December 16-17, 1996, p.7-23.
- [11] N.B. Skachkov, V.F. Konoplyanikov, D.V. Bandourin, “ $\gamma$ -direct + 1 jet events for HCAL calibration”. Third Annual RDMS CMS Collaboration Meeting. CMS-Document, 1997–168. CERN, December 16-17, 1997, p.139-153.
- [12] D.V. Bandourin, V.F. Konoplyanikov, N.B. Skachkov. “Jet energy scale setting with “ $\gamma + jet$ ” events at LHC energies. Generalities, selection rules.” JINR Preprint E2-2000-251, JINR, Dubna, hep-ex/0011012.
- [13] D.V. Bandourin, V.F. Konoplyanikov, N.B. Skachkov. “Jet energy scale setting with “ $\gamma + jet$ ” events at LHC energies. Event rates,  $P_t$  structure of jet.” JINR Preprint E2-2000-252, JINR, Dubna, hep-ex/0011013.
- [14] D.V. Bandourin, V.F. Konoplyanikov, N.B. Skachkov. “Jet energy scale setting with “ $\gamma + jet$ ” events at LHC energies. Minijets and cluster suppression and  $P_t^\gamma - P_t^{jet}$  disbalance.” JINR Preprint E2-2000-253, JINR, Dubna, hep-ex/0011084.
- [15] D.V. Bandourin, V.F. Konoplyanikov, N.B. Skachkov. “Jet energy scale setting with “ $\gamma + jet$ ” events at LHC energies. Selection of events with a clean “ $\gamma + jet$ ” topology and  $P_t^\gamma - P_t^{jet}$  disbalance.” JINR Preprint E2-2000-254, JINR, Dubna, hep-ex/0011014.
- [16] D.V. Bandourin, V.F. Konoplyanikov, N.B. Skachkov. “Jet energy scale setting with “ $\gamma + jet$ ” events at LHC energies. Detailed study of the background suppression.” JINR Preprint E2-2000-255, JINR, Dubna, hep-ex/0011017.
- [17] CMS Muon Project, Technical Design Report, CERN/LHCC 97–32, CMS TDR 3, CERN, 1997.
- [18] S. Abdullin, A. Khanov, N. Stepanov, CMS Note CMS TN/94–180 “CMSJET”.
- [19] T. Sjostrand, Comp.Phys.Comm. **82** (1994)74.
- [20] D.V. Bandourin, V.F. Konoplyanikov, N.B. Skachkov, ““ $\gamma + jet$ ” events rate estimation for gluon distribution determination at LHC”, Part.Nucl.Lett.**103**:34-43,2000, hep-ex/0011015.
- [21] D.V. Bandourin, N.B. Skachkov, “Background estimation for determination of gluon density in a proton in the process of “direct photon + jet” production at LHC”, hep-ex/0210004 (To appear as CMS Note).
- [22] D.V. Bandourin, N.B. Skachkov. ““ $\gamma + jet$ ” process application for setting the absolute scale of jet energy and determining the gluon distribution at the Tevatron Run II.” D0 Note 3948, 2002.
- [23] 19. D.V. Bandourin, N.B. Skachkov, “Photon+jet event rate estimation for gluon distribution determination at the Tevatron RUN II”, Contributed to Proc. of XVI ISHEP “Relativistic Nuclear Physics and Quantum Chromodynamics”, Dubna, Russia, 2002. JINR Preprint E2-2002-154, hep-ex/0206040. *Submitted to Yad.Fiz.*
- [24] P. Aurenche *et al.* Proc. of ”ECFA LHC Workshop”, Aachen, Germany, 4-9 Oktob. 1990, edited by G. Jarlskog and D. Rein (CERN-Report No 90-10; Geneva, Switzerland 1990), Vol. **II**.
- [25] UA1 Collaboration, C. Albajar *et al.*, Phys.Lett, **209B** (1998)385.
- [26] UA2 Collaboration, R. Ansari *et al.*, Phys.Lett. **176B** (1986)239.
- [27] CDF Collaboration. F. Abe *et al.*, Phys.Rev.Lett. **68** (1992)2734; F. Abe *et al.*,Phys.Rev. **D48** (1993)2998; F. Abe *et al.*,Phys.Rev.Lett., **73** (1994)2662.
- [28] D0 Collaboration, F. Abachi *et al.*, Phys.Rev.Lett, **77** (1996)5011.
- [29] D0 Collaboration, B. Abbott *et al.*, Phys.Rev.Lett. **84** 2786-2791,2000.

- [30] T. Ferbel and W.R. Molzon, Rev.Mod.Phys. **56** (1984)181.
- [31] P. Aurenche, *et al.* Phys.Lett. **169B**441 (1986).
- [32] E.N. Argyres, A.P. Contogouris, N. Mebarki, add S. D.P. Vlassopoulos, Phys.Rev.D 35, 1584-1589 (1987).
- [33] P. Aurenche, *et al.* Phys.Rev. **D39** (1989)3275.
- [34] J.F. Owens, Rev.Mod.Phys. **59** (1987)465.
- [35] J. Huston *et al.*, Phys.Rev. **D51** (1995)6139.
- [36] W. Vogelsang and A. Vogt, Nucl.Phys. **B453** (1995)334.
- [37] J. Huston ATLAS Note ATL-Phys-99-008, CERN,1999.
- [38] W. Vogelsang and M. Whally, J.Phys. **G23** (1997)A1.
- [39] S. Frixione and W. Vogelsang, CERN-TH/99-247 hep-ph/9908387.
- [40] E706 Collaboration, L. Apanasevich *et al.*, Phys.Rev.Lett., **81** (1997)2642.
- [41] UA6 Collaboration, G. Ballocchi *et al.*, Phys.Lett.,**B436** (1998)222. 5Proc. of “CERN Workshop on Standard Model Physics
- [42] M. Dittmar, F. Pauss, D. Zurcher, Phys.Rev.D56:7284-7290,1997.
- [43] M. Dittmar, K.Mazumdar, “Measuring the parton distribution functions of charm, beauty and strange quark and antiquarks at the LHC”, CMS Note 2001/002.
- [44] ISR-AFS Collaboration, T.Akesson *et al.*, Zeit.Phys. **C34** (1987)293.
- [45] CDF Collaboration, F. Abe *et al.*,Phys.Rev. **D57** (1998)1359 (see also p.67).  
hep-ph/9801444.

**Appendix 1**

$$45 < P_t^Z < 55 \text{ GeV}/c$$

Table 1: Selection 1.  $\Delta\phi_{(Z,jet)} = 180^\circ \pm 15^\circ$ . UA1 algorithm.

$P_{tCUT}^{clust}$	30	20	15	10	5
$P_t^{jet}$	48.145	47.600	47.417	47.334	47.323
$P_t^{jet} - P_t^{jet}$	0.140	0.129	0.122	0.106	0.084
$P_t^{jet}_{(\nu)}$	0.141	0.130	0.123	0.107	0.085
$R_{event}^{\nu \in Jet}$	0.027	0.026	0.025	0.023	0.022
$P_t^{jet}_{(\mu)}$	0.046	0.042	0.043	0.038	0.029
$R_{event}^{\mu \in Jet}$	0.011	0.011	0.010	0.009	0.010
$P_t^{miss}$	5.009	4.897	4.777	4.577	4.239
$P_{t\nu \in Jet}^{miss}$	9.016	8.843	8.517	7.653	6.880
$N_{event(c)}$	2774	2300	1763	1027	201
$N_{event(b)}$	2129	1677	1257	626	80
$30sub/all$	0.71	0.70	0.69	0.68	0.65
$R_{gc}^{jet}$	0.65	0.65	0.65	0.65	0.64
Entries	33240	29704	25482	17162	3842

Table 2: Selection 1.  $\Delta\phi_{(Z,jet)} = 180^\circ \pm 15^\circ$ . UA2 algorithm.

$P_{tCUT}^{clust}$	30	20	15	10	5
$P_t^{jet}$	47.520	46.883	46.520	46.296	46.254
$P_t^{jet} - P_t^{jet}$	0.129	0.116	0.106	0.096	0.085
$P_t^{jet}_{(\nu)}$	0.131	0.117	0.107	0.097	0.086
$R_{event}^{\nu \in Jet}$	0.026	0.025	0.023	0.022	0.021
$P_t^{jet}_{(\mu)}$	0.048	0.045	0.044	0.042	0.038
$R_{event}^{\mu \in Jet}$	0.010	0.010	0.009	0.009	0.010
$P_t^{miss}$	5.012	4.890	4.765	4.571	4.221
$P_{t\nu \in Jet}^{miss}$	8.635	8.336	8.008	7.290	6.366
$N_{event(c)}$	2793	2322	1792	1057	187
$N_{event(b)}$	2354	1856	1386	693	91
$30sub/all$	0.69	0.68	0.66	0.64	0.61
$R_{gc}^{jet}$	0.56	0.56	0.55	0.55	0.56
Entries	32326	29057	25154	17041	3706

Table 3: Selection 1.  $\Delta\phi_{(Z,jet)} = 180^\circ \pm 15^\circ$ . LUCELL algorithm.

$P_{tCUT}^{clust}$	30	20	15	10	5
$P_t^{jet}$	47.326	46.854	46.677	46.732	47.016
$P_t^{jet} - P_t^{jet}$	0.144	0.133	0.128	0.118	0.095
$P_t^{jet}_{(\nu)}$	0.145	0.134	0.129	0.119	0.096
$R_{event}^{\nu \in Jet}$	0.028	0.027	0.026	0.025	0.023
$P_t^{jet}_{(\mu)}$	0.049	0.048	0.043	0.040	0.034
$R_{event}^{\mu \in Jet}$	0.010	0.010	0.009	0.009	0.010
$P_t^{miss}$	5.007	4.902	4.791	4.600	4.255
$P_{t\nu \in Jet}^{miss}$	9.104	8.871	8.666	8.140	7.124
$N_{event(c)}$	2961	2488	1921	1086	195
$N_{event(b)}$	2282	1811	1335	642	64
$30sub/all$	0.72	0.71	0.70	0.69	0.67
$R_{gc}^{jet}$	0.66	0.66	0.66	0.66	0.65
Entries	36434	32748	28104	18599	3948

$$70 < P_t^Z < 85 \text{ GeV}/c$$

Table 4: Selection 1.  $\Delta\phi_{(Z,jet)} = 180^\circ \pm 15^\circ$ . UA1 algorithm.

$P_{tCUT}^{clust}$	30	20	15	10	5
$P_t^{jet}$	71.393	72.833	73.509	74.073	74.192
$P_t^{Jet} - P_t^{jet}$	0.339	0.326	0.319	0.270	0.271
$P_t^{jet}_{(\nu)}$	0.341	0.328	0.321	0.271	0.272
$R_{event}^{\nu \in Jet}$	0.039	0.037	0.036	0.031	0.027
$P_t^{jet}_{(\mu)}$	0.147	0.144	0.141	0.124	0.126
$R_{event}^{\mu \in Jet}$	0.019	0.018	0.018	0.016	0.016
$P_t^{miss}$	5.489	5.324	5.230	5.056	4.662
$P_{t\nu \in Jet}^{miss}$	14.357	14.273	14.484	14.504	15.842
$N_{event(c)}$	1478	1025	710	396	62
$N_{event(b)}$	1173	787	528	263	35
$30sub/all$	0.81	0.80	0.79	0.77	0.74
$R_{gc}^{jet}$	0.65	0.65	0.65	0.65	0.65
Entries	21649	17169	13309	8132	1628

Table 5: Selection 1.  $\Delta\phi_{(Z,jet)} = 180^\circ \pm 15^\circ$ . UA2 algorithm.

$P_{tCUT}^{clust}$	30	20	15	10	5
$P_t^{jet}$	71.065	72.035	72.483	72.896	72.976
$P_t^{Jet} - P_t^{jet}$	0.329	0.319	0.316	0.274	0.319
$P_t^{jet}_{(\nu)}$	0.331	0.322	0.318	0.276	0.320
$R_{event}^{\nu \in Jet}$	0.039	0.037	0.036	0.031	0.030
$P_t^{jet}_{(\mu)}$	0.147	0.144	0.141	0.124	0.138
$R_{event}^{\mu \in Jet}$	0.019	0.018	0.018	0.017	0.018
$P_t^{miss}$	5.465	5.308	5.216	4.999	4.577
$P_{t\nu \in Jet}^{miss}$	13.783	13.586	13.684	13.688	15.203
$N_{event(c)}$	1557	1114	787	440	67
$N_{event(b)}$	1349	924	624	324	40
$30sub/all$	0.79	0.78	0.77	0.75	0.71
$R_{gc}^{jet}$	0.58	0.58	0.58	0.58	0.57
Entries	22238	17993	14199	8656	1719

Table 6: Selection 1.  $\Delta\phi_{(Z,jet)} = 180^\circ \pm 15^\circ$ . LUCELL algorithm.

$P_{tCUT}^{clust}$	30	20	15	10	5
$P_t^{jet}$	71.054	72.235	72.910	73.608	73.869
$P_t^{Jet} - P_t^{jet}$	0.334	0.328	0.318	0.264	0.258
$P_t^{jet}_{(\nu)}$	0.336	0.330	0.319	0.265	0.258
$R_{event}^{\nu \in Jet}$	0.038	0.037	0.035	0.031	0.026
$P_t^{jet}_{(\mu)}$	0.151	0.150	0.148	0.126	0.129
$R_{event}^{\mu \in Jet}$	0.019	0.018	0.018	0.017	0.018
$P_t^{miss}$	5.480	5.336	5.229	5.040	4.615
$P_{t\nu \in Jet}^{miss}$	14.412	14.301	14.423	14.095	15.959
$N_{event(c)}$	1488	1057	735	401	64
$N_{event(b)}$	1166	812	547	270	34
$30sub/all$	0.81	0.80	0.79	0.78	0.75
$R_{gc}^{jet}$	0.66	0.66	0.66	0.65	0.64
Entries	22439	18123	14046	8434	1600

$$100 < P_t^Z < 120 \text{ GeV}/c$$

Table 7: Selection 1.  $\Delta\phi_{(Z,jet)} = 180^\circ \pm 15^\circ$ . UA1 algorithm.

$P_{tCUT}^{clust}$	30	20	15	10	5
$P_t^{jet}$	105.311	106.781	107.596	108.186	108.211
$P_t^{Jet} - P_t^{jet}$	0.579	0.536	0.503	0.464	0.306
$P_t^{jet}_{(\nu)}$	0.582	0.538	0.505	0.465	0.308
$R_{event}^{\nu \in Jet}$	0.043	0.040	0.038	0.035	0.027
$P_t^{jet}_{(\mu)}$	0.256	0.236	0.229	0.248	0.190
$R_{event}^{\mu \in Jet}$	0.021	0.021	0.020	0.019	0.017
$P_t^{miss}$	6.021	5.773	5.565	5.410	4.998
$P_{t\nu \in Jet}^{miss}$	21.291	20.555	19.968	19.964	20.603
$N_{event(c)}$	1101	837	611	348	71
$N_{event(b)}$	804	584	418	214	27
$30sub/all$	0.84	0.83	0.82	0.81	0.78
$R_{gc}^{jet}$	0.65	0.65	0.65	0.65	0.65
Entries	26365	19658	14669	8491	1690

Table 8: Selection 1.  $\Delta\phi_{(Z,jet)} = 180^\circ \pm 15^\circ$ . UA2 algorithm.

$P_{tCUT}^{clust}$	30	20	15	10	5
$P_t^{jet}$	105.053	106.086	106.624	107.032	107.226
$P_t^{Jet} - P_t^{jet}$	0.584	0.536	0.499	0.458	0.300
$P_t^{jet}_{(\nu)}$	0.587	0.539	0.502	0.461	0.302
$R_{event}^{\nu \in Jet}$	0.045	0.041	0.038	0.036	0.028
$P_t^{jet}_{(\mu)}$	0.258	0.236	0.229	0.218	0.209
$R_{event}^{\mu \in Jet}$	0.022	0.022	0.021	0.018	0.017
$P_t^{miss}$	5.998	5.781	5.578	5.430	5.000
$P_{t\nu \in Jet}^{miss}$	20.530	19.980	19.456	19.427	18.699
$N_{event(c)}$	1136	881	652	372	76
$N_{event(b)}$	881	658	478	250	31
$30sub/all$	0.83	0.82	0.81	0.80	0.76
$R_{gc}^{jet}$	0.59	0.60	0.59	0.59	0.59
Entries	28311	21607	16358	9541	1845

Table 9: Selection 1.  $\Delta\phi_{(Z,jet)} = 180^\circ \pm 15^\circ$ . LUCELL algorithm.

$P_{tCUT}^{clust}$	30	20	15	10	5
$P_t^{jet}$	104.919	106.238	107.024	107.700	108.019
$P_t^{Jet} - P_t^{jet}$	0.579	0.539	0.511	0.468	0.318
$P_t^{jet}_{(\nu)}$	0.581	0.541	0.514	0.470	0.319
$R_{event}^{\nu \in Jet}$	0.043	0.040	0.038	0.035	0.026
$P_t^{jet}_{(\mu)}$	0.264	0.247	0.244	0.222	0.188
$R_{event}^{\mu \in Jet}$	0.022	0.022	0.021	0.019	0.018
$P_t^{miss}$	6.014	5.787	5.602	5.424	4.991
$P_{t\nu \in Jet}^{miss}$	21.514	20.833	20.528	20.390	21.456
$N_{event(c)}$	1131	878	641	354	71
$N_{event(b)}$	818	612	438	219	25
$30sub/all$	0.84	0.83	0.82	0.82	0.80
$R_{gc}^{jet}$	0.66	0.66	0.66	0.65	0.64
Entries	26920	20362	15184	8643	1636

$$150 < P_t^Z < 200 \text{ GeV}/c$$

Table 10: Selection 1.  $\Delta\phi_{(Z,jet)} = 180^\circ \pm 15^\circ$ . UA1 algorithm.

$P_{tCUT}^{clust}$	30	20	15	10	5
$P_t^{jet}$	166.611	167.904	168.504	168.711	169.574
$P_t^{Jet} - P_t^{jet}$	0.808	0.763	0.732	0.652	0.548
$P_t^{jet}_{(\nu)}$	0.811	0.766	0.734	0.655	0.551
$R_{event}^{\nu \in Jet}$	0.043	0.041	0.041	0.038	0.034
$P_t^{jet}_{(\mu)}$	0.368	0.357	0.348	0.302	0.261
$R_{event}^{\mu \in Jet}$	0.021	0.021	0.021	0.020	0.019
$P_t^{miss}$	6.647	6.468	6.306	6.086	5.462
$P_{t\nu \in Jet}^{miss}$	29.802	29.934	29.081	28.699	22.469
$N_{event(c)}$	629	429	306	173	29
$N_{event(b)}$	459	305	201	97	14
$30sub/all$	0.85	0.84	0.83	0.81	0.77
$R_{gc}^{jet}$	0.66	0.66	0.66	0.66	0.65
Entries	27148	19298	14089	8022	1517

Table 11: Selection 1.  $\Delta\phi_{(Z,jet)} = 180^\circ \pm 15^\circ$ . UA2 algorithm.

$P_{tCUT}^{clust}$	30	20	15	10	5
$P_t^{jet}$	166.410	167.275	167.612	167.794	168.717
$P_t^{Jet} - P_t^{jet}$	0.797	0.736	0.722	0.648	0.486
$P_t^{jet}_{(\nu)}$	0.801	0.740	0.725	0.652	0.490
$R_{event}^{\nu \in Jet}$	0.044	0.041	0.041	0.037	0.035
$P_t^{jet}_{(\mu)}$	0.377	0.352	0.344	0.322	0.237
$R_{event}^{\mu \in Jet}$	0.023	0.022	0.022	0.021	0.020
$P_t^{miss}$	6.616	6.385	6.250	6.042	5.382
$P_{t\nu \in Jet}^{miss}$	28.727	28.831	28.168	28.360	20.770
$N_{event(c)}$	698	476	348	193	33
$N_{event(b)}$	545	364	247	119	15
$30sub/all$	0.84	0.83	0.82	0.80	0.76
$R_{gc}^{jet}$	0.62	0.62	0.62	0.62	0.63
Entries	30379	22130	16501	9520	1731

Table 12: Selection 1.  $\Delta\phi_{(Z,jet)} = 180^\circ \pm 15^\circ$ . LUCELL algorithm.

$P_{tCUT}^{clust}$	30	20	15	10	5
$P_t^{jet}$	166.046	167.273	167.865	168.298	169.319
$P_t^{Jet} - P_t^{jet}$	0.800	0.739	0.714	0.629	0.594
$P_t^{jet}_{(\nu)}$	0.803	0.742	0.716	0.631	0.596
$R_{event}^{\nu \in Jet}$	0.043	0.040	0.040	0.036	0.036
$P_t^{jet}_{(\mu)}$	0.396	0.361	0.352	0.326	0.297
$R_{event}^{\mu \in Jet}$	0.022	0.021	0.021	0.019	0.018
$P_t^{miss}$	6.644	6.446	6.292	6.072	5.555
$P_{t\nu \in Jet}^{miss}$	29.840	30.057	29.270	29.107	22.946
$N_{event(c)}$	626	434	313	169	28
$N_{event(b)}$	457	304	200	91	13
$30sub/all$	0.85	0.84	0.83	0.82	0.79
$R_{gc}^{jet}$	0.66	0.66	0.65	0.65	0.64
Entries	27334	19833	14494	8069	1430

**Appendix 2** $45 < P_t^Z < 55 \text{ GeV}/c$ Table 1: Selection 1.  $\Delta\phi_{(Z,jet)} = 180^\circ \pm 180^\circ$ . UA1 algorithm.

$P_t^{clust}_{CUT}$	30	20	15	10	5
Nevent*	44812	33355	25413	15342	3246
$P_t^{56}$	19.6	15.0	12.4	9.9	7.4
$\Delta\phi$	13.8	9.8	7.9	6.0	4.2
$P_t^{out}$	15.3	11.9	10.0	7.9	5.6
$P_t^{\eta>5}$	5.1	4.9	4.9	4.8	4.3
$(P_t^Z - P_t^{part})/P_t^Z$	0.0487	0.0315	0.0189	0.0113	0.0026
$(P_t^J - P_t^{part})/P_t^J$	0.0140	-0.0016	-0.0069	-0.0032	-0.0057
$(P_t^Z - P_t^J)/P_t^Z$	0.0243	0.0262	0.0200	0.0109	0.0064
$P_t(O+\eta>5)/P_t^Z$	-0.0300	-0.0005	0.0031	0.0011	0.0014
$1 - \cos(\Delta\phi)$	0.0543	0.0267	0.0170	0.0098	0.0050
$\sigma(Db[Z, J])^{**}$	0.2140	0.1814	0.1591	0.1304	0.1010
Entries	18857	14036	10694	6456	1366

Table 2: Selection 1.  $\Delta\phi_{(Z,jet)} = 180^\circ \pm 180^\circ$ . UA2 algorithm.

$P_t^{clust}_{CUT}$	30	20	15	10	5
Nevent	43198	32713	25458	15489	3189
$P_t^{56}$	19.3	14.8	12.4	10.0	7.6
$\Delta\phi$	13.3	9.6	7.7	5.9	4.1
$P_t^{out}$	15.0	11.8	10.0	8.0	5.8
$P_t^{\eta>5}$	5.0	4.9	4.9	4.8	4.4
$(P_t^Z - P_t^{part})/P_t^Z$	0.0399	0.0239	0.0153	0.0119	0.0080
$(P_t^J - P_t^{part})/P_t^J$	-0.0048	-0.0257	-0.0333	-0.0295	-0.0259
$(P_t^Z - P_t^J)/P_t^Z$	0.0330	0.0405	0.0405	0.0357	0.0302
$P_t(O+\eta>5)/P_t^Z$	-0.0175	0.0152	0.0241	0.0263	0.0254
$1 - \cos(\Delta\phi)$	0.0505	0.0253	0.0165	0.0094	0.0048
$\sigma(Db[Z, J])$	0.2088	0.1773	0.1563	0.1305	0.1009
Entries	18178	13766	10713	6518	1342

Table 3: Selection 1.  $\Delta\phi_{(Z,jet)} = 180^\circ \pm 180^\circ$ . LUCELL algorithm.

$P_t^{clust}_{CUT}$	30	20	15	10	5
Nevent	48402	36720	27923	16411	3296
$P_t^{56}$	19.4	15.2	12.6	10.0	7.3
$\Delta\phi$	13.6	10.0	8.0	6.1	4.3
$P_t^{out}$	15.2	12.2	10.2	8.0	5.7
$P_t^{\eta>5}$	5.0	4.9	4.9	4.8	4.4
$(P_t^Z - P_t^{part})/P_t^Z$	0.0552	0.0378	0.0250	0.0142	0.0009
$(P_t^J - P_t^{part})/P_t^J$	0.0043	-0.0120	-0.0170	-0.0123	-0.0119
$(P_t^Z - P_t^J)/P_t^Z$	0.0413	0.0420	0.0355	0.0223	0.0105
$P_t(O+\eta>5)/P_t^Z$	-0.0108	0.0143	0.0182	0.0122	0.0047
$1 - \cos(\Delta\phi)$	0.0521	0.0278	0.0173	0.0102	0.0058
$\sigma(Db[Z, J])$	0.2121	0.1842	0.1626	0.1337	0.1031
Entries	20368	15452	11750	6906	1387

\*Number of events (Nevent) is given in this and in the following tables for integrated luminosity  $L_{int} = 10 \text{ fb}^{-1}$ \*\*  $Db[Z, J] \equiv (P_t^Z - P_t^J)/P_t^Z$

Table 4: Selection 1.  $\Delta\phi_{(Z,jet)} = 180^\circ \pm 15^\circ$ . UA1 algorithm.

$P_t^{clust}_{CUT}$	30	20	15	10	5
Nevent	29624	26022	21782	14320	3189
$P_t 56$	14.5	12.5	11.0	9.3	7.2
$\Delta\phi$	6.1	5.9	5.6	4.9	3.9
$P_t^{out}$	10.5	9.6	8.7	7.4	5.5
$P_t^{\eta>5}$	4.9	4.8	4.7	4.6	4.2
$(P_t^Z - P_t^{part})/P_t^Z$	0.0156	0.0156	0.0107	0.0078	0.0004
$(P_t^J - P_t^{part})/P_t^J$	0.0015	-0.0047	-0.0062	-0.0033	-0.0054
$(P_t^Z - P_t^J)/P_t^Z$	0.0051	0.0140	0.0120	0.0077	0.0039
$P_t(O+\eta>5)/P_t^Z$	-0.0033	0.0060	0.0047	0.0019	0.0001
$1 - \cos(\Delta\phi)$	0.0084	0.0080	0.0073	0.0058	0.0039
$\sigma(Db[Z, J])$	0.2025	0.1745	0.1543	0.1282	0.0992
Entries	12466	10950	9166	6026	1342

 Table 5: Selection 1.  $\Delta\phi_{(Z,jet)} = 180^\circ \pm 15^\circ$ . UA2 algorithm.

$P_t^{clust}_{CUT}$	30	20	15	10	5
Nevent	29089	25734	21915	14491	3144
$P_t 56$	14.3	12.4	11.0	9.4	7.4
$\Delta\phi$	6.0	5.9	5.5	4.9	3.9
$P_t^{out}$	10.4	9.5	8.7	7.5	5.8
$P_t^{\eta>5}$	4.9	4.8	4.7	4.6	4.3
$(P_t^Z - P_t^{part})/P_t^Z$	0.0087	0.0093	0.0081	0.0093	0.0064
$(P_t^J - P_t^{part})/P_t^J$	-0.0203	-0.0292	-0.0324	-0.0293	-0.0262
$(P_t^Z - P_t^J)/P_t^Z$	0.0187	0.0302	0.0335	0.0332	0.0289
$P_t(O+\eta>5)/P_t^Z$	0.0105	0.0225	0.0264	0.0275	0.0252
$1 - \cos(\Delta\phi)$	0.0082	0.0078	0.0071	0.0057	0.0038
$\sigma(Db[Z, J])$	0.1972	0.1704	0.1513	0.1286	0.0998
Entries	12241	10829	9222	6098	1323

 Table 6: Selection 1.  $\Delta\phi_{(Z,jet)} = 180^\circ \pm 15^\circ$ . LUCELL algorithm.

$P_t^{clust}_{CUT}$	30	20	15	10	5
Nevent	32153	28405	23849	15294	3237
$P_t 56$	14.5	12.6	11.2	9.3	7.0
$\Delta\phi$	6.2	6.0	5.7	5.0	4.0
$P_t^{out}$	10.6	9.7	8.9	7.5	5.6
$P_t^{\eta>5}$	4.9	4.8	4.8	4.6	4.2
$(P_t^Z - P_t^{part})/P_t^Z$	0.0213	0.0206	0.0164	0.0103	-0.0013
$(P_t^J - P_t^{part})/P_t^J$	-0.0081	-0.0145	-0.0161	-0.0120	-0.0118
$(P_t^Z - P_t^J)/P_t^Z$	0.0207	0.0281	0.0268	0.0184	0.0082
$P_t(O+\eta>5)/P_t^Z$	0.0122	0.0200	0.0195	0.0124	0.0043
$1 - \cos(\Delta\phi)$	0.0085	0.0081	0.0074	0.0060	0.0039
$\sigma(Db[Z, J])$	0.2017	0.1768	0.1578	0.1312	0.1009
Entries	13530	11953	10036	6436	1362

Table 7: Selection 1.  $\Delta\phi_{(Z,jet)} = 180^\circ \pm 10^\circ$ . UA1 algorithm.

$P_t^{clust}_{CUT}$	30	20	15	10	5
Nevent	23075	20713	17892	12512	2985
$P_t 56$	13.0	11.3	10.1	8.6	6.8
$\Delta\phi$	4.3	4.3	4.2	3.9	3.4
$P_t^{out}$	9.4	8.6	7.9	6.9	5.3
$P_t^{\eta>5}$	4.8	4.8	4.7	4.5	4.1
$(P_t^Z - P_t^{part})/P_t^Z$	0.0079	0.0091	0.0069	0.0048	-0.0024
$(P_t^J - P_t^{part})/P_t^J$	-0.0009	-0.0053	-0.0051	-0.0027	-0.0061
$(P_t^Z - P_t^J)/P_t^Z$	0.0011	0.0085	0.0070	0.0044	0.0018
$P_t(O+\eta>5)/P_t^Z$	-0.0030	0.0045	0.0032	0.0009	-0.0009
$1 - \cos(\Delta\phi)$	0.0041	0.0040	0.0038	0.0034	0.0026
$\sigma(Db[Z, J])$	0.1944	0.1691	0.1496	0.1255	0.0980
Entries	9710	8716	7529	5265	1256

 Table 8: Selection 1.  $\Delta\phi_{(Z,jet)} = 180^\circ \pm 10^\circ$ . UA2 algorithm.

$P_t^{clust}_{CUT}$	30	20	15	10	5
Nevent	22965	20713	18196	12780	2966
$P_t 56$	13.0	11.3	10.1	8.8	7.1
$\Delta\phi$	4.3	4.3	4.2	3.9	3.4
$P_t^{out}$	9.3	8.6	8.0	7.1	5.6
$P_t^{\eta>5}$	4.8	4.8	4.7	4.6	4.2
$(P_t^Z - P_t^{part})/P_t^Z$	0.0050	0.0069	0.0070	0.0063	0.0046
$(P_t^J - P_t^{part})/P_t^J$	-0.0226	-0.0294	-0.0308	-0.0296	-0.0260
$(P_t^Z - P_t^J)/P_t^Z$	0.0183	0.0285	0.0309	0.0307	0.0271
$P_t(O+\eta>5)/P_t^Z$	0.0142	0.0245	0.0271	0.0273	0.0245
$1 - \cos(\Delta\phi)$	0.0041	0.0040	0.0038	0.0035	0.0026
$\sigma(Db[Z, J])$	0.1895	0.1643	0.1468	0.1258	0.0983
Entries	9664	8716	7657	5378	1248

 Table 9: Selection 1.  $\Delta\phi_{(Z,jet)} = 180^\circ \pm 10^\circ$ . LUCELL algorithm.

$P_t^{clust}_{CUT}$	30	20	15	10	5
Nevent	25028	22564	19532	13332	3035
$P_t 56$	13.1	11.5	10.3	8.7	6.7
$\Delta\phi$	4.4	4.3	4.2	4.0	3.4
$P_t^{out}$	9.5	8.8	8.1	7.0	5.4
$P_t^{\eta>5}$	4.8	4.8	4.7	4.5	4.1
$(P_t^Z - P_t^{part})/P_t^Z$	0.0140	0.0147	0.0129	0.0070	-0.0035
$(P_t^J - P_t^{part})/P_t^J$	-0.0102	-0.0141	-0.0144	-0.0118	-0.0115
$(P_t^Z - P_t^J)/P_t^Z$	0.0166	0.0225	0.0220	0.0151	0.0058
$P_t(O+\eta>5)/P_t^Z$	0.0125	0.0185	0.0181	0.0116	0.0032
$1 - \cos(\Delta\phi)$	0.0042	0.0041	0.0039	0.0035	0.0027
$\sigma(Db[Z, J])$	0.1944	0.1721	0.1535	0.1282	0.0997
Entries	10532	9495	8219	5610	1277

Table 10: Selection 1.  $\Delta\phi_{(Z,jet)} = 180^\circ \pm 5^\circ$ . UA1 algorithm.

$P_t^{clust}_{CUT}$	30	20	15	10	5
Nevent	14078	12852	11364	8477	2246
$P_t 56$	11.6	10.1	9.1	7.8	6.2
$\Delta\phi$	2.4	2.4	2.3	2.3	2.2
$P_t^{out}$	8.4	7.7	7.1	6.2	4.9
$P_t^{\eta>5}$	4.8	4.7	4.6	4.4	4.0
$(P_t^Z - P_t^{part})/P_t^Z$	0.0082	0.0090	0.0074	0.0038	-0.0029
$(P_t^J - P_t^{part})/P_t^J$	0.0001	-0.0035	-0.0028	-0.0025	-0.0065
$(P_t^Z - P_t^J)/P_t^Z$	0.0013	0.0070	0.0055	0.0031	0.0013
$P_t(O+\eta>5)/P_t^Z$	0.0001	0.0059	0.0044	0.0020	0.0003
$1 - \cos(\Delta\phi)$	0.0012	0.0012	0.0012	0.0011	0.0010
$\sigma(Db[Z, J])$	0.1847	0.1611	0.1432	0.1203	0.0938
Entries	5924	5408	4782	3567	945

 Table 11: Selection 1.  $\Delta\phi_{(Z,jet)} = 180^\circ \pm 5^\circ$ . UA2 algorithm.

$P_t^{clust}_{CUT}$	30	20	15	10	5
Nevent	13961	12775	11511	8607	2243
$P_t 56$	11.5	10.0	9.1	8.0	6.5
$\Delta\phi$	2.4	2.4	2.3	2.3	2.2
$P_t^{out}$	8.4	7.6	7.1	6.3	5.2
$P_t^{\eta>5}$	4.8	4.7	4.6	4.5	4.0
$(P_t^Z - P_t^{part})/P_t^Z$	0.0033	0.0048	0.0060	0.0046	0.0032
$(P_t^J - P_t^{part})/P_t^J$	-0.0242	-0.0301	-0.0307	-0.0300	-0.0271
$(P_t^Z - P_t^J)/P_t^Z$	0.0186	0.0275	0.0300	0.0292	0.0264
$P_t(O+\eta>5)/P_t^Z$	0.0174	0.0263	0.0289	0.0281	0.0254
$1 - \cos(\Delta\phi)$	0.0012	0.0012	0.0011	0.0011	0.0010
$\sigma(Db[Z, J])$	0.1832	0.1583	0.1414	0.1216	0.0936
Entries	5875	5376	4844	3622	944

 Table 12: Selection 1.  $\Delta\phi_{(Z,jet)} = 180^\circ \pm 5^\circ$ . LUCELL algorithm.

$P_t^{clust}_{CUT}$	30	20	15	10	5
Nevent	15114	13840	12286	8930	2272
$P_t 56$	11.7	10.3	9.2	7.8	6.1
$\Delta\phi$	2.4	2.4	2.4	2.3	2.2
$P_t^{out}$	8.5	7.8	7.2	6.3	5.0
$P_t^{\eta>5}$	4.7	4.7	4.6	4.5	4.0
$(P_t^Z - P_t^{part})/P_t^Z$	0.0121	0.0124	0.0111	0.0053	-0.0032
$(P_t^J - P_t^{part})/P_t^J$	-0.0097	-0.0129	-0.0138	-0.0119	-0.0127
$(P_t^Z - P_t^J)/P_t^Z$	0.0146	0.0194	0.0197	0.0135	0.0070
$P_t(O+\eta>5)/P_t^Z$	0.0134	0.0183	0.0185	0.0123	0.0060
$1 - \cos(\Delta\phi)$	0.0012	0.0012	0.0012	0.0011	0.0011
$\sigma(Db[Z, J])$	0.1849	0.1639	0.1470	0.1225	0.0959
Entries	6360	5824	5170	3758	956

Table 13: Selection 2.  $\Delta\phi_{(Z,jet)} = 180^\circ \pm 15^\circ$ ,  $\epsilon^{jet} < 9\%$ . UA1 algorithm.

$P_t^{clust}_{CUT}$	30	20	15	10	5
Nevent	23186	20758	17956	12419	3011
$P_t 56$	13.8	11.9	10.6	9.0	7.1
$\Delta\phi$	5.9	5.8	5.5	4.8	3.9
$P_t^{out}$	10.2	9.2	8.5	7.2	5.5
$P_t^{\eta>5}$	4.9	4.8	4.8	4.6	4.2
$(P_t^Z - P_t^{part})/P_t^Z$	-0.0088	-0.0057	-0.0060	-0.0023	-0.0023
$(P_t^J - P_t^{part})/P_t^J$	0.0136	0.0048	-0.0002	-0.0004	-0.0042
$(P_t^Z - P_t^J)/P_t^Z$	-0.0299	-0.0153	-0.0098	-0.0048	0.0000
$P_t(O+\eta>5)/P_t^Z$	-0.0379	-0.0229	-0.0168	-0.0105	-0.0037
$1 - \cos(\Delta\phi)$	0.0080	0.0076	0.0070	0.0057	0.0038
$\sigma(Db[Z, J])$	0.1986	0.1682	0.1487	0.1246	0.0984
Entries	9757	8735	7556	5226	1267

Table 14: Selection 2.  $\Delta\phi_{(Z,jet)} = 180^\circ \pm 15^\circ$ ,  $\epsilon^{jet} < 6\%$ . UA2 algorithm.

$P_t^{clust}_{CUT}$	30	20	15	10	5
Nevent	12671	11321	9895	6946	1811
$P_t 56$	13.6	11.5	10.2	8.7	6.8
$\Delta\phi$	5.8	5.6	5.3	4.7	3.7
$P_t^{out}$	10.2	9.2	8.3	7.1	5.5
$P_t^{\eta>5}$	4.9	4.8	4.8	4.6	4.3
$(P_t^Z - P_t^{part})/P_t^Z$	-0.0467	-0.0385	-0.0314	-0.0213	-0.0175
$(P_t^J - P_t^{part})/P_t^J$	-0.0118	-0.0229	-0.0272	-0.0290	-0.0341
$(P_t^Z - P_t^J)/P_t^Z$	-0.0421	-0.0206	-0.0083	0.0042	0.0103
$P_t(O+\eta>5)/P_t^Z$	-0.0497	-0.0278	-0.0149	-0.0010	0.0068
$1 - \cos(\Delta\phi)$	0.0077	0.0072	0.0066	0.0053	0.0035
$\sigma(Db[Z, J])$	0.2024	0.1694	0.1494	0.1252	0.0992
Entries	5332	4764	4164	2923	762

Table 15: Selection 2.  $\Delta\phi_{(Z,jet)} = 180^\circ \pm 15^\circ$ ,  $\epsilon^{jet} < 9\%$ . LUCELL algorithm.

$P_t^{clust}_{CUT}$	30	20	15	10	5
Nevent	24510	22048	19047	13027	3068
$P_t 56$	13.6	11.9	10.5	9.0	7.0
$\Delta\phi$	6.0	5.8	5.5	4.9	3.9
$P_t^{out}$	10.1	9.3	8.5	7.3	5.5
$P_t^{\eta>5}$	4.9	4.8	4.8	4.6	4.2
$(P_t^Z - P_t^{part})/P_t^Z$	-0.0089	-0.0054	-0.0055	-0.0026	-0.0039
$(P_t^J - P_t^{part})/P_t^J$	0.0019	-0.0058	-0.0104	-0.0089	-0.0098
$(P_t^Z - P_t^J)/P_t^Z$	-0.0179	-0.0049	0.0003	0.0029	0.0038
$P_t(O+\eta>5)/P_t^Z$	-0.0259	-0.0125	-0.0067	-0.0029	0.0000
$1 - \cos(\Delta\phi)$	0.0081	0.0077	0.0071	0.0057	0.0039
$\sigma(Db[Z, J])$	0.1979	0.1705	0.1510	0.1263	0.0993
Entries	10314	9278	8015	5482	1291

Table 16: Selection 3.  $\Delta\phi_{(Z,jet)} = 180^\circ \pm 15^\circ$ ,  $\epsilon^{jet} < 9\%$ . UA1 algorithm.

$P_t^{clust}_{CUT}$	30	20	15	10	5
Nevent	17640	15872	13835	9541	2224
$P_t 56$	13.4	11.6	10.3	8.8	7.0
$\Delta\phi$	5.8	5.6	5.4	4.7	3.8
$P_t^{out}$	10.0	9.0	8.3	7.1	5.4
$P_t^{\eta>5}$	4.9	4.8	4.7	4.6	4.3
$(P_t^Z - P_t^{part})/P_t^Z$	-0.0221	-0.0171	-0.0153	-0.0083	-0.0059
$(P_t^J - P_t^{part})/P_t^J$	0.0132	0.0046	-0.0006	-0.0007	-0.0061
$(P_t^Z - P_t^J)/P_t^Z$	-0.0422	-0.0261	-0.0182	-0.0102	-0.0016
$P_t(O+\eta>5)/P_t^Z$	-0.0498	-0.0334	-0.0249	-0.0155	-0.0051
$1 - \cos(\Delta\phi)$	0.0076	0.0073	0.0067	0.0054	0.0037
$\sigma(Db[Z, J])$	0.1948	0.1646	0.1460	0.1225	0.0971
Entries	7423	6679	5822	4015	936

Table 17: Selection 3.  $\Delta\phi_{(Z,jet)} = 180^\circ \pm 15^\circ$ ,  $\epsilon^{jet} < 6\%$ . UA2 algorithm.

$P_t^{clust}_{CUT}$	30	20	15	10	5
Nevent	17640	15872	13835	9541	2224
$P_t 56$	13.4	11.6	10.3	8.8	7.0
$\Delta\phi$	5.8	5.7	5.4	4.8	3.9
$P_t^{out}$	10.0	9.1	8.4	7.2	5.6
$P_t^{\eta>5}$	4.9	4.8	4.7	4.6	4.3
$(P_t^Z - P_t^{part})/P_t^Z$	-0.0221	-0.0171	-0.0153	-0.0083	-0.0059
$(P_t^J - P_t^{part})/P_t^J$	-0.0174	-0.0266	-0.0319	-0.0320	-0.0339
$(P_t^Z - P_t^J)/P_t^Z$	-0.0124	0.0037	0.0115	0.0166	0.0217
$P_t(O+\eta>5)/P_t^Z$	-0.0200	-0.0036	0.0048	0.0113	0.0181
$1 - \cos(\Delta\phi)$	0.0077	0.0073	0.0068	0.0054	0.0038
$\sigma(Db[Z, J])$	0.1958	0.1658	0.1475	0.1243	0.0992
Entries	7423	6679	5822	4015	936

Table 18: Selection 3.  $\Delta\phi_{(Z,jet)} = 180^\circ \pm 15^\circ$ ,  $\epsilon^{jet} < 9\%$ . LUCELL algorithm.

$P_t^{clust}_{CUT}$	30	20	15	10	5
Nevent	17640	15872	13835	9541	2224
$P_t 56$	13.4	11.6	10.3	8.8	7.0
$\Delta\phi$	5.8	5.7	5.4	4.8	3.8
$P_t^{out}$	10.0	9.1	8.4	7.2	5.5
$P_t^{\eta>5}$	4.9	4.8	4.7	4.6	4.3
$(P_t^Z - P_t^{part})/P_t^Z$	-0.0221	-0.0171	-0.0153	-0.0083	-0.0059
$(P_t^J - P_t^{part})/P_t^J$	0.0065	-0.0024	-0.0076	-0.0070	-0.0096
$(P_t^Z - P_t^J)/P_t^Z$	-0.0355	-0.0194	-0.0116	-0.0041	0.0019
$P_t(O+\eta>5)/P_t^Z$	-0.0431	-0.0268	-0.0183	-0.0095	-0.0016
$1 - \cos(\Delta\phi)$	0.0077	0.0074	0.0068	0.0055	0.0037
$\sigma(Db[Z, J])$	0.1950	0.1653	0.1469	0.1237	0.0975
Entries	7423	6679	5822	4015	936

Table 19: Selection 3.  $\Delta\phi_{(Z,jet)} = 180^\circ \pm 15^\circ$ ,  $\epsilon^{jet} < 9\%$ . UA1 algorithm.

$P_t^{clust}_{CUT}$	30	20	15	10	5
Nevent	22010	19805	17153	11818	2795
$P_t^{56}$	13.5	11.8	10.4	8.9	7.0
$\Delta\phi$	5.9	5.7	5.4	4.8	3.9
$P_t^{out}$	10.1	9.2	8.4	7.2	5.5
$P_t^{\eta>5}$	4.9	4.8	4.8	4.6	4.2
$(P_t^Z - P_t^{part})/P_t^Z$	-0.0125	-0.0089	-0.0086	-0.0040	-0.0044
$(P_t^J - P_t^{part})/P_t^J$	0.0107	0.0028	-0.0018	-0.0017	-0.0055
$(P_t^Z - P_t^J)/P_t^Z$	-0.0302	-0.0165	-0.0108	-0.0052	-0.0009
$P_t(O+\eta>5)/P_t^Z$	-0.0383	-0.0243	-0.0179	-0.0111	-0.0045
$1 - \cos(\Delta\phi)$	0.0079	0.0075	0.0069	0.0056	0.0038
$\sigma(Db[Z, J])$	0.1971	0.1683	0.1488	0.1246	0.0986
Entries	9262	8334	7218	4973	1176

Table 20: Selection 3.  $\Delta\phi_{(Z,jet)} = 180^\circ \pm 15^\circ$ ,  $\epsilon^{jet} < 9\%$ . LUCELL algorithm.

$P_t^{clust}_{CUT}$	30	20	15	10	5
Nevent	22010	19805	17153	11818	2795
$P_t^{56}$	13.5	11.8	10.4	8.9	7.0
$\Delta\phi$	5.9	5.8	5.5	4.9	3.9
$P_t^{out}$	10.1	9.2	8.5	7.3	5.5
$P_t^{\eta>5}$	4.9	4.8	4.8	4.6	4.2
$(P_t^Z - P_t^{part})/P_t^Z$	-0.0125	-0.0089	-0.0086	-0.0040	-0.0044
$(P_t^J - P_t^{part})/P_t^J$	0.0041	-0.0040	-0.0087	-0.0078	-0.0089
$(P_t^Z - P_t^J)/P_t^Z$	-0.0237	-0.0099	-0.0042	0.0005	0.0024
$P_t(O+\eta>5)/P_t^Z$	-0.0318	-0.0178	-0.0114	-0.0054	-0.0012
$1 - \cos(\Delta\phi)$	0.0080	0.0076	0.0070	0.0057	0.0038
$\sigma(Db[Z, J])$	0.1971	0.1689	0.1495	0.1257	0.0993
Entries	9262	8334	7218	4973	1176

**Appendix 3** $70 < P_t^Z < 85 \text{ GeV}/c$ Table 1: Selection 1.  $\Delta\phi_{(Z,jet)} = 180^\circ \pm 180^\circ$ . UA1 algorithm.

$P_t^{clust}_{CUT}$	30	20	15	10	5
Nevent*	17258	12124	8956	5313	1058
$P_t 56$	21.0	16.0	13.3	10.7	8.0
$\Delta\phi$	9.0	6.4	5.1	3.9	2.8
$P_t^{out}$	17.3	12.8	10.3	8.0	5.7
$P_t^{\eta>5}$	5.4	5.3	5.2	5.1	4.7
$(P_t^Z - P_t^{part})/P_t^Z$	0.0508	0.0227	0.0137	0.0090	0.0049
$(P_t^J - P_t^{part})/P_t^J$	-0.0273	-0.0163	-0.0100	-0.0037	-0.0068
$(P_t^Z - P_t^J)/P_t^Z$	0.0648	0.0316	0.0186	0.0092	0.0081
$P_t(O+\eta>5)/P_t^Z$	0.0365	0.0158	0.0072	0.0015	0.0022
$1 - \cos(\Delta\phi)$	0.0236	0.0113	0.0071	0.0040	0.0023
$\sigma(Db[Z, J])^{**}$	0.1915	0.1478	0.1219	0.0968	0.0801
Entries	26667	18734	13839	8209	1635

Table 2: Selection 1.  $\Delta\phi_{(Z,jet)} = 180^\circ \pm 180^\circ$ . UA2 algorithm.

$P_t^{clust}_{CUT}$	30	20	15	10	5
Nevent	17564	12705	9563	5664	1120
$P_t 56$	20.9	16.2	13.6	11.0	8.5
$\Delta\phi$	8.8	6.3	5.1	3.9	2.9
$P_t^{out}$	16.9	12.7	10.5	8.1	5.8
$P_t^{\eta>5}$	5.4	5.3	5.2	5.0	4.7
$(P_t^Z - P_t^{part})/P_t^Z$	0.0489	0.0243	0.0161	0.0128	0.0103
$(P_t^J - P_t^{part})/P_t^J$	-0.0309	-0.0258	-0.0226	-0.0165	-0.0182
$(P_t^Z - P_t^J)/P_t^Z$	0.0670	0.0421	0.0325	0.0252	0.0240
$P_t(O+\eta>5)/P_t^Z$	0.0401	0.0265	0.0212	0.0174	0.0174
$1 - \cos(\Delta\phi)$	0.0224	0.0112	0.0071	0.0041	0.0024
$\sigma(Db[Z, J])$	0.1856	0.1450	0.1207	0.0962	0.0792
Entries	27139	19631	14776	8752	1730

Table 3: Selection 1.  $\Delta\phi_{(Z,jet)} = 180^\circ \pm 180^\circ$ . LUCELL algorithm.

$P_t^{clust}_{CUT}$	30	20	15	10	5
Nevent	17643	12828	9459	5512	1041
$P_t 56$	20.5	16.1	13.3	10.5	7.6
$\Delta\phi$	8.7	6.4	5.1	3.9	2.8
$P_t^{out}$	16.9	12.9	10.5	8.1	5.7
$P_t^{\eta>5}$	5.4	5.3	5.2	5.1	4.7
$(P_t^Z - P_t^{part})/P_t^Z$	0.0492	0.0249	0.0143	0.0079	0.0012
$(P_t^J - P_t^{part})/P_t^J$	-0.0302	-0.0227	-0.0180	-0.0108	-0.0143
$(P_t^Z - P_t^J)/P_t^Z$	0.0673	0.0400	0.0267	0.0152	0.0121
$P_t(O+\eta>5)/P_t^Z$	0.0404	0.0239	0.0152	0.0075	0.0063
$1 - \cos(\Delta\phi)$	0.0223	0.0116	0.0072	0.0041	0.0024
$\sigma(Db[Z, J])$	0.1865	0.1489	0.1232	0.0974	0.0803
Entries	27262	19821	14615	8517	1608

\*Number of events (Nevent) is given in this and in the following tables for integrated luminosity  $L_{int} = 10 \text{ fb}^{-1}$ \*\*  $Db[Z, J] \equiv (P_t^Z - P_t^J)/P_t^Z$

Table 4: Selection 1.  $\Delta\phi_{(Z,jet)} = 180^\circ \pm 15^\circ$ . UA1 algorithm.

$P_t^{clust}_{CUT}$	30	20	15	10	5
Nevent	14012	11112	8613	5263	1054
$P_t 56$	17.5	14.6	12.7	10.5	7.9
$\Delta\phi$	5.6	5.1	4.5	3.8	2.7
$P_t^{out}$	13.7	11.5	9.8	7.9	5.7
$P_t^{\eta>5}$	5.2	5.1	5.1	5.0	4.6
$(P_t^Z - P_t^{part})/P_t^Z$	0.0320	0.0171	0.0113	0.0083	0.0042
$(P_t^J - P_t^{part})/P_t^J$	-0.0243	-0.0148	-0.0094	-0.0037	-0.0068
$(P_t^Z - P_t^J)/P_t^Z$	0.0447	0.0252	0.0158	0.0085	0.0074
$P_t(O+\eta>5)/P_t^Z$	0.0330	0.0147	0.0066	0.0014	0.0018
$1 - \cos(\Delta\phi)$	0.0072	0.0061	0.0050	0.0035	0.0020
$\sigma(Db[Z, J])$	0.1783	0.1420	0.1191	0.0958	0.0787
Entries	21651	17170	13309	8132	1628

 Table 5: Selection 1.  $\Delta\phi_{(Z,jet)} = 180^\circ \pm 15^\circ$ . UA2 algorithm.

$P_t^{clust}_{CUT}$	30	20	15	10	5
Nevent	14394	11646	9190	5603	1113
$P_t 56$	17.7	14.9	13.0	10.8	8.4
$\Delta\phi$	5.5	5.0	4.5	3.7	2.8
$P_t^{out}$	13.5	11.5	9.9	8.0	5.8
$P_t^{\eta>5}$	5.2	5.1	5.1	4.9	4.5
$(P_t^Z - P_t^{part})/P_t^Z$	0.0316	0.0189	0.0139	0.0120	0.0094
$(P_t^J - P_t^{part})/P_t^J$	-0.0287	-0.0246	-0.0219	-0.0165	-0.0180
$(P_t^Z - P_t^J)/P_t^Z$	0.0494	0.0361	0.0299	0.0244	0.0229
$P_t(O+\eta>5)/P_t^Z$	0.0379	0.0257	0.0207	0.0173	0.0167
$1 - \cos(\Delta\phi)$	0.0071	0.0061	0.0050	0.0035	0.0020
$\sigma(Db[Z, J])$	0.1729	0.1391	0.1182	0.0950	0.0772
Entries	22241	17995	14200	8657	1720

 Table 6: Selection 1.  $\Delta\phi_{(Z,jet)} = 180^\circ \pm 15^\circ$ . LUCELL algorithm.

$P_t^{clust}_{CUT}$	30	20	15	10	5
Nevent	14523	11730	9090	5458	1035
$P_t 56$	17.4	14.7	12.7	10.3	7.5
$\Delta\phi$	5.6	5.1	4.6	3.8	2.7
$P_t^{out}$	13.6	11.6	10.0	8.0	5.7
$P_t^{\eta>5}$	5.2	5.2	5.1	5.0	4.6
$(P_t^Z - P_t^{part})/P_t^Z$	0.0322	0.0185	0.0115	0.0072	0.0003
$(P_t^J - P_t^{part})/P_t^J$	-0.0273	-0.0214	-0.0175	-0.0108	-0.0142
$(P_t^Z - P_t^J)/P_t^Z$	0.0491	0.0330	0.0237	0.0145	0.0112
$P_t(O+\eta>5)/P_t^Z$	0.0375	0.0224	0.0144	0.0074	0.0057
$1 - \cos(\Delta\phi)$	0.0072	0.0062	0.0051	0.0036	0.0020
$\sigma(Db[Z, J])$	0.1744	0.1426	0.1204	0.0965	0.0786
Entries	22441	18124	14046	8434	1600

Table 7: Selection 1.  $\Delta\phi_{(Z,jet)} = 180^\circ \pm 10^\circ$ . UA1 algorithm.

$P_t^{clust}_{CUT}$	30	20	15	10	5
Nevent	11553	9597	7794	5014	1039
$P_t 56$	16.0	13.5	11.9	10.1	7.8
$\Delta\phi$	4.1	3.9	3.7	3.3	2.6
$P_t^{out}$	12.2	10.4	9.1	7.6	5.7
$P_t^{\eta>5}$	5.2	5.1	5.0	4.9	4.6
$(P_t^Z - P_t^{part})/P_t^Z$	0.0267	0.0141	0.0091	0.0076	0.0047
$(P_t^J - P_t^{part})/P_t^J$	-0.0222	-0.0137	-0.0089	-0.0037	-0.0066
$(P_t^Z - P_t^J)/P_t^Z$	0.0384	0.0214	0.0133	0.0079	0.0077
$P_t(O+\eta>5)/P_t^Z$	0.0303	0.0137	0.0061	0.0017	0.0024
$1 - \cos(\Delta\phi)$	0.0037	0.0035	0.0032	0.0026	0.0017
$\sigma(Db[Z, J])$	0.1721	0.1382	0.1163	0.0944	0.0778
Entries	17852	14829	12043	7748	1606

 Table 8: Selection 1.  $\Delta\phi_{(Z,jet)} = 180^\circ \pm 10^\circ$ . UA2 algorithm.

$P_t^{clust}_{CUT}$	30	20	15	10	5
Nevent	11917	10088	8332	5350	1099
$P_t 56$	16.1	13.8	12.2	10.5	8.3
$\Delta\phi$	4.1	3.9	3.7	3.4	2.6
$P_t^{out}$	12.0	10.4	9.2	7.7	5.8
$P_t^{\eta>5}$	5.1	5.1	5.0	4.9	4.5
$(P_t^Z - P_t^{part})/P_t^Z$	0.0266	0.0162	0.0122	0.0111	0.0093
$(P_t^J - P_t^{part})/P_t^J$	-0.0275	-0.0238	-0.0209	-0.0166	-0.0181
$(P_t^Z - P_t^J)/P_t^Z$	0.0441	0.0328	0.0276	0.0237	0.0230
$P_t(O+\eta>5)/P_t^Z$	0.0362	0.0252	0.0203	0.0175	0.0170
$1 - \cos(\Delta\phi)$	0.0037	0.0035	0.0032	0.0026	0.0018
$\sigma(Db[Z, J])$	0.1655	0.1347	0.1152	0.0938	0.0763
Entries	18413	15588	12874	8267	1698

 Table 9: Selection 1.  $\Delta\phi_{(Z,jet)} = 180^\circ \pm 10^\circ$ . LUCELL algorithm.

$P_t^{clust}_{CUT}$	30	20	15	10	5
Nevent	11986	10121	8209	5192	1021
$P_t 56$	15.9	13.6	11.9	9.9	7.4
$\Delta\phi$	4.1	4.0	3.8	3.4	2.6
$P_t^{out}$	12.2	10.5	9.2	7.7	5.7
$P_t^{\eta>5}$	5.2	5.1	5.0	4.9	4.5
$(P_t^Z - P_t^{part})/P_t^Z$	0.0270	0.0158	0.0093	0.0063	0.0006
$(P_t^J - P_t^{part})/P_t^J$	-0.0250	-0.0198	-0.0161	-0.0104	-0.0142
$(P_t^Z - P_t^J)/P_t^Z$	0.0427	0.0291	0.0206	0.0134	0.0114
$P_t(O+\eta>5)/P_t^Z$	0.0347	0.0214	0.0134	0.0073	0.0062
$1 - \cos(\Delta\phi)$	0.0038	0.0035	0.0032	0.0027	0.0017
$\sigma(Db[Z, J])$	0.1684	0.1391	0.1174	0.0948	0.0771
Entries	18520	15639	12684	8023	1577

Table 10: Selection 1.  $\Delta\phi_{(Z,jet)} = 180^\circ \pm 5^\circ$ . UA1 algorithm.

$P_t^{clust}_{CUT}$	30	20	15	10	5
Nevent	7410	6408	5471	3787	899
$P_t 56$	14.1	12.0	10.8	9.1	7.2
$\Delta\phi$	2.3	2.3	2.3	2.2	2.0
$P_t^{out}$	10.5	8.9	7.9	6.7	5.3
$P_t^{\eta>5}$	5.0	5.0	4.9	4.8	4.3
$(P_t^Z - P_t^{part})/P_t^Z$	0.0221	0.0115	0.0081	0.0061	0.0031
$(P_t^J - P_t^{part})/P_t^J$	-0.0171	-0.0091	-0.0054	-0.0018	-0.0053
$(P_t^Z - P_t^J)/P_t^Z$	0.0302	0.0152	0.0093	0.0047	0.0051
$P_t(O+\eta>5)/P_t^Z$	0.0252	0.0103	0.0044	0.0006	0.0010
$1 - \cos(\Delta\phi)$	0.0011	0.0011	0.0011	0.0010	0.0009
$\sigma(Db[Z, J])$	0.1597	0.1294	0.1112	0.0905	0.0728
Entries	11449	9901	8454	5851	1389

 Table 11: Selection 1.  $\Delta\phi_{(Z,jet)} = 180^\circ \pm 5^\circ$ . UA2 algorithm.

$P_t^{clust}_{CUT}$	30	20	15	10	5
Nevent	7657	6737	5821	4029	942
$P_t 56$	14.1	12.2	11.1	9.5	7.7
$\Delta\phi$	2.3	2.3	2.3	2.2	2.0
$P_t^{out}$	10.3	8.9	8.0	6.9	5.4
$P_t^{\eta>5}$	5.0	4.9	4.9	4.7	4.2
$(P_t^Z - P_t^{part})/P_t^Z$	0.0217	0.0127	0.0109	0.0096	0.0087
$(P_t^J - P_t^{part})/P_t^J$	-0.0242	-0.0205	-0.0181	-0.0153	-0.0162
$(P_t^Z - P_t^J)/P_t^Z$	0.0372	0.0270	0.0240	0.0214	0.0209
$P_t(O+\eta>5)/P_t^Z$	0.0320	0.0219	0.0188	0.0172	0.0163
$1 - \cos(\Delta\phi)$	0.0011	0.0011	0.0011	0.0010	0.0009
$\sigma(Db[Z, J])$	0.1538	0.1270	0.1105	0.0897	0.0733
Entries	11831	10409	8994	6225	1456

 Table 12: Selection 1.  $\Delta\phi_{(Z,jet)} = 180^\circ \pm 5^\circ$ . LUCELL algorithm.

$P_t^{clust}_{CUT}$	30	20	15	10	5
Nevent	7648	6700	5713	3892	876
$P_t 56$	14.0	12.1	10.7	8.9	6.7
$\Delta\phi$	2.3	2.3	2.3	2.2	1.9
$P_t^{out}$	10.4	9.0	8.1	6.8	5.3
$P_t^{\eta>5}$	5.0	5.0	4.9	4.7	4.3
$(P_t^Z - P_t^{part})/P_t^Z$	0.0231	0.0134	0.0083	0.0045	-0.0027
$(P_t^J - P_t^{part})/P_t^J$	-0.0196	-0.0154	-0.0129	-0.0089	-0.0142
$(P_t^Z - P_t^J)/P_t^Z$	0.0349	0.0232	0.0167	0.0101	0.0084
$P_t(O+\eta>5)/P_t^Z$	0.0300	0.0184	0.0118	0.0060	0.0045
$1 - \cos(\Delta\phi)$	0.0011	0.0011	0.0011	0.0010	0.0008
$\sigma(Db[Z, J])$	0.1566	0.1310	0.1127	0.0911	0.0723
Entries	11818	10353	8827	6014	1354

Table 13: Selection 2.  $\Delta\phi_{(Z,jet)} = 180^\circ \pm 15^\circ$ ,  $\epsilon^{jet} < 5\%$ . UA1 algorithm.

$P_t^{clust}_{CUT}$	30	20	15	10	5
Nevent	7623	6466	5291	3473	818
$P_t 56$	15.8	13.6	11.9	9.9	7.5
$\Delta\phi$	5.3	4.9	4.4	3.7	2.7
$P_t^{out}$	12.4	10.7	9.4	7.7	5.7
$P_t^{\eta>5}$	5.1	5.1	5.0	4.9	4.5
$(P_t^Z - P_t^{part})/P_t^Z$	-0.0125	-0.0126	-0.0107	-0.0069	-0.0052
$(P_t^J - P_t^{part})/P_t^J$	-0.0016	-0.0031	-0.0028	-0.0021	-0.0052
$(P_t^Z - P_t^J)/P_t^Z$	-0.0146	-0.0125	-0.0105	-0.0070	-0.0018
$P_t(O+\eta>5)/P_t^Z$	-0.0246	-0.0214	-0.0181	-0.0129	-0.0058
$1 - \cos(\Delta\phi)$	0.0067	0.0058	0.0047	0.0034	0.0020
$\sigma(Db[Z, J])$	0.1534	0.1263	0.1085	0.0891	0.0686
Entries	11778	9991	8175	5367	1264

Table 14: Selection 2.  $\Delta\phi_{(Z,jet)} = 180^\circ \pm 15^\circ$ ,  $\epsilon^{jet} < 4\%$ . UA2 algorithm.

$P_t^{clust}_{CUT}$	30	20	15	10	5
Nevent	4198	3593	2975	1975	485
$P_t 56$	15.5	13.3	11.7	9.7	7.4
$\Delta\phi$	5.2	4.8	4.3	3.6	2.7
$P_t^{out}$	12.2	10.6	9.3	7.7	5.6
$P_t^{\eta>5}$	5.1	5.0	5.0	4.9	4.4
$(P_t^Z - P_t^{part})/P_t^Z$	-0.0294	-0.0261	-0.0215	-0.0146	-0.0095
$(P_t^J - P_t^{part})/P_t^J$	-0.0205	-0.0220	-0.0213	-0.0192	-0.0214
$(P_t^Z - P_t^J)/P_t^Z$	-0.0127	-0.0075	-0.0030	0.0025	0.0097
$P_t(O+\eta>5)/P_t^Z$	-0.0227	-0.0163	-0.0108	-0.0031	0.0059
$1 - \cos(\Delta\phi)$	0.0065	0.0056	0.0046	0.0032	0.0019
$\sigma(Db[Z, J])$	0.1509	0.1260	0.1089	0.0896	0.0695
Entries	6487	5552	4597	3052	749

Table 15: Selection 2.  $\Delta\phi_{(Z,jet)} = 180^\circ \pm 15^\circ$ ,  $\epsilon^{jet} < 5\%$ . LUCELL algorithm.

$P_t^{clust}_{CUT}$	30	20	15	10	5
Nevent	7835	6688	5471	3569	814
$P_t 56$	15.6	13.5	11.8	9.8	7.3
$\Delta\phi$	5.3	4.9	4.4	3.7	2.7
$P_t^{out}$	12.3	10.8	9.4	7.7	5.6
$P_t^{\eta>5}$	5.1	5.1	5.0	4.9	4.5
$(P_t^Z - P_t^{part})/P_t^Z$	-0.0130	-0.0131	-0.0115	-0.0084	-0.0066
$(P_t^J - P_t^{part})/P_t^J$	-0.0080	-0.0087	-0.0085	-0.0076	-0.0106
$(P_t^Z - P_t^J)/P_t^Z$	-0.0088	-0.0075	-0.0056	-0.0030	0.0022
$P_t(O+\eta>5)/P_t^Z$	-0.0189	-0.0165	-0.0133	-0.0090	-0.0019
$1 - \cos(\Delta\phi)$	0.0067	0.0058	0.0048	0.0035	0.0020
$\sigma(Db[Z, J])$	0.1523	0.1269	0.1092	0.0894	0.0692
Entries	12107	10334	8454	5515	1258

Table 16: Selection 3.  $\Delta\phi_{(Z,jet)} = 180^\circ \pm 15^\circ$ ,  $\epsilon^{jet} < 5\%$ . UA1 algorithm.

$P_t^{clust}_{CUT}$	30	20	15	10	5
Nevent	4945	4250	3496	2275	539
$P_t 56$	15.4	13.4	11.8	9.7	7.3
$\Delta\phi$	5.1	4.8	4.3	3.6	2.7
$P_t^{out}$	12.2	10.7	9.4	7.7	5.6
$P_t^{\eta>5}$	5.0	5.0	5.0	4.9	4.4
$(P_t^Z - P_t^{part})/P_t^Z$	-0.0233	-0.0209	-0.0182	-0.0126	-0.0081
$(P_t^J - P_t^{part})/P_t^J$	-0.0019	-0.0041	-0.0032	-0.0031	-0.0065
$(P_t^Z - P_t^J)/P_t^Z$	-0.0247	-0.0197	-0.0174	-0.0116	-0.0033
$P_t(O+\eta>5)/P_t^Z$	-0.0344	-0.0285	-0.0250	-0.0175	-0.0073
$1 - \cos(\Delta\phi)$	0.0064	0.0056	0.0046	0.0033	0.0020
$\sigma(Db[Z, J])$	0.1487	0.1257	0.1078	0.0889	0.0684
Entries	7641	6567	5402	3515	833

Table 17: Selection 3.  $\Delta\phi_{(Z,jet)} = 180^\circ \pm 15^\circ$ ,  $\epsilon^{jet} < 5\%$ . UA2 algorithm.

$P_t^{clust}_{CUT}$	30	20	15	10	5
Nevent	4945	4250	3496	2275	539
$P_t 56$	15.4	13.4	11.8	9.7	7.3
$\Delta\phi$	5.2	4.8	4.3	3.6	2.7
$P_t^{out}$	12.1	10.6	9.3	7.7	5.7
$P_t^{\eta>5}$	5.0	5.0	5.0	4.9	4.4
$(P_t^Z - P_t^{part})/P_t^Z$	-0.0233	-0.0209	-0.0182	-0.0126	-0.0081
$(P_t^J - P_t^{part})/P_t^J$	-0.0201	-0.0220	-0.0207	-0.0204	-0.0228
$(P_t^Z - P_t^J)/P_t^Z$	-0.0070	-0.0022	-0.0002	0.0053	0.0126
$P_t(O+\eta>5)/P_t^Z$	-0.0167	-0.0111	-0.0079	-0.0007	0.0085
$1 - \cos(\Delta\phi)$	0.0064	0.0056	0.0046	0.0033	0.0020
$\sigma(Db[Z, J])$	0.1492	0.1259	0.1081	0.0897	0.0688
Entries	7641	6567	5402	3515	833

Table 18: Selection 3.  $\Delta\phi_{(Z,jet)} = 180^\circ \pm 15^\circ$ ,  $\epsilon^{jet} < 5\%$ . LUCELL algorithm.

$P_t^{clust}_{CUT}$	30	20	15	10	5
Nevent	4945	4250	3496	2275	539
$P_t 56$	15.4	13.4	11.8	9.7	7.3
$\Delta\phi$	5.2	4.8	4.3	3.6	2.7
$P_t^{out}$	12.2	10.7	9.4	7.7	5.6
$P_t^{\eta>5}$	5.0	5.0	5.0	4.9	4.4
$(P_t^Z - P_t^{part})/P_t^Z$	-0.0233	-0.0209	-0.0182	-0.0126	-0.0081
$(P_t^J - P_t^{part})/P_t^J$	-0.0063	-0.0080	-0.0072	-0.0065	-0.0089
$(P_t^Z - P_t^J)/P_t^Z$	-0.0205	-0.0159	-0.0135	-0.0082	-0.0009
$P_t(O+\eta>5)/P_t^Z$	-0.0302	-0.0247	-0.0212	-0.0142	-0.0050
$1 - \cos(\Delta\phi)$	0.0064	0.0056	0.0046	0.0033	0.0020
$\sigma(Db[Z, J])$	0.1494	0.1263	0.1085	0.0894	0.0682
Entries	7641	6567	5402	3515	833

**Appendix 4** $100 < P_t^Z < 120 \text{ GeV}/c$ Table 1: Selection 1.  $\Delta\phi_{(Z,jet)} = 180^\circ \pm 180^\circ$ . UA1 algorithm.

$P_t^{clust}_{CUT}$	30	20	15	10	5
Nevent*	9840	6949	5114	2944	586
$P_t 56$	21.9	17.0	14.4	11.7	8.6
$\Delta\phi$	6.0	4.4	3.6	2.8	2.1
$P_t^{out}$	17.4	13.0	10.6	8.0	5.6
$P_t^{\eta>5}$	5.8	5.6	5.5	5.4	5.1
$(P_t^Z - P_t^{part})/P_t^Z$	0.0322	0.0183	0.0129	0.0104	0.0052
$(P_t^J - P_t^{part})/P_t^J$	-0.0166	-0.0082	-0.0035	0.0007	-0.0014
$(P_t^Z - P_t^J)/P_t^Z$	0.0400	0.0208	0.0121	0.0061	0.0040
$P_t(O+\eta>5)/P_t^Z$	0.0244	0.0107	0.0040	-0.0002	-0.0001
$1 - \cos(\Delta\phi)$	0.0102	0.0052	0.0034	0.0020	0.0013
$\sigma(Db[Z, J])^{**}$	0.1442	0.1093	0.0920	0.0751	0.0602
Entries	28431	20078	14777	8505	1694

Table 2: Selection 1.  $\Delta\phi_{(Z,jet)} = 180^\circ \pm 180^\circ$ . UA2 algorithm.

$P_t^{clust}_{CUT}$	30	20	15	10	5
Nevent	10518	7623	5697	3306	640
$P_t 56$	22.2	17.6	15.1	12.5	9.5
$\Delta\phi$	5.9	4.3	3.6	2.8	2.1
$P_t^{out}$	17.0	12.9	10.6	8.2	5.8
$P_t^{\eta>5}$	5.8	5.6	5.5	5.4	5.0
$(P_t^Z - P_t^{part})/P_t^Z$	0.0341	0.0225	0.0181	0.0162	0.0121
$(P_t^J - P_t^{part})/P_t^J$	-0.0164	-0.0110	-0.0081	-0.0049	-0.0043
$(P_t^Z - P_t^J)/P_t^Z$	0.0422	0.0275	0.0214	0.0169	0.0141
$P_t(O+\eta>5)/P_t^Z$	0.0269	0.0174	0.0135	0.0107	0.0100
$1 - \cos(\Delta\phi)$	0.0098	0.0051	0.0034	0.0020	0.0013
$\sigma(Db[Z, J])$	0.1394	0.1076	0.0913	0.0759	0.0596
Entries	30391	22026	16462	9553	1848

Table 3: Selection 1.  $\Delta\phi_{(Z,jet)} = 180^\circ \pm 180^\circ$ . LUCELL algorithm.

$P_t^{clust}_{CUT}$	30	20	15	10	5
Nevent	9967	7202	5295	2996	568
$P_t 56$	21.4	17.0	14.3	11.4	8.1
$\Delta\phi$	5.8	4.4	3.6	2.8	2.1
$P_t^{out}$	17.0	13.1	10.7	8.1	5.6
$P_t^{\eta>5}$	5.8	5.7	5.5	5.4	5.1
$(P_t^Z - P_t^{part})/P_t^Z$	0.0311	0.0185	0.0120	0.0083	0.0008
$(P_t^J - P_t^{part})/P_t^J$	-0.0195	-0.0132	-0.0099	-0.0059	-0.0072
$(P_t^Z - P_t^J)/P_t^Z$	0.0424	0.0259	0.0172	0.0101	0.0053
$P_t(O+\eta>5)/P_t^Z$	0.0275	0.0156	0.0090	0.0038	0.0012
$1 - \cos(\Delta\phi)$	0.0095	0.0053	0.0035	0.0021	0.0013
$\sigma(Db[Z, J])$	0.1399	0.1101	0.0933	0.0767	0.0609
Entries	28798	20809	15300	8658	1640

\*Number of events (Nevent) is given in this and in the following tables for integrated luminosity  $L_{int} = 10 \text{ fb}^{-1}$   
\*\*  $Db[Z, J] \equiv (P_t^Z - P_t^J)/P_t^Z$

Table 4: Selection 1.  $\Delta\phi_{(Z,jet)} = 180^\circ \pm 15^\circ$ . UA1 algorithm.

$P_t^{clust}_{CUT}$	30	20	15	10	5
Nevent	9125	6803	5077	2939	585
$P_t 56$	20.3	16.6	14.2	11.6	8.5
$\Delta\phi$	4.9	4.1	3.5	2.7	2.0
$P_t^{out}$	15.7	12.5	10.5	8.0	5.6
$P_t^{\eta>5}$	5.7	5.6	5.4	5.4	5.0
$(P_t^Z - P_t^{part})/P_t^Z$	0.0266	0.0170	0.0123	0.0103	0.0048
$(P_t^J - P_t^{part})/P_t^J$	-0.0150	-0.0080	-0.0036	0.0007	-0.0014
$(P_t^Z - P_t^J)/P_t^Z$	0.0336	0.0195	0.0115	0.0060	0.0036
$P_t(O+\eta>5)/P_t^Z$	0.0225	0.0104	0.0038	-0.0002	-0.0003
$1 - \cos(\Delta\phi)$	0.0058	0.0042	0.0031	0.0019	0.0011
$\sigma(Db[Z, J])$	0.1382	0.1080	0.0916	0.0750	0.0596
Entries	26365	19658	14669	8491	1690

 Table 5: Selection 1.  $\Delta\phi_{(Z,jet)} = 180^\circ \pm 15^\circ$ . UA2 algorithm.

$P_t^{clust}_{CUT}$	30	20	15	10	5
Nevent	9798	7478	5661	3302	639
$P_t 56$	20.6	17.3	14.9	12.5	9.5
$\Delta\phi$	4.8	4.1	3.5	2.7	2.0
$P_t^{out}$	15.4	12.5	10.5	8.2	5.8
$P_t^{\eta>5}$	5.7	5.6	5.4	5.4	5.0
$(P_t^Z - P_t^{part})/P_t^Z$	0.0286	0.0215	0.0177	0.0162	0.0119
$(P_t^J - P_t^{part})/P_t^J$	-0.0152	-0.0106	-0.0080	-0.0049	-0.0042
$(P_t^Z - P_t^J)/P_t^Z$	0.0362	0.0262	0.0209	0.0168	0.0139
$P_t(O+\eta>5)/P_t^Z$	0.0251	0.0171	0.0133	0.0107	0.0100
$1 - \cos(\Delta\phi)$	0.0057	0.0042	0.0031	0.0020	0.0011
$\sigma(Db[Z, J])$	0.1337	0.1064	0.0907	0.0758	0.0593
Entries	28311	21607	16358	9541	1845

 Table 6: Selection 1.  $\Delta\phi_{(Z,jet)} = 180^\circ \pm 15^\circ$ . LUCELL algorithm.

$P_t^{clust}_{CUT}$	30	20	15	10	5
Nevent	9317	7047	5255	2991	566
$P_t 56$	20.0	16.6	14.1	11.4	8.0
$\Delta\phi$	4.8	4.1	3.5	2.7	2.0
$P_t^{out}$	15.5	12.7	10.6	8.1	5.6
$P_t^{\eta>5}$	5.7	5.6	5.5	5.4	5.0
$(P_t^Z - P_t^{part})/P_t^Z$	0.0265	0.0172	0.0115	0.0082	0.0005
$(P_t^J - P_t^{part})/P_t^J$	-0.0181	-0.0128	-0.0097	-0.0058	-0.0072
$(P_t^Z - P_t^J)/P_t^Z$	0.0370	0.0244	0.0166	0.0100	0.0050
$P_t(O+\eta>5)/P_t^Z$	0.0260	0.0152	0.0087	0.0038	0.0010
$1 - \cos(\Delta\phi)$	0.0057	0.0043	0.0032	0.0020	0.0011
$\sigma(Db[Z, J])$	0.1349	0.1087	0.0927	0.0766	0.0604
Entries	26920	20362	15184	8643	1636

Table 7: Selection 1.  $\Delta\phi_{(Z,jet)} = 180^\circ \pm 10^\circ$ . UA1 algorithm.

$P_t^{clust}_{CUT}$	30	20	15	10	5
Nevent	7979	6323	4882	2897	581
$P_t 56$	18.7	15.7	13.7	11.4	8.4
$\Delta\phi$	3.8	3.5	3.1	2.6	2.0
$P_t^{out}$	14.0	11.7	10.0	7.9	5.6
$P_t^{\eta>5}$	5.6	5.5	5.4	5.3	4.9
$(P_t^Z - P_t^{part})/P_t^Z$	0.0233	0.0155	0.0114	0.0098	0.0049
$(P_t^J - P_t^{part})/P_t^J$	-0.0126	-0.0072	-0.0032	0.0007	-0.0014
$(P_t^Z - P_t^J)/P_t^Z$	0.0288	0.0175	0.0103	0.0055	0.0037
$P_t(O+\eta>5)/P_t^Z$	0.0204	0.0099	0.0034	-0.0004	-0.0001
$1 - \cos(\Delta\phi)$	0.0033	0.0029	0.0024	0.0017	0.0010
$\sigma(Db[Z, J])$	0.1332	0.1061	0.0901	0.0742	0.0591
Entries	23056	18271	14105	8371	1679

 Table 8: Selection 1.  $\Delta\phi_{(Z,jet)} = 180^\circ \pm 10^\circ$ . UA2 algorithm.

$P_t^{clust}_{CUT}$	30	20	15	10	5
Nevent	8590	6952	5449	3256	634
$P_t 56$	19.1	16.4	14.5	12.3	9.3
$\Delta\phi$	3.8	3.5	3.1	2.6	2.0
$P_t^{out}$	13.8	11.7	10.1	8.1	5.8
$P_t^{\eta>5}$	5.6	5.5	5.4	5.3	4.8
$(P_t^Z - P_t^{part})/P_t^Z$	0.0250	0.0199	0.0165	0.0157	0.0116
$(P_t^J - P_t^{part})/P_t^J$	-0.0140	-0.0101	-0.0080	-0.0050	-0.0042
$(P_t^Z - P_t^J)/P_t^Z$	0.0319	0.0243	0.0198	0.0164	0.0135
$P_t(O+\eta>5)/P_t^Z$	0.0235	0.0168	0.0129	0.0106	0.0097
$1 - \cos(\Delta\phi)$	0.0033	0.0028	0.0024	0.0017	0.0010
$\sigma(Db[Z, J])$	0.1290	0.1044	0.0894	0.0749	0.0574
Entries	24819	20086	15744	9407	1832

 Table 9: Selection 1.  $\Delta\phi_{(Z,jet)} = 180^\circ \pm 10^\circ$ . LUCELL algorithm.

$P_t^{clust}_{CUT}$	30	20	15	10	5
Nevent	8188	6546	5051	2951	563
$P_t 56$	18.5	15.7	13.6	11.2	7.9
$\Delta\phi$	3.8	3.5	3.2	2.6	2.0
$P_t^{out}$	14.0	11.8	10.1	8.0	5.6
$P_t^{\eta>5}$	5.6	5.5	5.4	5.3	4.9
$(P_t^Z - P_t^{part})/P_t^Z$	0.0229	0.0155	0.0103	0.0079	0.0007
$(P_t^J - P_t^{part})/P_t^J$	-0.0163	-0.0123	-0.0096	-0.0058	-0.0072
$(P_t^Z - P_t^J)/P_t^Z$	0.0324	0.0224	0.0152	0.0096	0.0052
$P_t(O+\eta>5)/P_t^Z$	0.0240	0.0148	0.0082	0.0037	0.0012
$1 - \cos(\Delta\phi)$	0.0033	0.0029	0.0024	0.0017	0.0010
$\sigma(Db[Z, J])$	0.1308	0.1069	0.0915	0.0760	0.0601
Entries	23659	18915	14593	8528	1628

Table 10: Selection 1.  $\Delta\phi_{(Z,jet)} = 180^\circ \pm 5^\circ$ . UA1 algorithm.

$P_t^{clust}_{CUT}$	30	20	15	10	5
Nevent	5491	4657	3850	2514	546
$P_t 56$	16.4	14.0	12.4	10.6	8.0
$\Delta\phi$	2.2	2.2	2.1	2.0	1.7
$P_t^{out}$	11.7	9.9	8.7	7.3	5.4
$P_t^{\eta>5}$	5.5	5.3	5.2	5.1	4.7
$(P_t^Z - P_t^{part})/P_t^Z$	0.0203	0.0141	0.0108	0.0090	0.0055
$(P_t^J - P_t^{part})/P_t^J$	-0.0090	-0.0049	-0.0017	0.0007	-0.0005
$(P_t^Z - P_t^J)/P_t^Z$	0.0229	0.0141	0.0086	0.0047	0.0038
$P_t(O+\eta>5)/P_t^Z$	0.0172	0.0087	0.0035	-0.0001	0.0005
$1 - \cos(\Delta\phi)$	0.0011	0.0010	0.0010	0.0009	0.0007
$\sigma(Db[Z, J])$	0.1248	0.1018	0.0869	0.0724	0.0561
Entries	15866	13457	11125	7263	1579

 Table 11: Selection 1.  $\Delta\phi_{(Z,jet)} = 180^\circ \pm 5^\circ$ . UA2 algorithm.

$P_t^{clust}_{CUT}$	30	20	15	10	5
Nevent	5935	5124	4285	2822	597
$P_t 56$	16.7	14.7	13.2	11.5	9.0
$\Delta\phi$	2.2	2.2	2.1	2.0	1.7
$P_t^{out}$	11.5	9.9	8.8	7.4	5.6
$P_t^{\eta>5}$	5.4	5.3	5.2	5.1	4.6
$(P_t^Z - P_t^{part})/P_t^Z$	0.0224	0.0185	0.0162	0.0150	0.0127
$(P_t^J - P_t^{part})/P_t^J$	-0.0108	-0.0080	-0.0060	-0.0044	-0.0029
$(P_t^Z - P_t^J)/P_t^Z$	0.0271	0.0215	0.0180	0.0155	0.0137
$P_t(O+\eta>5)/P_t^Z$	0.0213	0.0162	0.0131	0.0110	0.0104
$1 - \cos(\Delta\phi)$	0.0011	0.0010	0.0010	0.0009	0.0007
$\sigma(Db[Z, J])$	0.1205	0.0999	0.0856	0.0723	0.0545
Entries	17150	14806	12380	8153	1726

 Table 12: Selection 1.  $\Delta\phi_{(Z,jet)} = 180^\circ \pm 5^\circ$ . LUCELL algorithm.

$P_t^{clust}_{CUT}$	30	20	15	10	5
Nevent	5621	4788	3958	2556	531
$P_t 56$	16.2	13.9	12.2	10.3	7.5
$\Delta\phi$	2.2	2.2	2.1	2.0	1.7
$P_t^{out}$	11.6	10.0	8.8	7.3	5.4
$P_t^{\eta>5}$	5.5	5.4	5.2	5.1	4.7
$(P_t^Z - P_t^{part})/P_t^Z$	0.0195	0.0137	0.0094	0.0067	0.0013
$(P_t^J - P_t^{part})/P_t^J$	-0.0136	-0.0101	-0.0082	-0.0059	-0.0061
$(P_t^Z - P_t^J)/P_t^Z$	0.0268	0.0187	0.0132	0.0086	0.0051
$P_t(O+\eta>5)/P_t^Z$	0.0211	0.0134	0.0081	0.0037	0.0018
$1 - \cos(\Delta\phi)$	0.0011	0.0010	0.0010	0.0009	0.0007
$\sigma(Db[Z, J])$	0.1228	0.1023	0.0880	0.0738	0.0565
Entries	16241	13834	11437	7385	1534

Table 13: Selection 2.  $\Delta\phi_{(Z,jet)} = 180^\circ \pm 15^\circ$ ,  $\epsilon^{jet} < 4\%$ . UA1 algorithm.

$P_t^{clust}_{CUT}$	30	20	15	10	5
Nevent	5597	4453	3499	2187	493
$P_t 56$	18.3	15.2	13.1	10.8	8.0
$\Delta\phi$	4.6	3.9	3.3	2.7	2.0
$P_t^{out}$	14.2	11.7	9.9	7.8	5.5
$P_t^{\eta>5}$	5.5	5.4	5.3	5.2	5.0
$(P_t^Z - P_t^{part})/P_t^Z$	-0.0041	-0.0034	-0.0037	-0.0009	-0.0021
$(P_t^J - P_t^{part})/P_t^J$	-0.0037	-0.0026	-0.0017	0.0001	-0.0044
$(P_t^Z - P_t^J)/P_t^Z$	-0.0038	-0.0035	-0.0045	-0.0029	0.0000
$P_t(O+\eta>5)/P_t^Z$	-0.0130	-0.0109	-0.0105	-0.0076	-0.0037
$1 - \cos(\Delta\phi)$	0.0053	0.0039	0.0029	0.0019	0.0011
$\sigma(Db[Z, J])$	0.1206	0.0963	0.0822	0.0668	0.0575
Entries	16173	12867	10110	6319	1424

Table 14: Selection 2.  $\Delta\phi_{(Z,jet)} = 180^\circ \pm 15^\circ$ ,  $\epsilon^{jet} < 4\%$ . UA2 algorithm.

$P_t^{clust}_{CUT}$	30	20	15	10	5
Nevent	5859	4677	3664	2290	502
$P_t 56$	18.3	15.3	13.2	11.0	8.3
$\Delta\phi$	4.6	3.9	3.3	2.7	2.0
$P_t^{out}$	14.2	11.7	10.0	7.9	5.6
$P_t^{\eta>5}$	5.5	5.4	5.3	5.2	4.9
$(P_t^Z - P_t^{part})/P_t^Z$	-0.0053	-0.0035	-0.0032	0.0000	0.0001
$(P_t^J - P_t^{part})/P_t^J$	-0.0155	-0.0143	-0.0131	-0.0110	-0.0126
$(P_t^Z - P_t^J)/P_t^Z$	0.0067	0.0079	0.0074	0.0090	0.0108
$P_t(O+\eta>5)/P_t^Z$	-0.0024	0.0006	0.0016	0.0044	0.0073
$1 - \cos(\Delta\phi)$	0.0053	0.0039	0.0029	0.0019	0.0012
$\sigma(Db[Z, J])$	0.1181	0.0959	0.0817	0.0672	0.0567
Entries	16928	13513	10586	6617	1450

Table 15: Selection 2.  $\Delta\phi_{(Z,jet)} = 180^\circ \pm 15^\circ$ ,  $\epsilon^{jet} < 4\%$ . LUCELL algorithm.

$P_t^{clust}_{CUT}$	30	20	15	10	5
Nevent	5639	4525	3554	2205	493
$P_t 56$	17.9	15.0	12.9	10.5	7.8
$\Delta\phi$	4.6	3.9	3.3	2.7	2.0
$P_t^{out}$	14.1	11.7	10.0	7.8	5.5
$P_t^{\eta>5}$	5.5	5.4	5.3	5.2	4.9
$(P_t^Z - P_t^{part})/P_t^Z$	-0.0046	-0.0045	-0.0051	-0.0029	-0.0040
$(P_t^J - P_t^{part})/P_t^J$	-0.0083	-0.0072	-0.0065	-0.0043	-0.0073
$(P_t^Z - P_t^J)/P_t^Z$	0.0004	-0.0001	-0.0011	-0.0005	0.0010
$P_t(O+\eta>5)/P_t^Z$	-0.0088	-0.0075	-0.0072	-0.0053	-0.0026
$1 - \cos(\Delta\phi)$	0.0052	0.0039	0.0029	0.0019	0.0011
$\sigma(Db[Z, J])$	0.1189	0.0966	0.0830	0.0672	0.0572
Entries	16292	13074	10268	6371	1425

Table 16: Selection 3.  $\Delta\phi_{(Z,jet)} = 180^\circ \pm 15^\circ$ ,  $\epsilon^{jet} < 4\%$ . UA1 algorithm.

$P_t^{clust}_{CUT}$	30	20	15	10	5
Nevent	4686	3785	2962	1846	400
$P_t 56$	17.8	15.0	12.8	10.5	7.7
$\Delta\phi$	4.5	3.9	3.3	2.7	2.0
$P_t^{out}$	13.9	11.7	9.9	7.8	5.5
$P_t^{\eta>5}$	5.5	5.4	5.3	5.2	4.9
$(P_t^Z - P_t^{part})/P_t^Z$	-0.0074	-0.0067	-0.0066	-0.0034	-0.0058
$(P_t^J - P_t^{part})/P_t^J$	-0.0048	-0.0042	-0.0034	-0.0023	-0.0061
$(P_t^Z - P_t^J)/P_t^Z$	-0.0058	-0.0052	-0.0055	-0.0031	-0.0015
$P_t(O+\eta>5)/P_t^Z$	-0.0149	-0.0125	-0.0115	-0.0079	-0.0049
$1 - \cos(\Delta\phi)$	0.0051	0.0038	0.0028	0.0019	0.0012
$\sigma(Db[Z, J])$	0.1169	0.0960	0.0815	0.0669	0.0553
Entries	13541	10935	8559	5333	1157

Table 17: Selection 3.  $\Delta\phi_{(Z,jet)} = 180^\circ \pm 15^\circ$ ,  $\epsilon^{jet} < 4\%$ . UA2 algorithm.

$P_t^{clust}_{CUT}$	30	20	15	10	5
Nevent	4686	3785	2962	1846	400
$P_t 56$	17.8	15.0	12.8	10.5	7.7
$\Delta\phi$	4.5	3.9	3.3	2.7	2.0
$P_t^{out}$	13.9	11.7	9.9	7.8	5.6
$P_t^{\eta>5}$	5.5	5.4	5.3	5.2	4.9
$(P_t^Z - P_t^{part})/P_t^Z$	-0.0074	-0.0067	-0.0066	-0.0034	-0.0058
$(P_t^J - P_t^{part})/P_t^J$	-0.0176	-0.0169	-0.0160	-0.0147	-0.0169
$(P_t^Z - P_t^J)/P_t^Z$	0.0065	0.0071	0.0067	0.0090	0.0090
$P_t(O+\eta>5)/P_t^Z$	-0.0026	-0.0003	0.0008	0.0042	0.0056
$1 - \cos(\Delta\phi)$	0.0051	0.0039	0.0029	0.0019	0.0012
$\sigma(Db[Z, J])$	0.1171	0.0963	0.0820	0.0673	0.0555
Entries	13541	10935	8559	5333	1157

Table 18: Selection 3.  $\Delta\phi_{(Z,jet)} = 180^\circ \pm 15^\circ$ ,  $\epsilon^{jet} < 4\%$ . LUCELL algorithm.

$P_t^{clust}_{CUT}$	30	20	15	10	5
Nevent	4686	3785	2962	1846	400
$P_t 56$	17.8	15.0	12.8	10.5	7.7
$\Delta\phi$	4.5	3.9	3.3	2.7	2.0
$P_t^{out}$	14.0	11.7	9.9	7.8	5.5
$P_t^{\eta>5}$	5.5	5.4	5.3	5.2	4.9
$(P_t^Z - P_t^{part})/P_t^Z$	-0.0074	-0.0067	-0.0066	-0.0034	-0.0058
$(P_t^J - P_t^{part})/P_t^J$	-0.0082	-0.0073	-0.0062	-0.0047	-0.0077
$(P_t^Z - P_t^J)/P_t^Z$	-0.0025	-0.0021	-0.0027	-0.0007	0.0000
$P_t(O+\eta>5)/P_t^Z$	-0.0116	-0.0095	-0.0087	-0.0056	-0.0034
$1 - \cos(\Delta\phi)$	0.0051	0.0038	0.0029	0.0019	0.0012
$\sigma(Db[Z, J])$	0.1174	0.0964	0.0819	0.0672	0.0556
Entries	13541	10935	8559	5333	1157

**Appendix 5** $150 < P_t^Z < 200 \text{ GeV}/c$ Table 1: Selection 1.  $\Delta\phi_{(Z,jet)} = 180^\circ \pm 180^\circ$ . UA1 algorithm.

$P_t^{clust}_{CUT}$	30	20	15	10	5
Nevent*	4103	2886	2104	1198	227
$P_t 56$	23.4	18.6	15.8	13.0	10.0
$\Delta\phi$	3.9	2.9	2.4	1.9	1.4
$P_t^{out}$	17.6	13.2	10.8	8.4	6.0
$P_t^{\eta>5}$	6.4	6.3	6.2	6.0	5.5
$(P_t^Z - P_t^{part})/P_t^Z$	0.0186	0.0133	0.0112	0.0104	0.0067
$(P_t^J - P_t^{part})/P_t^J$	-0.0081	-0.0036	-0.0009	0.0012	0.0018
$(P_t^Z - P_t^J)/P_t^Z$	0.0214	0.0126	0.0085	0.0061	0.0028
$P_t(O+\eta>5)/P_t^Z$	0.0123	0.0058	0.0027	0.0014	-0.0011
$1 - \cos(\Delta\phi)$	0.0042	0.0024	0.0015	0.0009	0.0006
$\sigma(Db[Z, J])^{**}$	0.0990	0.0791	0.0684	0.0586	0.0465
Entries	27490	19335	14096	8024	1518

Table 2: Selection 1.  $\Delta\phi_{(Z,jet)} = 180^\circ \pm 180^\circ$ . UA2 algorithm.

$P_t^{clust}_{CUT}$	30	20	15	10	5
Nevent	4585	3309	2464	1421	259
$P_t 56$	24.2	19.7	17.1	14.3	11.3
$\Delta\phi$	3.8	2.9	2.4	1.9	1.4
$P_t^{out}$	17.1	13.1	10.8	8.5	6.0
$P_t^{\eta>5}$	6.4	6.2	6.2	6.0	5.4
$(P_t^Z - P_t^{part})/P_t^Z$	0.0234	0.0186	0.0173	0.0156	0.0110
$(P_t^J - P_t^{part})/P_t^J$	-0.0048	-0.0023	-0.0004	0.0004	0.0013
$(P_t^Z - P_t^J)/P_t^Z$	0.0231	0.0168	0.0142	0.0121	0.0082
$P_t(O+\eta>5)/P_t^Z$	0.0142	0.0101	0.0085	0.0074	0.0048
$1 - \cos(\Delta\phi)$	0.0040	0.0023	0.0015	0.0009	0.0006
$\sigma(Db[Z, J])$	0.0959	0.0772	0.0675	0.0580	0.0439
Entries	30719	22169	16509	9522	1732

Table 3: Selection 1.  $\Delta\phi_{(Z,jet)} = 180^\circ \pm 180^\circ$ . LUCELL algorithm.

$P_t^{clust}_{CUT}$	30	20	15	10	5
Nevent	4123	2966	2165	1205	214
$P_t 56$	22.8	18.4	15.6	12.5	9.4
$\Delta\phi$	3.8	2.9	2.4	1.9	1.4
$P_t^{out}$	17.3	13.4	11.0	8.5	6.0
$P_t^{\eta>5}$	6.4	6.3	6.2	6.0	5.6
$(P_t^Z - P_t^{part})/P_t^Z$	0.0180	0.0125	0.0103	0.0081	0.0039
$(P_t^J - P_t^{part})/P_t^J$	-0.0115	-0.0078	-0.0055	-0.0036	-0.0029
$(P_t^Z - P_t^J)/P_t^Z$	0.0242	0.0161	0.0121	0.0087	0.0042
$P_t(O+\eta>5)/P_t^Z$	0.0153	0.0093	0.0064	0.0040	0.0001
$1 - \cos(\Delta\phi)$	0.0040	0.0024	0.0015	0.0009	0.0006
$\sigma(Db[Z, J])$	0.0974	0.0792	0.0691	0.0585	0.0478
Entries	27621	19870	14502	8071	1431

\*Number of events (Nevent) is given in this and in the following tables for integrated luminosity  $L_{int} = 10 \text{ fb}^{-1}$ \*\*  $Db[Z, J] \equiv (P_t^Z - P_t^J)/P_t^Z$

Table 4: Selection 1.  $\Delta\phi_{(Z,jet)} = 180^\circ \pm 15^\circ$ . UA1 algorithm.

$P_t^{clust}_{CUT}$	30	20	15	10	5
Nevent	4052	2880	2103	1197	226
$P_t 56$	22.9	18.5	15.8	13.0	10.0
$\Delta\phi$	3.7	2.9	2.4	1.9	1.4
$P_t^{out}$	17.1	13.2	10.8	8.4	6.0
$P_t^{\eta>5}$	6.3	6.3	6.2	6.0	5.4
$(P_t^Z - P_t^{part})/P_t^Z$	0.0178	0.0131	0.0111	0.0104	0.0067
$(P_t^J - P_t^{part})/P_t^J$	-0.0078	-0.0036	-0.0009	0.0012	0.0018
$(P_t^Z - P_t^J)/P_t^Z$	0.0204	0.0124	0.0085	0.0061	0.0028
$P_t(O+\eta>5)/P_t^Z$	0.0120	0.0057	0.0027	0.0014	-0.0010
$1 - \cos(\Delta\phi)$	0.0036	0.0022	0.0015	0.0009	0.0005
$\sigma(Db[Z, J])$	0.0976	0.0787	0.0683	0.0586	0.0465
Entries	27148	19298	14089	8022	1517

 Table 5: Selection 1.  $\Delta\phi_{(Z,jet)} = 180^\circ \pm 10^\circ$ . UA2 algorithm.

$P_t^{clust}_{CUT}$	30	20	15	10	5
Nevent	4534	3303	2463	1421	258
$P_t 56$	23.8	19.6	17.1	14.3	11.2
$\Delta\phi$	3.6	2.9	2.4	1.9	1.4
$P_t^{out}$	16.7	13.1	10.8	8.5	6.0
$P_t^{\eta>5}$	6.3	6.2	6.1	6.0	5.4
$(P_t^Z - P_t^{part})/P_t^Z$	0.0227	0.0185	0.0173	0.0156	0.0110
$(P_t^J - P_t^{part})/P_t^J$	-0.0044	-0.0023	-0.0005	0.0004	0.0013
$(P_t^Z - P_t^J)/P_t^Z$	0.0222	0.0166	0.0142	0.0121	0.0083
$P_t(O+\eta>5)/P_t^Z$	0.0140	0.0101	0.0085	0.0074	0.0048
$1 - \cos(\Delta\phi)$	0.0035	0.0022	0.0015	0.0009	0.0005
$\sigma(Db[Z, J])$	0.0946	0.0769	0.0674	0.0580	0.0439
Entries	30379	22130	16501	9520	1731

 Table 6: Selection 1.  $\Delta\phi_{(Z,jet)} = 180^\circ \pm 15^\circ$ . LUCELL algorithm.

$P_t^{clust}_{CUT}$	30	20	15	10	5
Nevent	4080	2960	2163	1204	213
$P_t 56$	22.5	18.3	15.6	12.5	9.4
$\Delta\phi$	3.6	2.9	2.4	1.9	1.4
$P_t^{out}$	16.9	13.3	11.0	8.5	6.0
$P_t^{\eta>5}$	6.3	6.3	6.2	6.0	5.5
$(P_t^Z - P_t^{part})/P_t^Z$	0.0175	0.0123	0.0102	0.0081	0.0039
$(P_t^J - P_t^{part})/P_t^J$	-0.0110	-0.0078	-0.0055	-0.0036	-0.0029
$(P_t^Z - P_t^J)/P_t^Z$	0.0233	0.0159	0.0121	0.0087	0.0043
$P_t(O+\eta>5)/P_t^Z$	0.0152	0.0093	0.0064	0.0041	0.0002
$1 - \cos(\Delta\phi)$	0.0035	0.0022	0.0015	0.0009	0.0005
$\sigma(Db[Z, J])$	0.0963	0.0788	0.0689	0.0585	0.0478
Entries	27334	19833	14494	8069	1430

Table 7: Selection 1.  $\Delta\phi_{(Z,jet)} = 180^\circ \pm 10^\circ$ . UA1 algorithm.

$P_t^{clust}_{CUT}$	30	20	15	10	5
Nevent	3842	2831	2091	1195	226
$P_t 56$	21.9	18.2	15.7	12.9	10.0
$\Delta\phi$	3.2	2.7	2.3	1.9	1.4
$P_t^{out}$	16.0	12.8	10.7	8.4	6.0
$P_t^{\eta>5}$	6.3	6.2	6.2	6.0	5.4
$(P_t^Z - P_t^{part})/P_t^Z$	0.0165	0.0127	0.0110	0.0103	0.0068
$(P_t^J - P_t^{part})/P_t^J$	-0.0074	-0.0034	-0.0008	0.0014	0.0019
$(P_t^Z - P_t^J)/P_t^Z$	0.0188	0.0119	0.0083	0.0060	0.0028
$P_t(O+\eta>5)/P_t^Z$	0.0114	0.0056	0.0026	0.0013	-0.0010
$1 - \cos(\Delta\phi)$	0.0026	0.0019	0.0014	0.0009	0.0005
$\sigma(Db[Z, J])$	0.0959	0.0782	0.0680	0.0583	0.0465
Entries	25739	18965	14012	8009	1515

 Table 8: Selection 1.  $\Delta\phi_{(Z,jet)} = 180^\circ \pm 10^\circ$ . UA2 algorithm.

$P_t^{clust}_{CUT}$	30	20	15	10	5
Nevent	4308	3245	2449	1418	258
$P_t 56$	22.8	19.3	17.0	14.2	11.2
$\Delta\phi$	3.2	2.7	2.3	1.9	1.4
$P_t^{out}$	15.7	12.7	10.7	8.5	6.1
$P_t^{\eta>5}$	6.3	6.2	6.1	5.9	5.3
$(P_t^Z - P_t^{part})/P_t^Z$	0.0214	0.0180	0.0171	0.0156	0.0111
$(P_t^J - P_t^{part})/P_t^J$	-0.0042	-0.0021	-0.0004	0.0005	0.0013
$(P_t^Z - P_t^J)/P_t^Z$	0.0207	0.0160	0.0139	0.0119	0.0083
$P_t(O+\eta>5)/P_t^Z$	0.0136	0.0099	0.0084	0.0073	0.0049
$1 - \cos(\Delta\phi)$	0.0025	0.0019	0.0014	0.0009	0.0005
$\sigma(Db[Z, J])$	0.0930	0.0763	0.0670	0.0577	0.0439
Entries	28861	21739	16409	9500	1727

 Table 9: Selection 1.  $\Delta\phi_{(Z,jet)} = 180^\circ \pm 10^\circ$ . LUCELL algorithm.

$P_t^{clust}_{CUT}$	30	20	15	10	5
Nevent	3884	2907	2152	1202	213
$P_t 56$	21.5	17.9	15.5	12.5	9.4
$\Delta\phi$	3.2	2.8	2.4	1.9	1.4
$P_t^{out}$	15.9	12.9	10.9	8.5	6.0
$P_t^{\eta>5}$	6.3	6.2	6.1	6.0	5.5
$(P_t^Z - P_t^{part})/P_t^Z$	0.0161	0.0117	0.0100	0.0080	0.0039
$(P_t^J - P_t^{part})/P_t^J$	-0.0109	-0.0077	-0.0055	-0.0036	-0.0029
$(P_t^Z - P_t^J)/P_t^Z$	0.0220	0.0153	0.0119	0.0086	0.0043
$P_t(O+\eta>5)/P_t^Z$	0.0148	0.0091	0.0063	0.0040	0.0002
$1 - \cos(\Delta\phi)$	0.0025	0.0019	0.0014	0.0009	0.0005
$\sigma(Db[Z, J])$	0.0948	0.0783	0.0687	0.0584	0.0478
Entries	26020	19473	14415	8056	1428

Table 10: Selection 1.  $\Delta\phi_{(Z,jet)} = 180^\circ \pm 5^\circ$ . UA1 algorithm.

$P_t^{clust}_{CUT}$	30	20	15	10	5
Nevent	2937	2388	1884	1143	223
$P_t 56$	19.3	16.6	14.7	12.5	9.8
$\Delta\phi$	2.1	2.0	1.9	1.7	1.3
$P_t^{out}$	13.2	11.2	9.8	8.1	6.0
$P_t^{\eta>5}$	6.2	6.1	6.0	5.8	5.2
$(P_t^Z - P_t^{part})/P_t^Z$	0.0148	0.0118	0.0102	0.0098	0.0064
$(P_t^J - P_t^{part})/P_t^J$	-0.0052	-0.0021	-0.0004	0.0012	0.0020
$(P_t^Z - P_t^J)/P_t^Z$	0.0152	0.0101	0.0072	0.0056	0.0023
$P_t(O+\eta>5)/P_t^Z$	0.0096	0.0049	0.0022	0.0012	-0.0012
$1 - \cos(\Delta\phi)$	0.0010	0.0009	0.0008	0.0007	0.0004
$\sigma(Db[Z, J])$	0.0909	0.0754	0.0665	0.0577	0.0448
Entries	19676	15996	12622	7657	1495

 Table 11: Selection 1.  $\Delta\phi_{(Z,jet)} = 180^\circ \pm 5^\circ$ . UA2 algorithm.

$P_t^{clust}_{CUT}$	30	20	15	10	5
Nevent	3317	2740	2204	1357	254
$P_t 56$	20.3	17.7	16.1	13.8	11.1
$\Delta\phi$	2.1	2.0	1.9	1.7	1.3
$P_t^{out}$	13.0	11.1	9.8	8.2	6.0
$P_t^{\eta>5}$	6.1	6.0	6.0	5.8	5.1
$(P_t^Z - P_t^{part})/P_t^Z$	0.0196	0.0172	0.0165	0.0153	0.0113
$(P_t^J - P_t^{part})/P_t^J$	-0.0026	-0.0008	0.0006	0.0009	0.0022
$(P_t^Z - P_t^J)/P_t^Z$	0.0177	0.0141	0.0126	0.0115	0.0080
$P_t(O+\eta>5)/P_t^Z$	0.0123	0.0092	0.0078	0.0072	0.0049
$1 - \cos(\Delta\phi)$	0.0009	0.0009	0.0008	0.0007	0.0004
$\sigma(Db[Z, J])$	0.0883	0.0735	0.0652	0.0566	0.0416
Entries	22222	18359	14764	9089	1705

 Table 12: Selection 1.  $\Delta\phi_{(Z,jet)} = 180^\circ \pm 5^\circ$ . UA2 algorithm.

$P_t^{clust}_{CUT}$	30	20	15	10	5
Nevent	2984	2443	1931	1149	210
$P_t 56$	19.0	16.3	14.5	12.1	9.2
$\Delta\phi$	2.1	2.0	1.9	1.7	1.3
$P_t^{out}$	13.2	11.3	9.9	8.2	6.0
$P_t^{\eta>5}$	6.2	6.1	6.0	5.8	5.3
$(P_t^Z - P_t^{part})/P_t^Z$	0.0141	0.0106	0.0093	0.0076	0.0040
$(P_t^J - P_t^{part})/P_t^J$	-0.0091	-0.0065	-0.0049	-0.0036	-0.0025
$(P_t^Z - P_t^J)/P_t^Z$	0.0185	0.0133	0.0107	0.0082	0.0041
$P_t(O+\eta>5)/P_t^Z$	0.0130	0.0083	0.0057	0.0039	0.0002
$1 - \cos(\Delta\phi)$	0.0010	0.0009	0.0008	0.0007	0.0004
$\sigma(Db[Z, J])$	0.0902	0.0754	0.0672	0.0576	0.0467
Entries	19995	16364	12936	7700	1409

Table 13: Selection 2.  $\Delta\phi_{(Z,jet)} = 180^\circ \pm 15^\circ$ ,  $\epsilon^{jet} < 3\%$ . UA1 algorithm.

$P_t^{clust}_{CUT}$	30	20	15	10	5
Nevent	3193	2403	1835	1093	217
$P_t 56$	21.4	17.5	15.0	12.3	9.6
$\Delta\phi$	3.5	2.8	2.3	1.9	1.4
$P_t^{out}$	16.0	12.6	10.5	8.3	5.9
$P_t^{\eta>5}$	6.1	6.1	6.0	5.9	5.3
$(P_t^Z - P_t^{part})/P_t^Z$	0.0049	0.0051	0.0052	0.0058	0.0044
$(P_t^J - P_t^{part})/P_t^J$	-0.0015	-0.0006	0.0000	0.0005	0.0028
$(P_t^Z - P_t^J)/P_t^Z$	0.0035	0.0029	0.0028	0.0032	0.0009
$P_t(O+\eta>5)/P_t^Z$	-0.0035	-0.0028	-0.0021	-0.0009	-0.0020
$1 - \cos(\Delta\phi)$	0.0033	0.0021	0.0014	0.0009	0.0005
$\sigma(Db[Z, J])$	0.0870	0.0714	0.0625	0.0539	0.0390
Entries	21392	16101	12291	7321	1457

Table 14: Selection 2.  $\Delta\phi_{(Z,jet)} = 180^\circ \pm 15^\circ$ ,  $\epsilon^{jet} < 3\%$ . UA2 algorithm.

$P_t^{clust}_{CUT}$	30	20	15	10	5
Nevent	3458	2605	2000	1198	229
$P_t 56$	21.4	17.6	15.2	12.5	9.8
$\Delta\phi$	3.5	2.8	2.3	1.9	1.4
$P_t^{out}$	15.9	12.6	10.5	8.4	6.0
$P_t^{\eta>5}$	6.1	6.1	6.0	5.9	5.4
$(P_t^Z - P_t^{part})/P_t^Z$	0.0055	0.0053	0.0059	0.0064	0.0046
$(P_t^J - P_t^{part})/P_t^J$	-0.0089	-0.0082	-0.0071	-0.0066	-0.0046
$(P_t^Z - P_t^J)/P_t^Z$	0.0111	0.0103	0.0102	0.0105	0.0080
$P_t(O+\eta>5)/P_t^Z$	0.0040	0.0046	0.0052	0.0062	0.0046
$1 - \cos(\Delta\phi)$	0.0033	0.0021	0.0014	0.0009	0.0006
$\sigma(Db[Z, J])$	0.0869	0.0721	0.0633	0.0548	0.0428
Entries	23169	17455	13397	8023	1537

Table 15: Selection 2.  $\Delta\phi_{(Z,jet)} = 180^\circ \pm 15^\circ$ ,  $\epsilon^{jet} < 3\%$ . LUCELL algorithm.

$P_t^{clust}_{CUT}$	30	20	15	10	5
Nevent	3184	2429	1851	1095	209
$P_t 56$	20.9	17.3	14.8	12.1	9.3
$\Delta\phi$	3.5	2.8	2.4	1.9	1.4
$P_t^{out}$	15.8	12.7	10.6	8.4	6.0
$P_t^{\eta>5}$	6.1	6.1	6.0	5.9	5.4
$(P_t^Z - P_t^{part})/P_t^Z$	0.0040	0.0039	0.0041	0.0049	0.0033
$(P_t^J - P_t^{part})/P_t^J$	-0.0056	-0.0047	-0.0037	-0.0023	-0.0004
$(P_t^Z - P_t^J)/P_t^Z$	0.0068	0.0059	0.0053	0.0052	0.0027
$P_t(O+\eta>5)/P_t^Z$	0.0000	0.0002	0.0004	0.0012	-0.0007
$1 - \cos(\Delta\phi)$	0.0032	0.0021	0.0014	0.0009	0.0005
$\sigma(Db[Z, J])$	0.0863	0.0720	0.0631	0.0536	0.0410
Entries	21330	16275	12399	7339	1400

Table 16: Selection 3.  $\Delta\phi_{(Z,jet)} = 180^\circ \pm 15^\circ$ ,  $\epsilon^{jet} < 3\%$ . UA1 algorithm.

$P_t^{clust}_{CUT}$	30	20	15	10	5
Nevent	2770	2119	1616	957	179
$P_t 56$	20.6	17.1	14.6	11.9	9.3
$\Delta\phi$	3.4	2.8	2.3	1.9	1.4
$P_t^{out}$	15.6	12.5	10.5	8.3	6.0
$P_t^{\eta>5}$	6.1	6.1	6.0	5.9	5.4
$(P_t^Z - P_t^{part})/P_t^Z$	0.0024	0.0027	0.0031	0.0038	0.0029
$(P_t^J - P_t^{part})/P_t^J$	-0.0032	-0.0028	-0.0018	-0.0011	0.0007
$(P_t^Z - P_t^J)/P_t^Z$	0.0027	0.0026	0.0024	0.0028	0.0013
$P_t(O+\eta>5)/P_t^Z$	-0.0042	-0.0031	-0.0025	-0.0012	-0.0021
$1 - \cos(\Delta\phi)$	0.0032	0.0021	0.0014	0.0009	0.0005
$\sigma(Db[Z, J])$	0.0848	0.0712	0.0626	0.0536	0.0406
Entries	18559	14199	10824	6409	1200

Table 17: Selection 3.  $\Delta\phi_{(Z,jet)} = 180^\circ \pm 15^\circ$ ,  $\epsilon^{jet} < 3\%$ . UA2 algorithm.

$P_t^{clust}_{CUT}$	30	20	15	10	5
Nevent	2770	2119	1616	957	179
$P_t 56$	20.6	17.1	14.6	11.9	9.3
$\Delta\phi$	3.4	2.8	2.3	1.9	1.4
$P_t^{out}$	15.6	12.5	10.5	8.4	6.1
$P_t^{\eta>5}$	6.1	6.1	6.0	5.9	5.4
$(P_t^Z - P_t^{part})/P_t^Z$	0.0024	0.0027	0.0031	0.0038	0.0029
$(P_t^J - P_t^{part})/P_t^J$	-0.0110	-0.0104	-0.0094	-0.0086	-0.0059
$(P_t^Z - P_t^J)/P_t^Z$	0.0101	0.0100	0.0098	0.0102	0.0078
$P_t(O+\eta>5)/P_t^Z$	0.0033	0.0043	0.0048	0.0061	0.0044
$1 - \cos(\Delta\phi)$	0.0032	0.0021	0.0014	0.0009	0.0005
$\sigma(Db[Z, J])$	0.0851	0.0714	0.0628	0.0538	0.0408
Entries	18559	14199	10824	6409	1200

Table 18: Selection 3.  $\Delta\phi_{(Z,jet)} = 180^\circ \pm 15^\circ$ ,  $\epsilon^{jet} < 3\%$ . LUCELL algorithm.

$P_t^{clust}_{CUT}$	30	20	15	10	5
Nevent	2770	2119	1616	957	179
$P_t 56$	20.6	17.1	14.6	11.9	9.3
$\Delta\phi$	3.5	2.8	2.3	1.9	1.4
$P_t^{out}$	15.7	12.6	10.5	8.4	6.0
$P_t^{\eta>5}$	6.1	6.1	6.0	5.9	5.4
$(P_t^Z - P_t^{part})/P_t^Z$	0.0024	0.0027	0.0031	0.0038	0.0029
$(P_t^J - P_t^{part})/P_t^J$	-0.0061	-0.0052	-0.0040	-0.0031	-0.0006
$(P_t^Z - P_t^J)/P_t^Z$	0.0055	0.0050	0.0047	0.0048	0.0027
$P_t(O+\eta>5)/P_t^Z$	-0.0014	-0.0007	-0.0003	0.0007	-0.0007
$1 - \cos(\Delta\phi)$	0.0032	0.0021	0.0014	0.0009	0.0005
$\sigma(Db[Z, J])$	0.0853	0.0714	0.0628	0.0539	0.0408
Entries	18559	14199	10824	6409	1200

## Appendix 6

$$40 \leq P_t^Z \leq 70 \text{ GeV}/c$$

Table 1: Number of events per  $L_{int} = 10 \text{ fb}^{-1}$ .

$P_{t\ max}^{clust}$ (GeV/c)	$P_{t\ max}^{out}$ (GeV/c)					
	5	10	15	20	30	1000
5	9700	17700	19200	19300	19300	19300
10	30700	69600	87300	91700	92400	92400
15	37700	92600	127400	141500	146600	146900
20	40000	100900	145400	167700	179200	180300
30	41400	106600	157600	187100	208900	213100

Table 2:  $\langle F \rangle$ ,  $F = (P_t^Z - P_t^{jet})/P_t^Z$ .

$P_{t\ max}^{clust}$ (GeV/c)	$P_{t\ max}^{out}$ (GeV/c)					
	5	10	15	20	30	1000
5	0.014	0.015	0.016	0.016	0.016	0.016
10	0.013	0.018	0.023	0.024	0.024	0.024
15	0.014	0.021	0.029	0.033	0.034	0.034
20	0.014	0.022	0.033	0.038	0.041	0.041
30	0.014	0.023	0.034	0.042	0.047	0.049

Table 3:  $\sigma(F)$ ,  $F = (P_t^Z - P_t^{jet})/P_t^Z$ .

$P_{t\ max}^{clust}$ (GeV/c)	$P_{t\ max}^{out}$ (GeV/c)					
	5	10	15	20	30	1000
5	0.079	0.088	0.093	0.094	0.095	0.095
10	0.085	0.103	0.115	0.121	0.124	0.124
15	0.086	0.107	0.126	0.140	0.150	0.151
20	0.088	0.109	0.131	0.151	0.168	0.173
30	0.088	0.110	0.134	0.158	0.187	0.200

$$70 \leq P_t^Z \leq 100 \text{ GeV}/c$$

Table 4: Number of events per  $L_{int} = 10 \text{ fb}^{-1}$ .

$P_{t\ max}^{clust}$ (GeV/c)	$P_{t\ max}^{out}$ (GeV/c)					
	5	10	15	20	30	1000
5	2500	4500	4900	5000	5000	5000
10	7600	18100	23000	24800	25200	25200
15	9500	24700	35000	40700	43900	44000
20	10100	27000	40300	50000	57900	59200
30	10600	28700	44500	57900	73200	79200

Table 5:  $\langle F \rangle$ ,  $F = (P_t^Z - P_t^{jet})/P_t^Z$ .

$P_{t\ max}^{clust}$ (GeV/c)	$P_{t\ max}^{out}$ (GeV/c)					
	5	10	15	20	30	1000
5	0.011	0.012	0.012	0.012	0.013	0.013
10	0.012	0.013	0.015	0.018	0.018	0.018
15	0.013	0.015	0.019	0.024	0.028	0.029
20	0.014	0.016	0.021	0.028	0.038	0.043
30	0.014	0.017	0.023	0.033	0.050	0.066

Table 6:  $\sigma(F)$ ,  $F = (P_t^Z - P_t^{jet})/P_t^Z$ .

$P_{t\ max}^{clust}$ (GeV/c)	$P_{t\ max}^{out}$ (GeV/c)					
	5	10	15	20	30	1000
5	0.069	0.070	0.074	0.075	0.077	0.077
10	0.071	0.078	0.088	0.093	0.095	0.096
15	0.071	0.082	0.094	0.105	0.116	0.118
20	0.072	0.083	0.097	0.111	0.131	0.141
30	0.073	0.084	0.100	0.118	0.149	0.178

$$100 \leq P_t^Z \leq 140 \text{ GeV}/c$$

Table 7: Number of events per  $L_{int} = 10 \text{ fb}^{-1}$ .

$P_{t\ max}^{clust}$ (GeV/c)	$P_{t\ max}^{out}$ (GeV/c)					
	5	10	15	20	30	1000
5	930	1710	1890	1920	1920	1920
10	3000	6860	9010	9660	9910	9930
15	3660	9320	13750	16110	17700	17910
20	3880	10320	15950	19880	23600	24330
30	4050	10970	17470	22910	30640	34110

Table 8:  $\langle F \rangle$ ,  $F = (P_t^Z - P_t^{jet})/P_t^Z$ .

$P_{t\ max}^{clust}$ (GeV/c)	$P_{t\ max}^{out}$ (GeV/c)					
	5	10	15	20	30	1000
5	0.007	0.006	0.009	0.008	0.008	0.008
10	0.005	0.012	0.014	0.014	0.015	0.015
15	0.005	0.011	0.015	0.017	0.018	0.019
20	0.006	0.012	0.017	0.019	0.024	0.026
30	0.005	0.013	0.017	0.022	0.033	0.036

Table 9:  $\sigma(F)$ ,  $F = (P_t^Z - P_t^{jet})/P_t^Z$ .

$P_{t\ max}^{clust}$ (GeV/c)	$P_{t\ max}^{out}$ (GeV/c)					
	5	10	15	20	30	1000
5	0.046	0.045	0.050	0.051	0.050	0.050
10	0.054	0.066	0.075	0.076	0.080	0.080
15	0.054	0.068	0.079	0.084	0.092	0.095
20	0.056	0.071	0.082	0.088	0.102	0.109
30	0.055	0.073	0.084	0.092	0.113	0.138

$$40 \leq P_t^Z \leq 70 \text{ GeV}/c$$

$$\epsilon^{jet} = 8\%$$

Table 10: Number of events per  $L_{int} = 10 \text{ fb}^{-1}$ .

$P_{t \max}^{clust}$ (GeV/c)	$P_{t \max}^{out}$ (GeV/c)					
	5	10	15	20	30	1000
5	8200	14800	16000	16100	16100	16100
10	23200	50800	62200	64800	65100	65100
15	27400	64200	85300	93200	95700	95900
20	28700	68700	94800	106900	112600	113200
30	29300	71300	100700	116200	127200	129500

Table 11:  $\langle F \rangle$ ,  $F = (P_t^Z - P_t^{jet})/P_t^Z$ .

$P_{t \max}^{clust}$ (GeV/c)	$P_{t \max}^{out}$ (GeV/c)					
	5	10	15	20	30	1000
5	0.007	0.006	0.005	0.005	0.005	0.005
10	0.006	0.003	0.002	0.001	0.000	0.000
15	0.007	0.005	0.003	0.001	-0.002	-0.002
20	0.007	0.005	0.004	0.002	-0.003	-0.004
30	0.007	0.006	0.006	0.004	-0.003	-0.010

Table 12:  $\sigma(F)$ ,  $F = (P_t^Z - P_t^{jet})/P_t^Z$ .

$P_{t \max}^{clust}$ (GeV/c)	$P_{t \max}^{out}$ (GeV/c)					
	5	10	15	20	30	1000
5	0.077	0.086	0.091	0.091	0.092	0.092
10	0.080	0.096	0.108	0.114	0.116	0.116
15	0.082	0.101	0.119	0.132	0.141	0.142
20	0.083	0.103	0.124	0.141	0.158	0.162
30	0.084	0.104	0.127	0.148	0.178	0.192

$$70 \leq P_t^Z \leq 100 \text{ GeV}/c$$

$$\epsilon^{jet} = 5\%$$

Table 13: Number of events per  $L_{int} = 10 \text{ fb}^{-1}$ .

$P_{t \max}^{clust}$ (GeV/c)	$P_{t \max}^{out}$ (GeV/c)					
	5	10	15	20	30	1000
5	2100	3700	4000	4100	4100	4100
10	5800	13200	16400	17400	17700	17700
15	7000	17000	23300	26600	28100	28200
20	7300	18200	26100	31400	35200	35600
30	7600	19100	28100	35300	42400	44300

Table 14:  $\langle F \rangle$ ,  $F = (P_t^Z - P_t^{jet})/P_t^Z$ .

$P_{t \max}^{clust}$ (GeV/c)	$P_{t \max}^{out}$ (GeV/c)					
	5	10	15	20	30	1000
5	0.010	0.009	0.008	0.008	0.007	0.007
10	0.010	0.005	0.004	0.004	0.003	0.003
15	0.009	0.006	0.005	0.005	0.003	0.003
20	0.009	0.006	0.006	0.006	0.006	0.006
30	0.009	0.007	0.007	0.009	0.011	0.009

Table 15:  $\sigma(F)$ ,  $F = (P_t^Z - P_t^{jet})/P_t^Z$ .

$P_{t \max}^{clust}$ (GeV/c)	$P_{t \max}^{out}$ (GeV/c)					
	5	10	15	20	30	1000
5	0.074	0.070	0.073	0.073	0.074	0.074
10	0.069	0.075	0.083	0.087	0.090	0.090
15	0.069	0.077	0.088	0.097	0.106	0.107
20	0.068	0.077	0.090	0.102	0.119	0.124
30	0.069	0.077	0.092	0.108	0.136	0.155

$$100 \leq P_t^Z \leq 140 \text{ GeV}/c$$

$$\epsilon^{jet} = 5\%$$

Table 16: Number of events per  $L_{int} = 10 \text{ fb}^{-1}$ .

$P_{t \max}^{clust}$ (GeV/c)	$P_{t \max}^{out}$ (GeV/c)					
	5	10	15	20	30	1000
5	910	1660	1810	1840	1850	1850
10	2730	6150	7870	8390	8590	8610
15	3220	8050	11460	13230	14380	14490
20	3370	8720	12900	15780	18300	18670
30	3490	9120	13910	17770	22860	24510

Table 17:  $\langle F \rangle$ ,  $F = (P_t^Z - P_t^{jet})/P_t^Z$ .

$P_{t \max}^{clust}$ (GeV/c)	$P_{t \max}^{out}$ (GeV/c)					
	5	10	15	20	30	1000
5	0.007	0.006	0.008	0.007	0.007	0.007
10	0.003	0.009	0.009	0.008	0.008	0.008
15	0.002	0.008	0.009	0.008	0.007	0.007
20	0.003	0.008	0.009	0.009	0.008	0.008
30	0.002	0.009	0.009	0.010	0.014	0.013

Table 18:  $\sigma(F)$ ,  $F = (P_t^Z - P_t^{jet})/P_t^Z$ .

$P_{t \max}^{clust}$ (GeV/c)	$P_{t \max}^{out}$ (GeV/c)					
	5	10	15	20	30	1000
5	0.046	0.045	0.049	0.049	0.049	0.049
10	0.046	0.059	0.065	0.068	0.071	0.071
15	0.046	0.063	0.071	0.076	0.084	0.086
20	0.049	0.063	0.072	0.080	0.093	0.098
30	0.048	0.064	0.075	0.084	0.105	0.120